



HEINRICH HEINE
UNIVERSITÄT DÜSSELDORF

**Magnetic resonance spectroscopy and
quantitative brain water imaging
in patients with hepatic encephalopathy**

Inaugural-Dissertation

zur

Erlangung des Doktorgrades der
Mathematisch-Naturwissenschaftlichen Fakultät
der Heinrich-Heine-Universität Düsseldorf

vorgelegt von

Georg Oeltzschner

aus **Leverkusen**

Düsseldorf, November 2015

Aus dem Institut für Klinische Neurowissenschaften und Medizinische
Psychologie
der Heinrich-Heine-Universität Düsseldorf

Gedruckt mit der Genehmigung der
Mathematisch-Naturwissenschaftlichen Fakultät der
Heinrich-Heine-Universität Düsseldorf

Referent: Prof. Dr. Alfons Schnitzler

Koreferent: Prof. Dr. Thomas Heinzel

Tag der mündlichen Prüfung:

16.12.2015

ACKNOWLEDGEMENTS

Ich bedanke mich mit der größten denkbaren Herzlichkeit bei Herrn Prof. Dr. Alfons Schnitzler für die Gelegenheit, an seinem Institut und unter seiner hervorragenden Anleitung meine Dissertation anfertigen zu dürfen. Die Unterstützung in jeglicher Hinsicht, die ich durch ihn erfahren durfte, war außerordentlich und alles andere als selbstverständlich.

Ein besonderer Dank gilt Herrn Prof. Dr. Thomas Heinzl für die Übernahme des Ko-referats sowie zahlreiche hilfreiche Hinweise beim Verfassen der Dissertation.

Herrn Prof. Dr. Dieter Häussinger sei für die Gelegenheit gedankt, im Rahmen des Sonderforschungsbereiches 974 an einem renommierten, aktuellen und spannenden Forschungsprojekt teilzuhaben. Weiter danke ich Herrn Prof. Dr. Gerald Antoch für die Aufnahme in das Institut für Diagnostische und Interventionelle Radiologie, ohne dessen Infrastruktur diese Arbeit niemals möglich gewesen wäre.

Besonders möchte ich mich bei Herrn Prof. Dr. Hans-Jörg Wittsack bedanken. Sein stets aufs Neue bewiesenes Nebeneinander von fachlicher Brillanz und großartiger Persönlichkeit hat mich verlässlich durch die vergangenen vier Jahre geführt und wird mir künftig als großes Vorbild dienen.

Herrn Dr. Markus Butz gilt ebenfalls eine besondere Danksagung. Auch ihn zeichnet die seltene Gabe aus, bei aller fachlichen Kompetenz ständig erreichbar, ansprechbar, hilfsbereit, aber auch im richtigen Moment kritisch und fordernd zu sein.

Bei der gesamten Arbeitsgruppe Medizinische Physik (Dr. Anja Müller-Lutz, Gael Pentang, Frithjof Wickrath) möchte ich mich für vier wunderbare Jahre bedanken, in denen ich mich stets heimisch gefühlt habe - und für stetige, unbedingte Unterstützung bei meinen Untersuchungen. Auch meine zweite Heimat, das Institut für Klinische Neurowissenschaft-

ten und Medizinische Psychologie, soll an dieser Stelle aus den gleichen Gründen nicht unerwähnt bleiben. Vor allem der feine Herr Thomas Baumgarten entwickelte sich zu einem hochgeschätzten Begleiter des Weges, der uns gemeinsam sogar bis nach Hawaii führte.

Frau Nur-Deniz Füllenbach gebührt ein herausragender Dank für ihr Engagement in der Patientenrekrutierung und -graduierung. Ohne sie wäre diese Arbeit unmöglich gewesen. Gleiches gilt für Frau Erika Rädisch, die bei unzähligen langen Messabenden wertvolle Unterstützung und Aufmunterung am MRT gab. Außerdem ist sie beim Quizduell nahezu unbesiegbar.

Eine gesonderte Erwähnung finden alle Last-Minute-Last-Second-Korrekturleser. Danke Imke, Hans-Jörg, Markus, Leona!

Leona! Hast Du wirklich gedacht, Du bekommst keine eigene Danksagung? Dir gebührt doch eine ganze Seite, oder eine ganze Arbeit. Vielen, vielen Dank - für jede gemeinsam verbrachte Sekunde, von denen mich jede einzelne unsagbar glücklich macht.

Weniger einen Dank als eine Huldigung verdient an dieser Stelle der beste denkbare Mitbewohner, Cocktailspezialist und Billardkollege Christian Kleinhans. 20 Jahre währt die Freundschaft, aber die Zeit der Promotion wird ganz besonders auf ewig hin untrennbar mit ihm verbunden sein. Es war mir eine Ehre, und es ist noch lange nicht vorbei!

Zu guter Letzt möchte ich mich bei meiner Mutter und meinem verstorbenen Vater bedanken, ohne die diese Arbeit erst recht nicht entstanden wäre. Eurer fortwährenden und unbedingten Unterstützung habe ich alles zu verdanken.

AUTHOR'S DECLARATION

I declare that the work in the dissertation was carried out autonomously and independently and without using any unauthorized help, and has not in the same or similar form been submitted at a different institution. This is my first attempt at obtaining a doctoral degree.

SIGNED: DATE:

CONTENTS

| | |
|--|------------|
| Contents | v |
| Abstract | vii |
| Zusammenfassung | ix |
| 1 Introduction | 1 |
| 2 Neurophysiological processing in the brain | 3 |
| 2.1 Neurotransmission | 3 |
| 2.2 Neural oscillations | 4 |
| 3 Glutathione in the brain | 7 |
| 4 Hepatic encephalopathy | 9 |
| 4.1 Symptoms, diagnosis, and grading | 9 |
| 4.1.1 <i>West-Haven</i> criteria and minimal HE | 10 |
| 4.1.2 Covert HE and overt HE | 11 |
| 4.1.3 Critical flicker frequency (CFF) | 11 |
| 4.2 Pathogenesis | 13 |
| 4.3 GABA in HE | 14 |
| 4.4 Oxidative stress, hyperammonemia and glutathione | 14 |
| 5 Magnetic resonance | 17 |
| 5.1 Background | 17 |

| | | |
|-----------|--|-----------|
| 5.1.1 | Proton spin in a magnetic field | 17 |
| 5.1.2 | Macroscopic magnetization and relaxation | 18 |
| 5.1.3 | Spin echo and gradient echo | 19 |
| 5.2 | Magnetic resonance imaging | 20 |
| 5.2.1 | Spatial encoding | 20 |
| 5.2.2 | Echo Planar Imaging (EPI) | 22 |
| 5.2.3 | Quantitative brain water content imaging | 23 |
| 5.3 | Magnetic resonance spectroscopy | 25 |
| 5.3.1 | Chemical shift | 25 |
| 5.3.2 | Localisation and acquisition | 26 |
| 5.3.3 | Analysis and quantification | 26 |
| 5.3.4 | Edited MR spectroscopy | 27 |
| 6 | Aims and hypotheses | 31 |
| 7 | Study 1: GABA spectroscopy in hepatic encephalopathy | 33 |
| 8 | Study 2: Covert hepatic encephalopathy: Elevated total glutathione and absence of brain water content changes | 39 |
| 9 | Methodological considerations: Water-scaled quantification of GABA | 47 |
| 10 | Conclusions and Outlook | 51 |

ABSTRACT

Hepatic encephalopathy (HE) is a set of neurological symptoms frequently occurring as a consequence of liver cirrhosis. HE affects many functional entities of the brain, including cognitive, executive and perceptive systems. Patients with HE exhibit an impaired performance of cognitive tasks, abnormal perception of temperature stimuli, behavioural changes, and motor dysfunctions. The severity of these symptoms is highly volatile and can range from subtle alterations to stupor and *coma hepaticum*.

The accumulation of neurotoxic ammonia in the brain due to impaired liver activity has been identified as a key feature of HE, triggering manifold responses such as neuroinflammation, oxidative stress, and formation of low-grade oedema. Recent magnetoencephalography (MEG) studies have provided evidence that HE symptoms are consistently associated with slowing of neural oscillations in their respective functional systems, but the underlying mechanisms remain elusive. While these and numerous other processes behind HE have been identified on microscopic and mesoscopic scales, they are yet to be integrated into a coherent pathophysiological concept, and at this point, it remains unclear how they contribute to pathological neural activity.

The present work investigated the role of the main inhibitory neurotransmitter γ -aminobutyric acid (GABA) for the pathogenesis of HE. As local GABA levels had previously been shown to influence the frequency of oscillations in the visual and the motor *gamma* frequency band, it was hypothesized that altered GABA concentrations contribute to HE symptoms via modulation of neural oscillations.

To test this hypothesis, magnetic resonance spectroscopy (MRS) was employed to determine in vivo levels of GABA in a cohort of 16 healthy controls and 30 HE patients. Results showed a decrease of GABA in the visual cortex in HE. Further, individual GABA levels correlated with the critical flicker frequency (CFF), a singular experimental parameter reliably reflecting HE severity. Low GABA was also linked to elevated blood ammonia levels. Beyond this, GABA was coupled to concentrations of glutamine and myo-inositol, two compounds that are highly involved in astrocytic regulation of hyperammonemia. However,

none of these relationships became evident in the sensorimotor region, giving rise to the assumption that the mechanisms mediating pathological behaviour are substantially different across brain regions.

In a second MRS investigation, the interplay of the major cerebral antioxidant glutathione, magnetic resonance imaging (MRI) measures of brain water content and HE characteristics was studied. Glutathione was elevated in HE, correlated with blood ammonia levels and closely followed alterations of glutamine and myo-inositol, suggesting an involvement in the interception of oxidative stress induced by ammonia. In contrast, measures of brain water content were not influenced by HE severity, blood ammonia or metabolite concentrations. This may imply that, at least in early stages of HE, the pathological impact of cerebral oedema may be smaller than previously assumed.

In conclusion, the novel findings presented in this work may help improve the understanding of the emergence of HE. GABA concentrations are presumably relevant for the development of HE symptoms in certain functional systems, but evidence prompts the notion that the exact pathways mediating abnormal oscillatory behaviour are highly region-specific. Further, glutathione appears to participate in the adaptation to hyperammonemia, whereas the relationship of brain water content and HE severity may be of more complex nature than previously expected.

ZUSAMMENFASSUNG

Die hepatische Enzephalopathie (HE) bezeichnet eine umfassende Reihe neurologischer Symptome, die als Folge einer Leberzirrhose auftreten können. Die HE kann verschiedene funktionale Einheiten des Gehirns beeinträchtigen, darunter Systeme, die für kognitive und exekutive Aufgaben oder die Wahrnehmung verantwortlich sind. Zu den Symptomen zählen unter anderem kognitive Verlangsamung, gestörte Temperaturwahrnehmung, Verhaltensänderungen und motorische Störungen. Dabei umfasst sie von im Alltag kaum wahrnehmbaren Veränderungen bis hin zu schwersten Störungen und *Coma hepaticum* eine große Bandbreite.

Hohe Ammoniakkonzentrationen infolge der Leberschädigung konnten als zentrale Ursache für vielfältige Folgevorgänge (u.a. entzündliche Prozesse, oxidativer Stress, Bildung niedriggradiger zerebraler Ödeme) identifiziert werden. Mit Hilfe der Magnetenzephalographie (MEG) konnte darüber hinaus in der Vergangenheit nachgewiesen werden, dass die Symptomatik der HE mit einer globalen, verschiedene funktionale Systeme betreffenden Verlangsamung neuronaler Oszillationen einhergeht. Eine vollständige und zusammenhängende Vorstellung von den zugrunde liegenden Mechanismen fehlt jedoch weiterhin, vor allem im Bezug darauf, wodurch die abnormale neuronale Aktivität hervorgerufen wird.

Im Rahmen der vorliegenden Arbeit wurde untersucht, inwieweit der wichtigste hemmende Neurotransmitter des Gehirns, γ -Aminobuttersäure (GABA), an der Pathophysiologie der HE beteiligt ist. In den vergangenen Jahren konnten verschiedene Studien lokale GABA-Konzentrationen mit der Frequenz der neuronalen Oszillationen im visuellen sowie im motorischen *Gamma*-Frequenzband in Verbindung bringen. In diesem Sinne wurde in der vorliegenden Dissertation die Hypothese geprüft, dass veränderte Konzentrationen von GABA – etwa durch Modulation der neuronalen Oszillationen – zur Entstehung der HE-Symptomatik beitragen.

In einer entsprechenden Studie wurden mit Hilfe der Magnetresonanzspektroskopie (MRS) die Spiegel von GABA in einem Kollektiv von 30 HE-Patienten und 16 gesunden Kontrollprobanden untersucht. Im visuellen Kortex von HE-Patienten wurden dabei

verminderte GABA-Konzentrationen nachgewiesen. Individuelle GABA-Spiegel korrelierten zudem mit der kritischen Flimmerfrequenz (CFF), einem routinemäßig erhobenen Diagnoseparameter, der den Schweregrad der HE nachweislich gut widerspiegelt. Niedrige GABA-Konzentrationen waren des Weiteren mit erhöhten Ammoniakspiegeln im Blut assoziiert. Zudem konnte gezeigt werden, dass GABA eng an die Konzentrationen von Glutamin und myo-Inositol gekoppelt ist, die wiederum zur Reaktion der Astrozyten auf den Ammoniaküberschuss beitragen. Keiner dieser Zusammenhänge konnte jedoch für das sensorimotorische Areal belegt werden. Dies legt nahe, dass die Mechanismen, die letztlich zur krankhaften Veränderung des Oszillationsverhaltens führen, nicht globaler Natur sind, sondern je nach Hirnregion stark variieren.

Eine weitere MRS-Untersuchung befasste sich mit der Rolle des wichtigsten Antioxidans im Gehirn, Glutathion, und seinen Wechselwirkungen mit dem HE-Schweregrad sowie dem Vorhandensein eines niedriggradigen zerebralen Ödems. Als Maß für dessen Ausprägung diente dabei eine quantitative Wassergehaltsbestimmung mittels Magnetresonanztomographie (MRT). Dabei konnte gezeigt werden, dass die Konzentration von Glutathion bei der HE erhöht ist, mit den Blutkonzentrationen von Ammoniak korreliert sowie dem Verhalten von Glutamin und myo-Inositol eng folgt. Diese Ergebnisse deuten auf eine prominente Rolle von Glutathion in der Bekämpfung des durch Ammoniak hervorgerufenen oxidativen Stress hin. Im Gegensatz dazu konnte keine maßgebliche Relevanz des Wassergehaltes festgestellt werden, der weder mit dem HE-Schweregrad noch den Blutammoniakspiegeln oder Metabolitenkonzentrationen zusammenhing. Dieser Befund könnte bedeuten, dass – zumindest im Falle der untersuchten niedriggradigen HE – die Rolle zerebraler Ödembildung für die Pathophysiologie geringer ist als bislang vermutet.

In der Gesamtschau könnten die in dieser Arbeit vorgestellten neuen Erkenntnisse das Verständnis der der HE zugrunde liegenden pathogenetischen Mechanismen verbessern. Die Konzentrationen von GABA sind in bestimmten funktionalen Systemen vermutlich maßgeblich an der Entwicklung der HE-Symptomatik beteiligt. Allerdings legen die vorgelegten Ergebnisse den Schluss nahe, dass die entscheidenden Störungen der neuronalen Oszillationen in verschiedenen Hirnregionen auf unterschiedlichen Wegen hervorgerufen werden. Glutathion nimmt indes offenbar eine wichtige Rolle in der Reaktion auf überschüssiges Ammoniak ein, während die Zusammenhänge vom HE-Schweregrad und erhöhten zerebralen Wassergehalts mutmaßlich komplexerer Natur sind, als bislang angenommen.

INTRODUCTION 1

The human brain is a biological entity of utmost sophistication. Employing the highest degree of complexity, structural specialization and functional organization, brain is capable of receiving, processing and evaluating sensory input from the outside world, while it coordinates our every interaction with the sources of these stimuli.

The brain orchestrates its function in a symphony of communication within a network of billions of neural cells, the *neurons*. Coordinated signal processing of large populations of neurons defines how—and which—information is relayed between different functional areas of the brain. Information is transported via modulation of electric signals, and neurons pass this information on through the release of distinct chemical compounds, the *neurotransmitters* [1, 2].

In the healthy brain, the underlying biochemical mechanisms are highly regulated. If these well-balanced equilibria are disturbed, information exchange within the brain may be severely impaired. A lot of research effort within clinical neuroscience is dedicated to the investigation of neurological diseases that may emerge as a consequence of erroneous neural communication, which can in turn be traced back to malfunctions on a molecular level. However, these deleterious impairments are not necessary brain-immanent. Damage to other organs may induce systemic stress with detrimental effect on brain function.

Hepatic encephalopathy (HE) constitutes an example for cerebral dysfunction that originates from other sites than the brain itself. HE evolves as a complication of liver damage with subsequent loss of detoxification capacity, causing accumulation of ammonia in the brain, which in turn has been recognized as a crucial force driving HE emergence and progression [3]. Its clinical manifestations (cognitive, behavioural and motor dysfunctions) have been attributed to abnormal neural communication patterns [4, 5]. Amongst others, oxidative stress and formation of a low-grade cerebral oedema have been hypothesized

to mediate deleterious effects of HE [6]. However, the exact origins and mechanisms of cerebral malfunction have not been completely understood.

The present work endeavours to elucidate the role of several aspects of HE pathogenesis, including neurotransmitter concentrations and cerebral water content. The following sections will provide brief summaries of the most relevant issues of the investigation. First, the important neurotransmitter γ -aminobutyric acid (GABA) will be presented in the framework of an introduction to the communication of neurons, followed by a concise explanation of the primary antioxidant compound glutathione. A review of the clinical symptoms, diagnosis and the current concept of the pathogenesis of hepatic encephalopathy (including the roles of GABA, glutathione and cerebral oedema) is presented afterwards. Finally, a brief introduction to the basic principles of magnetic resonance (MR) is given, including the key techniques of MR brain water imaging and MR spectroscopy that were employed in the present work.

NEUROPHYSIOLOGICAL PROCESSING IN THE BRAIN

2

In order to accomplish its tasks, the brain needs to collect, process and distribute information within its network of neurons. Neural signals are temporally and spatially limited inversions (*action potentials* or *spikes*) of the electric potential difference (*membrane potential*) between the inside and the outside of a neuron. Action potentials propagate along the membrane of branch-like structures of the neuron (*axons*) towards adjacent neurons, a process commonly referred to as *firing*. At the junction of two neurons, the *synapses*, the information needs to be relayed in order to facilitate further processing. The transfer of action potentials from one neuron to the next can be realised via direct electrical contact (*gap junctions*), but, in the brain, chemical synapses are predominant. These contacts convert an action potential into a chemical signal that bridges the gap to the next neuron where it elicits subsequent modulations of the membrane potential [7].

2.1 Neurotransmission

Several compounds in the brain, the *neurotransmitters*, accomplish the way of chemically forwarding an electric signal. One of them is γ -*aminobutyric acid* (*GABA*), a substance that is prevalent throughout the entire central nervous system. Chemically, GABA resembles another neurotransmitter, *glutamate*, a non-essential amino acid, from which it is also biosynthesized by the enzyme glutamate decarboxylase [1].

Neurotransmitters like GABA and glutamate are permanently held available in the *presynaptic terminals*. Once a propagating inversion of the membrane potential arrives, the neuron releases neurotransmitter molecules into the *synaptic cleft*. They diffuse through extracellular space to arrive at the postsynaptic site, where they can bind to specific proteins in the cell membrane, the *receptors*. In turn, these receptors modify the membrane

2.2 Neural oscillations

potential by allowing influx or efflux of positively (potassium, K^+ , calcium, Ca^{2+}) or negatively (chloride, Cl^-) charged ions. The membrane is consequently hyper- or depolarized. Depending on the receptor type, this modulation is mediated via different pathways and can be of varying extent and duration [1].

Despite their chemical resemblance, GABA and glutamate play opposing roles in the transmission of neural signals within the central nervous system. In most cases, GABA hyperpolarizes the postsynaptic neuron, i.e. makes it harder to elicit a subsequent action potential, whereas glutamate usually has a depolarizing effect and lowers the membrane potential towards its threshold of excitation. Consequently, GABA is labelled an *inhibitory* neurotransmitter and glutamate an *excitatory* one [1, 7].

2.2 Neural oscillations

Action potentials can be elicited successively and trigger repeated firing. Hence, they can influence post-synaptic potentials in subsequent neurons over time in various ways. Due to their abundant connectivity, neurons usually receive simultaneous synaptic signalling from numerous other neurons, with both excitatory and inhibitory input. As a result, the membrane potentials (and with them, the firing probability) within a population of many neurons can fluctuate. Post-synaptic potentials may now overlap, interfere constructively and synchronize across a neural ensemble to macroscopic *oscillations*. The amplitude of synchronized neural membrane potentials, i.e. their spatial average over a group of neurons, can reach such magnitude that it becomes measurable from outside the skull with electroencephalography (EEG) or magnetoencephalography (MEG) [8].

These techniques are used to noninvasively record neural activity on a time scale of milliseconds with coverage of the whole scalp. The collected time signals can be decomposed to yield the contribution of different frequencies. Oscillatory activity can be classified according to its frequency, encompassing the *delta* and *theta* bands (< 10 Hz), the *alpha* band (~ 10 Hz), the *beta* band (~ 20 Hz) and the *gamma* band (30 – 100 Hz) [9–11]. Cross-correlation analysis of neural activity recorded at different spatial locations can further provide measures of *coherence*, i.e. functional connectivity between brain areas [12]. Forming a bridge from activity on a cellular level to behaviour, different oscillatory networks are associated with distinct functions and tasks such as perception, attention modulation,

Chapter 2. Neurophysiological processing in the brain

memory or motor control [8, 10]. Oscillating networks convey information between distinct brain regions over large distances, and their disturbance in disease can result in various neurological dysfunctions [8].

Gamma oscillations are prevalent throughout cortex, involved in numerous cognitive tasks, and are known to emerge in neuronal networks from the interplay of glutamatergic and GABAergic activity [11, 13]. Computer simulations showed that inhibitory feedback connections within those networks are of special importance for the genesis of *gamma* rhythms [11]. Further, the peak *gamma* frequency is critically influenced by balance and nature of inhibitory and excitatory connections [14], with increased inhibition eliciting higher dominant frequencies.

Recent studies combined MEG and magnetic resonance spectroscopy (MRS) to scrutinize these associations in vivo in healthy humans. In both the motor cortex and the visual cortex, the peak *gamma* frequency during tasks did in fact correlate with the local resting GABA concentrations in the respective areas [15, 16].

GLUTATHIONE IN THE BRAIN

3

While the activity of neurons is the centrepiece of information processing in the brain, they require vital support from surrounding cells. *Astrocytes*, star-shaped brain cells, take over various maintenance and support duties throughout brain, e.g. the supply of nutrients and other important metabolites to neurons, maintaining brain water homeostasis etc. Further, they are crucially involved in the metabolism of *glutathione*, a chemical that is critical for the interception of deleterious oxygen compounds [17, 18].

During normal oxidative metabolism (i.e. generation of energy from nutrients), reactive oxygen species (ROS) are inadvertently generated in cells. Through various pathways, molecules like superoxide (O_2^-), hydrogen peroxide (H_2O_2), and hydroxyl radicals (OH) form [19]. These compounds are toxic and detrimental in many ways, including cell membrane destruction, protein modification and DNA alteration [18]. Given its large energy turnover and oxygen consumption, brain is particularly vulnerable to damage inferred by ROS, requiring a potent system to maintain its antioxidant capacity [17]. *Oxidative stress* describes circumstances in which this antioxidant system is thrown out of balance.

Reduced glutathione (GSH), a tripeptide composed from glutamate, cysteine and glycine, is a very important antioxidant compound in cells at a concentration of 1 – 10 mM [20]. GSH directly scavenges radicals under the formation of oxidized glutathione or glutathione disulfide (GSSG), and it catalyzes enzymatic antioxidant mechanisms [18]. To maintain antioxidant capacity, it is continuously restored from GSSG by enzymatic activity of glutathione reductase.

In brain, different cell types interact to provide protection against oxidative stress [17, 18]. Both neurons and astrocytes are able to synthesise GSH. However, astrocytes are the predominant site of synthesis and further provide precursor compounds to neighbouring cells. Hence, they prevent neuronal death and are therefore critical for the defence of brain integrity against ROS [21, 22].

Impairment of the glutathione defence system may be involved in various neurodegenerative disorders including Alzheimer's and Parkinson's disease [23].

HEPATIC ENCEPHALOPATHY

4

The liver is an organ with an enormous range of vital duties. Beyond the production of many important biochemical substances that are needed in almost all parts of the human body, its ability to detoxify deleterious compounds is of great importance.

Loss of liver filter function impairs the disposal of toxic substances which subsequently accumulate in the blood. Upon entering the brain, they affect cerebral mechanisms in multiple ways [24]. These alterations to cerebral functions are subsumed under the term *hepatic encephalopathy* (HE). HE can be classified with respect to the origin of hepatic dysfunction. The following typology has been adapted from the 1998 World Congress of Gastroenterology report [25].

- *Type A* (acute) describes HE associated with acute liver failure (e.g. following paracetamol intoxication)
- *Type B* (byypass) means HE associated with portal-systemic bypass (i.e. redirection of bloodflow bypassing the liver for reduction of blood pressure), but no intrinsic liver disease
- *Type C* (cirrhosis) indicates HE associated with cirrhosis (regardless of the pathogenesis, i.e. alcoholic liver disease, viral hepatitis etc.)

The present work focuses on HE Type C, i.e. as a consequence of chronic liver damage.

4.1 Symptoms, diagnosis, and grading

HE is associated with a range of neuropsychiatric impairments, affecting cognitive function, attention, consciousness and behaviour [24, 25]. Motor symptoms of HE include Parkinson-like hand tremor of varying amplitude such as *mini-asterixis* (fine tremulousness)

4.1 Symptoms, diagnosis, and grading

and *asterixis* (coarse flapping tremor) [24, 26]). HE affects a considerable fraction (30–45%) of patients with cirrhosis, resulting in frequent hospitalisation and great—probably underestimated—economic burden [27].

In the framework of chronic liver cirrhosis (as is the case in the present work), time course and severity of alterations allow for a differentiation between *overt* and *minimal* HE [25, 28]. Patients with overt HE exhibit clear manifestations of the aforementioned symptoms and are therefore diagnosed by clinical examination, whereas diagnosis of minimal HE requires additional neuropsychometric measurements (see below) [29].

4.1.1 West-Haven criteria and minimal HE

Grading of overt HE severity is routinely performed with the assessment of the mental state, focusing on consciousness and behaviour. The *West-Haven* criteria allow for a semiquantitative classification into four groups, ranging from comparably mild symptoms (grade 1) up to coma (grade 4). The following list is a compilation from various sources [25, 29, 30].

- *Grade 1*: Trivial lack of awareness, experience of euphoria or anxiety, shortened attention span, impaired performance of basic arithmetic operations, altered sleep rhythm
- *Grade 2*: Lethargy or apathy, minimal disorientation in time or space, subtle to obvious personality change, inappropriate behaviour, asterixis
- *Grade 3*: Somnolence to semistupor but responsive to verbal stimuli, confusion, gross disorientation, bizarre behaviour
- *Grade 4*: Coma (unresponsive to verbal or noxious stimuli)

The *West-Haven* scheme does, however, not apply to a considerable population of patients. These appear normal during clinical examination and do not present visible signs of brain dysfunction, but show significantly inferior results in psychometric tests revealing subtle impairments of psychomotor and executive performance [29, 30]. Originally, these patients were subsumed under the label of *subclinical HE* [31]. Subsequently, the term *minimal HE* (*mHE*) was introduced and used throughout the latest agreements on HE terminology [25, 29].

Per definition, diagnosis of mHE requires neuropsychometric testing [3], encompassing the assessment of fine motor performance, psychomotor speed and bimanual coordination. A number of test strategies exist, ranging from paper and pencil tests (portosystemic encephalopathy syndrome (PSE) test [32] or psychometric hepatic encephalopathy score (PHES) [33, 34]) over computerized psychometry [35] and reaction time assessment [36] to processing of incongruent colour stimuli (Stroop test [37]). However, single tests lack specificity [38] and standardization (e.g. across countries), which is why a combination of at least two test methods is recommended [29].

The prevalence of mHE is high. Between 30% to 84% of cirrhosis patients are reported to develop mHE [39]. The condition has not only been reported to predict episodes of higher-grade HE [40], but also has detrimental influence on life expectancy [41], quality of life [42, 43], fitness to drive [44] and other aspects of daily functioning.

4.1.2 Covert HE and overt HE

In 2011, the members of the International Society for Hepatic Encephalopathy and Nitrogen Metabolism (ISHEN) published a report of their 14th conference in 2010. Based on their experience of high subjectivity of the *West-Haven* criteria—especially considering the variability in identifying patients with HE of grade 1—they proposed an alternative classification [28]. The experts suggested to pool minimal HE and HE 1 patients to a *covert HE* group “with neuropsychometric/neurophysiological abnormalities in the absence of disorientation and asterixis” [28]. Covert HE should thus be delineated from an *overt HE* group including patients with grade II and above with clear physical signs of HE.

Fig. 4.1 summarizes the different grading agreements. Despite the diversity of classification schemes, it is important to recognize the continuous nature of HE, which hampers unambiguous grading and is the reason for the various revisions of classification agreements over the past years.

4.1.3 Critical flicker frequency (CFF)

A useful tool to describe HE severity on a non-discrete scale is the assessment of the critical flicker frequency (CFF). The CFF mirrors the individual ability to discern quickly oscillating visual stimuli, and is widely used to grade HE severity and clinically monitor symptom progression [45]. The measurement procedure—originally designed to investigate

4.1 Symptoms, diagnosis, and grading

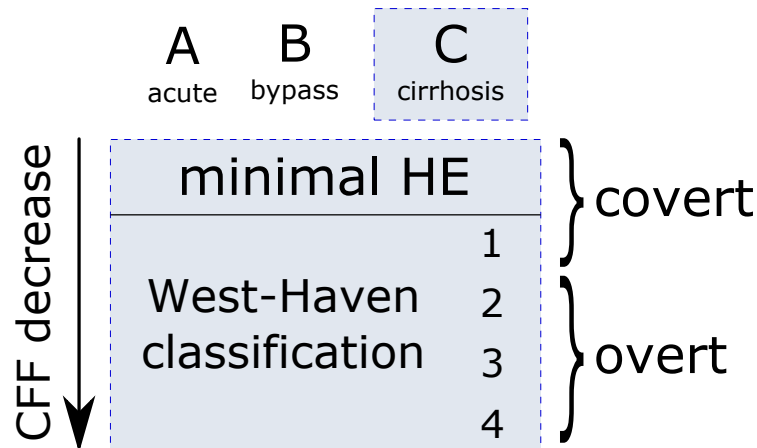


Figure 4.1: Schematic overview of HE typology and grading agreements [25, 28, 29]. The present work focuses on patients with covert HE (i.e. minimal HE and HE 1) of type C.

neurological dysfunction such as multiple sclerosis or Alzheimer’s disease—was adapted for the estimation of HE severity and is briefly outlined in the following paragraph [46].

The CFF device consists of a binocular-like display and a handheld switch. At the start of the measurement, the participant is being presented a visual stimulus in shape of a red light spot on the display. The spot initially flickers at a frequency of 60 Hz, giving the impression of a continuous fused light, and the flicker frequency is gradually decreased. The participant is instructed to press a button as soon as perception switches from steady to flickering light. The mean of the respective frequencies from 8 repeated measurements (with random frequency slopes to avoid habituation) is the individual CFF.

CFF in healthy controls is usually around 42 Hz, whereas deterioration of CFF is associated with increasing HE severity [46, 47]. Cut-off frequencies of 39 Hz and 38 Hz have been suggested for the discrimination between controls and patients [46, 48]. Potential benefits of CFF assessment for the delicate and elaborate diagnosis of mHE have been recognized [47, 48]. However, while it is regarded as a useful parameter and shows high specificity, CFF has been noted to have only moderate sensitivity to reliably distinguish mHE from controls or overt HE [45, 49]. The recommendation to use it as an addendum, but not a replacement to psychometric assessment, is therefore maintained [29, 49].

4.2 Pathogenesis

The exact pathogenetic concept of HE is complex, needs to consider a multitude of impacting factors and is still an important issue of current research [3, 30]. Numerous studies have unveiled a large array of phenomena which are potentially intertwined and may differentially contribute to different types, severity stages or symptoms of HE [6]. Amongst others, this array includes neuroinflammation (i.e. signs of systemic immune reaction in the brain [50, 51]), oxidative and nitrosative stress (i.e. formation of aggressive reactive oxygen and nitrogen oxide species [52]), low-grade oedema formation (i.e. tissue swelling due to disturbed cellular water homeostasis [6]) and alterations of neurotransmitter systems [30].

Many mechanisms relate to, are enforced by and interact with the common thread in the HE pathogenesis, *hyperammonemia*, meaning excess presence of neurotoxic ammonia in the brain due to failed hepatic clearance and subsequent accumulation in the blood. Within brain, ammonia is metabolized and incorporated into glutamine (Gln) by the enzyme glutamine synthetase which is primarily expressed in the astrocytes [6]. Accordingly, studies using proton magnetic resonance spectroscopy could consistently show increased concentrations of Gln, along with lower concentrations of myo-inositol (ml), a compound that is presumably released from the astrocyte to maintain the osmotic balance between intra- and extracellular space [53–56]. These findings are interpreted as a sign of abnormal cell volume regulation eliciting astrocyte swelling, leading to a low-grade cellular oedema [57, 58]. This hypothesis is corroborated by several studies demonstrating small changes in magnetic resonance imaging parameters that are either sensitive to or directly map brain water content [55, 59, 60] (reviewed in [61]).

HE symptoms are thought to emerge from a series of complex interactions of astrocyte swelling, oxidative stress, neuroinflammation, neurotransmitter system alterations and other HE-related phenomena. MEG experiments have linked disturbances in the several oscillatory systems to HE-induced abnormalities in numerous functional domains such as fine motor control [4, 62, 63], attention [64] and pain perception [65]. This is giving rise to a concept of global oscillatory slowing in HE across functional subsystems and oscillation frequency bands [4, 5, 66]. It is, though, currently not fully understood how oscillatory behaviour is deteriorated by the pathogenetic mechanisms of HE.

4.3 GABA in HE

For more than thirty years, it has been debated to what extent GABA is involved in the emergence of HE symptoms. Initially, a global increase of cerebral GABAergic tone was proposed and traced back to elevated bacterial synthesis of GABA in the gut [67], but subsequent attempts to substantiate potential effects on receptor architecture or regulation of GABAergic tone in the brain yielded controversial outcome [68]. A consistent notion of the role of GABA in HE is still lacking, although evidence against a generalized increase of GABAergic tone in HE grew stronger. Instead, recent concepts are in favour of localized, regionally selective and interdependent alterations of glutamatergic and GABAergic neurotransmission [69, 70]. These ideas are based on a number of experiments in rodent models of chronic HE. Rats with chronic liver failure showed hypokinesia along with increased thalamic GABA levels (in turn due to excessive glutamate receptor activation in the *substantia nigra*) [71]. In hyperammonemic rats, GABA levels were reported to be decreased in cortex, but elevated in cerebellum, and moreover linked to cognitive performance [72].

As mentioned above, disturbances of neurotransmitter systems might be mediating pathological oscillatory behaviour in HE, considering the link between GABA levels and oscillations in both the motor [15] and the visual cortex [16]. Hence, in **Study 1** GABA levels in HE patients were probed *in vivo* with magnetic resonance spectroscopy, and it was scrutinized whether clinical and behavioural indicators of HE severity are associated with altered GABA concentration.

4.4 Oxidative stress, hyperammonemia and glutathione

Oxidative stress is considered to be another key feature in the emergence of HE [6]. Formation of ROS has been shown to mediate ammonia neurotoxicity in cell cultures and in the rat brain (for a review see [73]), and recently, marker compounds indicating oxidative stress were also discovered in the brains of cirrhosis patients [74]. Oxidative stress in HE is closely interacting with astrocyte swelling, probably in a mutually self-amplifying way [58, 75], and its subsequent deleterious effects on RNA (ribonucleic acid) and protein synthesis may help explain various HE related deficits, including abnormalities of neurotransmitter systems [76].

Oxidative stress further seems to be critical for the emergence of cerebral oedema. Recent experiments demonstrated that only synergistic action with hyperammonemia, but not solitary action of one of both, elicited formation of cerebral oedema in animal models of chronic HE [77, 78].

The link between ammonia and oxidative stress sparked several studies investigating the effect of ammonia challenge on glutathione levels ¹. Increased glutathione concentrations and synthesis were found in cultured astrocytes [79] and in rodent brains [80, 81] under ammonia challenge, whereas cultured neurons show decreased GSx and subsequent cell death [82]. Rodent studies further revealed that hyperammonemia prompts astrocytes to synthesize and release GSH precursors into extracellular space, hence reinforcing their protection to neighbouring neurons [83].

In the light of these experiments, **Study 2** scrutinized whether altered glutathione levels can be shown in patients with HE and if they scale with HE severity or ammonia load. Given the close associations between oxidative stress, ammonia and cerebral oedema, it was further analysed whether brain water content measures are linked to glutathione levels.

¹If not stated otherwise, this refers to total glutathione or GSx, i.e. both reduced and oxidized glutathione (GSH+GSSG).

MAGNETIC RESONANCE 5

In the late 19th and early 20th century, the quantised nature of the angular momentum of elementary particles in the presence of an external magnetic field became apparent (most notably through the ZEEMAN effect [84] and the STERN-GERLACH experiment [85]). Soon, quantisation of energy levels in magnetic fields was demonstrated for protons (RABI in 1938 [86]). Manipulation of spins via nuclear magnetic resonance (NMR) followed (PURCELL [87] and BLOCH [88] in 1946), paving the way towards the first imaging applications (LAUTERBUR [89] and MANSFIELD [90, 91] in 1973/74).

5.1 Background

Today, magnetic resonance techniques are valuable tools for the noninvasive assessment of structural and biochemical properties in the living brain. This section intends to introduce the most important concepts behind magnetic resonance experiments and to present essentials of the techniques that were used within this work. It is based on the standard textbook by Haacke et al. [92]

5.1.1 Proton spin in a magnetic field

Elementary particles carry intrinsic properties such as mass and charge, defining their interactions with other particles and fields. Another of these intrinsic features is *spin*. The elements of the quantum mechanical spin operator \hat{S} do not commute, i.e. not all three spin components of a given system can be simultaneously assessed (HEISENBERG's uncertainty principle). In contrast, \hat{S}^2 and \hat{S}_z do commute. An eigenstate of \hat{S}^2 has an eigenvalue of $s(s+1)\hbar^2$, with the *spin quantum number* s and the reduced Planck constant \hbar . Eigenvalues of \hat{S}_z are $m_s\hbar$, where m_s assumes one of the $2s+1$ values between $-s$ and $+s$.

5.1 Background

Elementary particles have spin quantum numbers of $s = 1/2$ (fermions, e.g. electrons or protons) or $s = 1$ (bosons, e.g. photons).¹ Hence, protons have only two possible spin quantum states identified by $m_s = +1/2$ and $m_s = -1/2$. The intrinsic spin angular momentum \vec{S} is linearly associated with a magnetic moment

$$\vec{\mu} = \gamma \vec{S} \quad (5.1)$$

with the gyromagnetic ratio γ . Upon interaction with an external magnetic field \vec{B}_0 along the z-direction, the potential energy of a proton spin is found to be

$$E = -\vec{\mu} \cdot \vec{B}_0 = -\mu_z B_z = -\gamma m_s \hbar B_z \quad (5.2)$$

The proton spin system in presence of an external magnetic field therefore possesses two discrete energy configurations. In the state with $m_s = +1/2$, the z-component of \vec{S} is aligned along the external field (“spin up”), whereas in the state described by $m_s = -1/2$, the z-component is antiparallel to \vec{B}_0 (“spin down”). By plugging the values of m_s into Eq. 5.2, the energy difference between the two states is found to be

$$\Delta E = E(m_s = -1/2) - E(m_s = +1/2) = \frac{1}{2} \gamma \hbar B_0 - \left(-\frac{1}{2} \gamma \hbar B_0\right) = \hbar \omega_0 \quad (5.3)$$

where $\omega_0 = \gamma B_0$, the *Larmor frequency*, describes the precession that the tip of the spin angular momentum vector performs with respect to the magnetic field axis. This precession ultimately arises from the fact that magnitude and direction of \vec{S} are not precisely determined at the same time. Instead, its magnitude and z-component are constant in time, resulting in periodic modulation of the x- and y-components with angular frequency ω_0 .

Transition between the two spin states can be accomplished by absorption or emission of a photon with energy ΔE , i.e. with the Larmor frequency ω_0 (“spin flip”, Eq. 5.3).

5.1.2 Macroscopic magnetization and relaxation

The probability of meeting a system at a certain energy state (in thermal equilibrium at temperature T) is following BOLTZMANN’s distribution. The upper of the two proton spin

¹For particles containing more than one elementary particle, the total spin can be added up according to rules of quantum mechanical angular momenta. For example, ¹³C, ²³Na, ³¹P and other nuclei are widely employed for magnetic resonance experiments. The introduction will, however, stick to ¹H for the sake of simplicity.

states in an external magnetic field B_0 is therefore slightly less populated than the lower one, resulting in an excess macroscopic magnetization in direction of B_0 :

$$\vec{M}_0 \simeq \rho_0 \frac{\gamma^2 \hbar^2}{4kT} \vec{B}_0 \quad (5.4)$$

with the Boltzmann constant k . Here, M_0 is proportional to the local spin density ρ_0 . Although the relative spin excess contributing to M_0 is on the scale of 10^{-6} for room temperature and fields in the order of magnitude of 1 T, the vast number of spins in matter allows for actual detection of through induction in measurement coils.

The steady-state macroscopic magnetization \vec{M}_0 can be disturbed from outside through interaction with time-varying electromagnetic fields at Larmor frequency, i.e. irradiation of radiofrequency (RF) pulses. Such manipulation and subsequent observation of the then time-dependent $\vec{M}(t)$ is the essential of all NMR experiments. BLOCH introduced a set of motion equations for $\vec{M}(t)$, describing its return to thermal equilibrium after manipulation with exponential growth and decay terms (Eq. 5.5) [88]:

$$\vec{M}(t) = \begin{pmatrix} M_x(t) \\ M_y(t) \\ M_z(t) \end{pmatrix} = \begin{pmatrix} e^{-t/T_2} (M_x(0) \cos \omega_0 t + M_y(0) \sin \omega_0 t) \\ e^{-t/T_2} (M_y(0) \cos \omega_0 t - M_x(0) \sin \omega_0 t) \\ M_z(0) e^{-t/T_1} + M_0 (1 - e^{-t/T_1}) \end{pmatrix} \quad (5.5)$$

The relaxation processes are defined by the time constants T_1 and T_2 . T_1 , the spin-lattice or *longitudinal relaxation time*, characterizes the regrowth of M_z to the steady-state value M_0 . The parallel decay of magnetization in the x - y -plane (M_{xy}) is addressed as spin-spin or *transversal relaxation time*. Both T_1 and T_2 depend on microscopic properties of the magnetized domains, e.g. tissue. Standard MR imaging contrasts base on the utilization of differing relaxation behaviour across tissue types.

5.1.3 Spin echo and gradient echo

Decay of transverse magnetization M_{xy} (i.e. the signal induced in the receiver coil) after initial excitation of spins is not only due to spin-spin interaction. B_0 inhomogeneities further contribute to signal decay via additional dephasing of the spins. The total signal decay is characterised by the time constant T_2^* , which is consequently shorter than T_2 .

5.2 Magnetic resonance imaging

In order to partially recover M_{xy} for signal recording, the *spin echo* technique can be applied. First presented by HAHN, it makes use of an additional RF pulse at $t = \frac{TE}{2}$ that flips the phase of all spins by 180° in the x - y -plane, while their frequency is maintained [93]. After the *echo time* TE , the spins are back in phase (“refocused”) and interfere constructively. It is evident that this technique can only account for stationary sources of dephasing, i.e. B_0 inhomogeneities, but not intrinsic dephasing caused by spin-spin-interaction. Hence, spin echo is still subject to the T_2 decay.

A *gradient* is an additional superimposed magnetic field with linear increase along a defined direction. For instance, a z -gradient changes the total field to be $\vec{B}(x, y, z) = B_0\hat{z} + G_z z\hat{z}$ with the gradient strength $G_z = \frac{\partial B_z}{\partial z}$. Gradients are vital for the employment of magnetic resonance as an imaging technique (see next section). Application of a gradient is an artificial field inhomogeneity, hence amplifying spin dephasing. This can be countered by pre-applying an inverse gradient prior to the actual gradient. Rewinding of the spins subsequently induces a *gradient echo*. In contrast to the spin echo, the gradient echo will still suffer from stationary B_0 variation and thus be subject to the T_2^* decay. As the additional time for the refocusing pulse is saved, gradient echoes are nevertheless suitable for fast signal acquisition.

5.2 Magnetic resonance imaging

In order to enable imaging based on nuclear magnetic resonance, it is necessary to imprint spatial information on the signal that is induced in the measurement coil by precessing magnetization. Application of gradients to make the Larmor frequency and precession phase a function of position was the key concept applied by CARR (1D [94]), LAUTERBUR [89] and MANSFIELD [90, 91] (2D and 3D).

5.2.1 Spatial encoding

Adding spatial information to the signal is performed separately for the x -, y - and z -axis. These axes are defined as follows: z denominates the direction of the main magnetic field B_0 , x is the left-right-axis and y the up-down-axis (e.g. as perceived from a subject lying in an MRI scanner), hence $\vec{B}_0(x, y, z) = B_0\hat{z}$.

5.2.1.1 Slice selection is the process of delineating the desired imaging volume in z -direction.

To this end, a z -gradient is applied and renders the Larmor frequency dependent of the z position ($\omega(z) = \omega_0 + \gamma G_z z$). Irradiation of a rectangular RF pulse² of frequency $\omega = \omega_0 + \omega'$ and bandwidth $\Delta\omega$ will excite spins within a slice centered at $z = \frac{\omega'}{\gamma G_z}$ with a width of $\Delta z = \frac{\Delta\omega}{\gamma G_z}$. The slice thickness is hence determined by gradient strength and pulse bandwidth, its position by the center frequency of the RF pulse.

5.2.1.2 Frequency encoding: After slice selection, all spins within this slice precess with equal frequency and phase³. One direction (x in this example) is simply encoded by applying another gradient G_x , inducing Larmor frequency dependence from x within the slice. For this reason, x is referred to as the *frequency encoding direction*. As the gradient is active throughout the whole signal recording time t , it is also termed *readout* gradient. Its strength directly determines the range of frequencies contributing to the total recorded signal.

5.2.1.3 Phase encoding: The remaining direction (here y) needs to be encoded differently. Prior to frequency encoding, a *phase encoding gradient* G_y is therefore switched on for a brief period τ and then switched off again. Spins within the slice will afterwards precess at identical frequencies, but have acquired a phase shift $\Phi(y) = \gamma G_y y \tau$ linearly growing with y (further from $y = 0$, the acquired phase will be larger). Re-excitation of the slice with a small increment of the phase encoding gradient strength (ΔG_y) induces a different phase shift. This experiment is repeated to cover a range of maximum phase encoding gradients ($-G_{y,\max}$ to $+G_{y,\max}$). This allows to plot the phase shift from a given location over all gradient strengths ($\Phi(G_y)$). In this plot, the phase shift will oscillate quicker for large y values and not at all for $y = 0$. y position is hence encoded in a “rate of change” of phase over gradient strength, which is similar to a frequency in time. In that sense, phase encoding is indirect frequency encoding—instead of sampling a signal at constant phase over time, the signal is sampled at constant time points by varying its phase shift over the repeated acquisitions.

²This refers to the shape of the pulse in the frequency domain. It has to be noted that real RF pulses are never perfectly rectangular, as a boxcar-shaped pulse would require an infinite pulse length in the time domain. Hence, the excitation profile deviates slightly from an ideal boxcar.

³To rewind the frequency dependence in z -direction *within* the slice, i.e. reset all excited spins to identical phase, an inverted slice selection gradient needs to be applied directly after slice selection.

5.2 Magnetic resonance imaging

5.2.1.4 k-space and 2D Fourier transformation: Realising that a given volume element at (x, y) produces a signal $S(x, y, t)$ which is proportional to the local spin density $\rho(x, y)$ and is modulated by a phase $\Delta\Phi(x, y, t) = \gamma G_x x t + \gamma G_y y \tau$, one can rewrite the whole signal that is induced in the receiver as an integral over all (x, y) :

$$S(t) = \iint_{x,y} \rho(x, y) e^{i\gamma G_x x t + i\gamma G_y y \tau} dx dy \quad (5.6)$$

Defining $k_x = -\gamma G_x t$ and $k_y = -\gamma G_y \tau$, Eq. 5.6 becomes a 2D Fourier integral, and the desired spin distribution $\rho(x, y)$ can be obtained from the total signal by 2D Fourier transformation:

$$\rho(x, y) = \iint_{k_x, k_y} S(k_x, k_y) e^{ik_x x + ik_y y} dk_x dk_y \quad (5.7)$$

k -space (k_x, k_y) immediately becomes obvious as conjugate to real space (x, y) . Acquiring an image as outlined above simply means measuring the signal over discrete points in k -space. Frequency encoding corresponds to sampling the signal M times during the time t that a constant G_x gradient is active, thus recording M points with increasing k_x in k -space. N times increasing the gradient G_y for a constant phase encoding time τ is the equivalent of recording N such lines in k -space. 2-dimensional discrete Fourier transformation is finally performed on $S(k_x, k_y)$ to yield the desired spatial spin density distribution $\rho(x, y)$ (i.e. to reconstruct an image with $M \times N$ pixels).

5.2.2 Echo Planar Imaging (EPI)

Re-exciting the slice of interest for each k -space line can cost a considerable amount of time. *Echo Planar Imaging* (EPI) instead collects more than one k -space line after RF excitation [95]. With EPI, the whole of k -space (usually 64-128 phase encoding steps) is reached after one (single shot) or a low number (multi shot) of RF excitations.

EPI uses the frequency encoding gradient to refocus the precessing magnetization and collect a whole train of gradient echoes. Phase encoding starts with the maximum gradient and is gradually reduced by a small inverse gradient (“blip”). The readout gradient is inverted after every blip, leading to a zig-zag trajectory through k -space. Refocusing can

also be performed by a train of 180° pulses after excitation and normal readout of the resulting spin echoes. In this case, the label *fast spin echo* (FSE) instead of EPI is common.

EPI enables rapid imaging on a time scale of 100 ms per slice, but demands fast and strong gradient systems. It is further prone to inhomogeneities of the magnetic field.

5.2.3 Quantitative brain water content imaging

Radiological MR imaging for diagnostic purposes is mainly of qualitative nature, as its primary goal is to discern between pathological and healthy tissue. For research purposes, the assessment of quantitative parameters is particularly desirable. As the MR signal is directly proportional to the number of protons precessing at a given frequency, its assessment is intrinsically quantitative, but requires some kind of calibration. In the current work, a combination of several acquisitions has been used to provide a quantitative measure of cerebral water content. With these data, statements about the extent of the putative low-grade brain oedema in HE patients could be expressed. The method was originally proposed by Neeb and colleagues [96–98], and has subsequently been employed to investigate HE patients [60]. Its basic principles are briefly outlined below.

The foundation of this technique is a gradient echo sequence, hence, the signal decay can be expressed as

$$S(t) = S_{0,T_2^*} \cdot e^{-t/T_2^*} \quad (5.8)$$

The multi gradient echo sequence used for this technique measures the MR signal $S(t)$ at 8 subsequent time points, each separated by 5 ms, with the first echo acquired 4 ms after excitation. The signal curve is extrapolated backwards to obtain the signal at $t_0 = 0$ ms. As the macroscopic magnetization of abundant non-water protons (fat, macromolecules etc.) decays very quickly, their contribution is already negligible at the time of the first echo after 4 ms. Hence, the signal $S_{0,T_2^*} = S(t_0)$ is directly proportional to the number of water protons. By comparison with a reference signal from a probe containing 100% water, a measure for absolute localized water content can be calculated.

However, such measures require various corrections to compensate for different sources of spatial signal inhomogeneity:

- RF excitation is performed by a body coil, while the signal itself is acquired by a dedicated head coil. The spatial profile of the RF excitation field strength (B_1) may

5.2 Magnetic resonance imaging

not be homogeneous throughout the whole image volume. As a result, different image voxels will experience deviations from the ideal 90° excitation pulse. This directly affects the measured signal intensity during readout. For compensation, an effective flip angle is calculated from two EPI images with varying nominal flip angle (90° vs. 30°). This effective excitation angle is used to calculate a B_1 correction map for the signal intensity S_0 .

- As the receiving profile of the head coil is also not uniform over the investigated volume, it will directly affect the measured signal intensities, too. The 90° EPI image from B_1 correction can be combined with a third 90° EPI acquisition, this time with the body coil as the receiver coil. In combination with the transmission characteristics expressed by the effective flip angle, a correction map for receiver coil inhomogeneities can be computed.
- Lastly, spatial variations in tissue T_1 need to be accounted for, as the multi echo gradient sequence used to determine S_0 is performed with comparably short TR. Saturation effects will therefore modulate the measured signal intensities. T_1 mapping is performed with an additional two-echo gradient sequence (using a different RF excitation flip angle). It is subsequently used to calculate voxel-individual saturation correction.
- If a phantom probe is used as a 100 % water reference, additional correction for its temperature is required. In the present work, the cerebrospinal fluid in the individual brain was used as pure water reference, hence rendering temperature correction redundant.

Using this technique, reliable brain water maps (50 slices, 192×256 pixels, 1×1 mm resolution, 2 mm slice thickness) with whole-brain coverage can be obtained in roughly 11 minutes of measurement time. Three exemplary slices from a healthy control are displayed in Fig. 5.1. Average brain water content in healthy subjects roughly amounts to 70 % in white matter and 80 % in grey matter [97, 98].

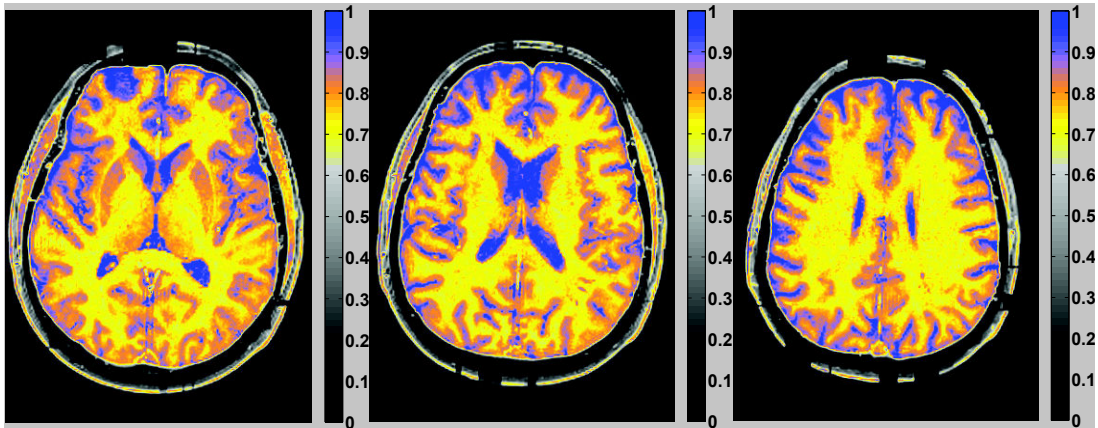


Figure 5.1: Exemplary quantitative brain water content slices from a healthy control. Images are scaled from 0 (0% water content) to 1.0 (100% water content). The lateral ventricles were used as an internal 100% water reference.

5.3 Magnetic resonance spectroscopy

Apart from imaging, magnetic resonance can also be utilized to obtain information about the chemical environment of nuclei. In the brain, *magnetic resonance spectroscopy* (MRS) is used to non-invasively probe concentrations of different compounds, e.g. neurotransmitters [99].

5.3.1 Chemical shift

Differentiation of chemical compounds is made possible by electrons. Under the influence of an external magnetic field B_0 , they vary the local magnetic fields at the nuclei through induction of an opposing field according to LENZ's law, thus effectively shielding protons from B_0 . Depending on the configuration of their electronic surrounding, non-equivalent protons experience different effective magnetic fields and hence precess at different Larmor frequencies. As the frequency ν obviously scales with B_0 , it is referenced against a reference frequency ν_0 (defined by protons in certain compounds such as TMS or DSS⁴). The normalized *chemical shift* $\delta = \frac{\nu - \nu_0}{\nu_0}$ is independent of the magnetic field strength and usually provided in units of parts per million (ppm) [100].

⁴Tetramethylsilane and Dimethyl-silapentane-sulfonate. Due to the low electronegativity of silicon, the protons in both compounds are surrounded by high electron density, hence experience strong shielding and precess at comparably low frequencies.

5.3 Magnetic resonance spectroscopy

5.3.2 Localisation and acquisition

Commonly, spectroscopic data is collected with single voxel spectroscopy (SVS), e.g. from a defined cuboid volume. On excitation with a 90° pulse, slice-selective gradients are played out in orthogonal directions, accompanied by an ensemble of RF pulses (180° for point resolved spectroscopy (PRESS) [101] or 90° for stimulated echo acquisition (STEAM) [102]). The water signal—around 10^4 times the magnitude of the metabolites of interest—is usually suppressed beforehand by frequency-selective excitation and dephasing gradients. The resulting signal after an echo time TE stems from the intersection of the three selected slices. It is recorded without any spatial encoding, as the frequency information is needed for correct assignment of chemical compounds. The resulting signal is Fourier transformed to yield a spectrum containing the contributions of each frequency (Fig. 5.2).

5.3.3 Analysis and quantification

In-vivo acquired MR spectra of the human brain suffer from low signal-to-noise ratio as well as from overlapping signals due to limited resolution in frequency. Therefore, special techniques for the analysis of the acquired spectra is essential. Computer-assisted fitting of MR spectra is hence performed to quantify the contribution of resonances or metabolites to the measured signal [103]. Several software implementations exist to decompose the total signal in either the time domain (jMRUI [104], TARQUIN [105]) or the frequency domain (LCModel [106, 107]). Some algorithms use prior knowledge in the form of simulated *basis spectra* of the most abundant brain metabolites. The amplitude of the respective signal in the time domain or the area under the peak in the frequency domain are directly proportional to the amount of protons that emit the signal. Hence, estimates of metabolite concentrations can be obtained, with consideration of the effects of longitudinal and transversal relaxation.

The exact proportionality factor (containing parameters like RF amplifier gain, impedance of the coil system, temperature etc.) between the amplitude or peak area of a given metabolite and the metabolite concentration in tissue (e.g. $\frac{\text{mol}}{\text{kg}}$) is unknown. In order to express measures of concentrations, it is common to use internal reference substances, as they are equally affected by the proportionality scaling [108].

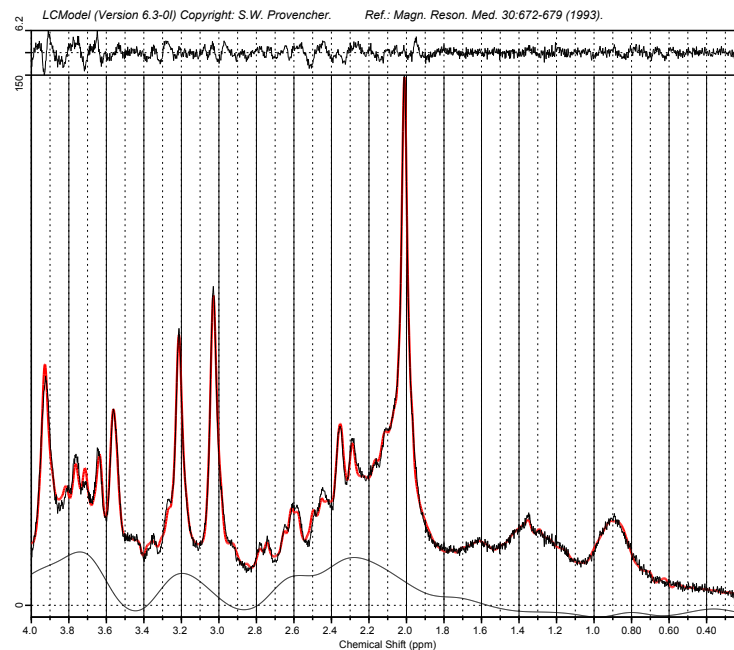


Figure 5.2: Exemplary PRESS spectrum of a healthy volunteer at $TE = 30$ ms. Prominent signals are from n-acetylaspartate (NAA, 2.01 ppm) and creatine (Cr, 3.02 ppm).

- Metabolite concentrations are most commonly expressed as **ratios** with respect to other metabolites, usually **Cr** or **NAA**, as these are of relatively low variance across healthy subjects. However, in certain pathologies, the assumption of constant Cr or NAA may not always be justified [109].
- Metabolite levels can also be normalized to the internal **water** signal from a spectrum without water suppression. With the assumption of standard molar concentration values for the water content of different brain tissue types, estimation of “absolute” metabolite levels (in mM) can be performed [109]. However, special care has to be dedicated to correction of partial volume effects (cerebrospinal fluid does not contain measurable amounts of metabolites) and to accounting for large impact of water relaxation times [110]. In the case of potential tissue water changes, water referencing has to be addressed in more elaborate ways [111, 112].

5.3.4 Edited MR spectroscopy

Analysis of in vivo MRS data acquired at common magnetic field strengths (i.e. 1.5 - 3 T) can be hampered because of spectral overlap of neighbouring resonances. This is especially true for metabolites with *J-coupled resonances* (e.g. glutamate (Glu), glutamine (Gln),

5.3 Magnetic resonance spectroscopy

GABA), as they exhibit complex spectral patterns. J-coupling arises from small local field modulations due to the magnetic moment of neighbouring protons. In an AX_2 spin system, the effective field at the position of spin A depends on the configuration of two equivalent adjacent spins X, resulting in threefold splitting of the resonance with a field-independent separation of J Hz.

This AX_2 triplet changes its shape with increasing echo time. After $TE = \frac{1}{2J}$, its outer wings have a phase shift of 180° . This behaviour can be utilized to unveil J-coupled resonances that are otherwise overlapped by much larger resonances.

A common sequence implementation of this principle is MEGA-PRESS [113]. It combines PRESS localization with selective refocusing of the 3 ppm triplet of GABA. This is accomplished by applying frequency selective 180° pulses to flip the 1.9 ppm spins which are J-coupled to the triplet. After $TE = 68$ ms, the outer peaks of the triplet point upwards again (*spectral editing*, Fig. 5.3). Upon subtraction of a spectrum without editing pulses, a pseudo-doublet representing only GABA is revealed [114, 115].

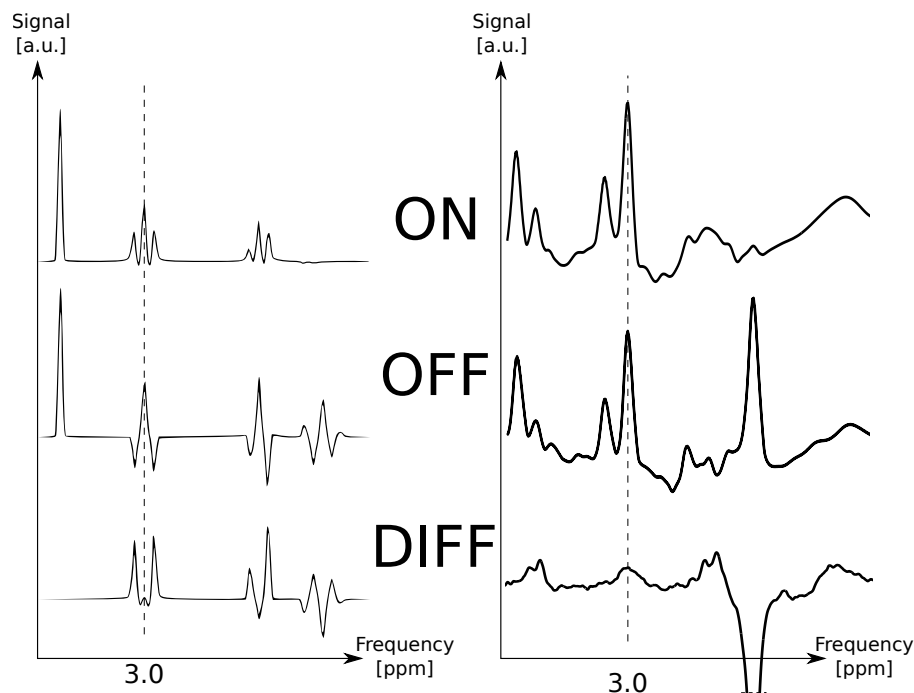


Figure 5.3: Spectral editing with MEGA-PRESS. Left panel: Editing of the 3 ppm GABA triplet. The normal phase evolution of the outer wings of the resonance (**OFF** resonance) is rewound by a frequency selective pulse applied to the coupled resonance at 1.9 ppm (**ON** resonance). Subtraction of the two acquisitions yields the edited pseudo-doublet of GABA. Right panel: In-vivo spectral editing to unveil the small GABA resonance upon subtraction of the large creatine peak at 3 ppm.

Due to in vivo line broadening, this GABA resonance is often fitted with a single Gaussian peak in the course of spectral analysis [115, 116]. A pitfall of MEGA-PRESS is the contamination of the GABA peak with macromolecule resonances at 1.7 ppm which are co-edited due to the spectral width of the editing pulses [115, 117–120]. The exact contribution is not precisely known and may vary across subjects and brain regions [121].

AIMS AND HYPOTHESES

6

The aim of the present dissertation was to investigate the pathogenetic roles of the inhibitory neurotransmitter GABA, the cellular antioxidant glutathione and individual brain water content measures for development and severity of hepatic encephalopathy in liver cirrhosis patients.

Study 1 analysed concentrations of GABA in patients with hepatic encephalopathy of varying grade, compared to healthy controls. Magnetic resonance spectroscopy was used to determine GABA levels in defined regions in the sensorimotor and visual cortex. GABA levels were further investigated with regard to associations with psychometric and clinical parameters. Based on previous observations of oscillatory slowing in HE and links between GABA levels and the peak *gamma* frequency, it was hypothesized that GABA levels are altered in HE, and reflect measures of disease severity.

Study 2 examined MR spectroscopic levels of glutathione and MR brain water imaging data from the subjects in Study 1. Considering reports of increasing glutathione levels in hyperammonemia and oxidative stress, it was hypothesized that glutathione levels are altered in HE patients. Study 2 further investigated whether the extent of the proposed cerebral oedema is related to glutathione or GABA levels.

In the course of these studies, several **methodological considerations** led to potential improvements of the quantification of GABA spectroscopy measures. The calculation of individual concentration references from brain water imaging was proposed to improve GABA quantification in pathology.

The overarching goal of this thesis was to reveal potential associations between HE severity, brain water content, antioxidant levels and neurotransmitter concentrations. Therefore, its main purpose was to help extend the understanding of mechanisms that underlie the chain of events from chronic liver failure to cerebral dysfunction.

STUDY 1: LOW VISUAL CORTEX GABA LEVELS IN HEPATIC ENCEPHALOPATHY: LINKS TO BLOOD AMMONIA, CRITICAL FLICKER FREQUENCY, AND BRAIN OSMOLYTES 7

J-edited magnetic resonance spectroscopy was utilized in **Study 1** to measure GABA levels in visual and sensorimotor areas of healthy controls and HE patients. Further, levels of glutamate, glutamine and myo-inositol were determined. Relations between metabolite measures and HE severity, psychometric data, CFF and venous blood ammonia levels were investigated. Beyond this, interrelations between metabolites were examined. The primary goal of **Study 1** was to reveal potential alterations of GABA concentration in HE, and to scrutinize potential links to relevant aspects of HE pathophysiology. The respective publication can be found in Appendix 1.

Methods

For this study, thirty HE patients and sixteen age-matched healthy controls were enrolled. HE classification into two groups was performed with a combination of *West-Haven* criteria and psychometric testing, complemented by measurement of the critical flicker frequency [46] and determination of the venous blood ammonia levels.

Computer-based psychometric test tasks (Vienna Test System, Dr. Schuhfried GmbH, Mödling, Austria) yielded the following scores: COG1 and COG2 (comparing geometrical shapes to control shapes), LVT1 and LVT2 (line following test), MLS1 (hand steadiness), MLS2 (precision of arm and hand movement), MLS3 (speed of arm and hand movement), MLS4 (finger tapping speed), WRT1 and WRT2 (reaction times). Comparison with age-

matched control cohorts resulted in age-validated percentage ranks indicating the performance in the respective task. Results were considered abnormal if they deviated from the control cohort mean by more than one standard deviation.

Patients were assigned to the *minimal HE* (mHE) group if they did not show clinical signs of HE, but more than 2 abnormal psychometric test results. If they exhibited clear clinical symptoms of manifest HE according to *West-Haven* criteria, they were attributed to the HE of grade 1 group (HE 1). Healthy, age-matched control subjects formed the third group.

All participants subsequently underwent magnetic resonance spectroscopy measurements at rest in a clinical 3T MRI scanner (Siemens MAGNETOM Trio A TIM, Siemens Healthcare AG, Erlangen, Germany). To this end, MEGA-PRESS spectra were recorded from three spectroscopic volumes: one in the visual area (occipital cortex), and one in the left and the right sensorimotor area, respectively (centered on the hand knob, a prominent landmark of the precentral gyrus [122]). Spectroscopic data were analysed with LCModel [107] and Gannet 2.0 [116] to obtain metabolite-to-creatine ratios of GABA, glutamate, glutamine, and myo-inositol. Measures from the left and right sensorimotor MRS volume were averaged within each subject.

To test for HE-related effects, metabolite levels were compared between the three groups (controls, mHE, HE 1). Further, their correlations with each other and with CFF, blood ammonia and psychometric testing were assessed.

Results

The most striking findings of **Study 1** were a reduction of visual GABA/Cr levels in both HE groups and their associations with CFF, blood ammonia and osmolytes ml and Gln. None of these could be confirmed for the sensorimotor GABA/Cr ratios.

HE-related GABA decrease in visual, but not in sensorimotor cortex

Compared with the control group, GABA/Cr ratios from the visual spectroscopic volume were significantly reduced in both the mHE and the HE 1 group. Visual GABA/Cr did, however, not differ between the two HE groups (Appendix 1, Table 2 and Fig. 4a).

Chapter 7. Study 1: GABA spectroscopy in hepatic encephalopathy

In contrast, GABA/Cr measures from the sensorimotor spectroscopic volume did not differ between any of the three groups (Appendix 1, Table 2 and Fig. 4c).

GABA vs. CFF, blood ammonia, psychometrics and metabolite levels

Across all subjects, data from the visual MRS volume revealed a positive correlation between GABA/Cr and the critical flicker frequency, and a negative correlation between GABA/Cr and blood ammonia levels (Appendix 1, Table 2 and Fig. 4b). Further, GABA/Cr correlated with ml/Cr and anticorrelated with Gln/Cr (Appendix 1, Table 3). Lastly, a positive correlation with COG1 scores was observed (Appendix 1, Table 4).

Again, none of these relations were found for the sensorimotor data (Appendix 1, Table 2 and Fig. 4d).

Glutamine, glutamate and myo-inositol

Data demonstrated elevated Gln/Cr and reduced ml/Cr levels for both MRS volumes in both HE groups, whereas Glu/Cr did not exhibit any alterations. In all cases, Gln/Cr correlated positively with ammonia and negatively with the CFF, while ml/Cr showed the adverse behaviour. Glu/Cr was neither linked to ammonia nor to the CFF (Appendix 1, Table 2).

Gln/Cr and ml/Cr were strongly mutually anticorrelated in both MRS volumes. Glu/Cr was only correlated to ml/Cr in the visual area (Appendix 1, Table 3). In both regions, Gln/Cr and ml/Cr were correlated with various psychometric test scores.

Discussion

The goal of **Study 1** was to explore whether levels of the inhibitory neurotransmitter GABA are altered in patients with HE, and whether they are related to parameters reflecting HE severity. Decreased levels of GABA were confirmed for both HE groups, and further found to correlate with the critical flicker frequency, blood ammonia levels, osmolytic actors glutamine and myo-inositol, and psychometric scores. This was, however, only true for GABA levels from the visual, but not from the sensorimotor cortex.

GABA in HE

The observed reduction of visual GABA/Cr was in accordance with a previous report of decreased cortical GABAergic tone in a rodent model of chronic HE [72]. **Study 1** further confirmed and extended findings from a preliminary observation by Behar and colleagues in only four HE patients [123]. The present study included more subjects and was the first experiment to examine different disease grades along with clinical and behavioural parameters.

The positive association of visual GABA/Cr with the CFF suggests that discrimination of a quick succession of visual stimuli is enhanced in individuals with higher visual GABA levels. Subjects with high visual GABA have previously also been shown to perceive time intervals in a more contracted manner [124], and to show superior performance in visual orientation discrimination tasks [125]. The positive association between visual GABA/Cr and COG1 score is further in line with an observation that higher occipital GABA levels predict lower occurrence of cognitive failure in everyday life [126]. Deterioration of CFF and cognitive performance in HE may be mediated by GABA decrease, as suggested by the negative correlation between blood ammonia and GABA/Cr.

In light of global oscillatory slowing in HE [4, 5, 66] (especially regarding occipital *gamma* activity [64]), and given the observed positive correlation of *gamma* peak frequency with occipital GABA levels [16], the observed HE-related GABA/Cr decrease also seems plausible.

It is all the more striking that this prominent GABA/Cr reduction in HE was not demonstrated for the sensorimotor cortex, despite a previous report proposing a link between oscillations and GABA levels in the motor region [15].

The most likely conclusion is that cortical GABA concentrations are not *globally*, but rather *locally* affected in HE. This is suggested by the observation that GABA/Cr measures from the sensorimotor MRS volume were, unlike the visual GABA/Cr levels, not linked to CFF, blood ammonia or the compounds involved in cell volume regulation, glutamine and myo-inositol. Reports from the rodent model of chronic HE have previously underlined the regional specificity of alterations in the GABAergic tone [70, 72], and indicated that motor symptoms of HE might rather originate in increased GABA levels in the ventromedial thalamus [127].

Glutamine and myo-inositol in HE

Data from **Study 1** consistently confirm the well-established pattern of increased glutamine and depleted myo-inositol in HE [53, 61, 128, 129] and their association with disease severity [54, 55]. Their important role in cell volume regulation is mirrored by the substantial anticorrelation between both osmolytes.

Summary

Study 1 extends the understanding of the role of resting GABA concentrations in patients with HE. Decreased visual GABA levels—already evident in mHE—may contribute to the HE-related deterioration of visual and cognitive performance. The absence of HE effects on sensorimotor GABA levels lends further support to previous findings of region specific alterations of the GABAergic system in HE.

STUDY 2: COVERT HEPATIC ENCEPHALOPATHY: ELEVATED TOTAL GLUTATHIONE AND ABSENCE OF BRAIN WATER CONTENT CHANGES



Re-analysis of the magnetic resonance spectroscopy data from **Study 1** was performed in **Study 2** to quantify the levels of the cellular antioxidant glutathione in patients with hepatic encephalopathy. Additionally, data from a quantitative brain water mapping technique were evaluated and related to spectroscopic measures of glutathione, GABA, glutamate, glutamine and myo-inositol. Further, potential associations of all results with clinical parameters of HE severity were tested.

Study 2 aimed to investigate potential relationships between glutathione levels, neurometabolite levels and the extent of local low-grade cerebral oedema, which have previously been suspected to trigger HE symptoms. The respective publication appears in Appendix 2.

Methods

The MR spectroscopy data acquired in the course of **Study 1** were re-analyzed with respect to total glutathione (GSx, i.e. GSH + GSSG). Recruitment of patient and healthy controls, clinical assessment, HE grading, psychometry, MRS acquisition and spectroscopy analysis were therefore as described in section 7.

In addition to spectroscopy, quantitative whole-brain water maps were calculated from imaging data that was acquired during the same MR scanning sessions. Brain water content mapping was carried out according to a previously published and established method [96–98] (for details, please see section 5.2.3).

The resulting maps were evaluated in distinct ways to yield several individual water content measures:

- Global tissue class specific analysis: Calculation of the average individual water content across all grey and white matter voxels
- Spectroscopic volume specific analysis: Calculation of the average individual water content across all grey and white matter voxels within the three MR spectroscopic volumes (left sensorimotor, right sensorimotor, visual)
- Individual region of interest (ROI) analysis: Calculation of the average individual water content from 10 regions of interest interactively drawn to cover distinct brain regions

As in **Study 1**, all parameters and measures were tested for group effects between controls, mHE and HE 1. To unveil potential links between metabolite levels, brain water content measures, CFF and blood ammonia, correlation analyses were performed.

Results

Study 2 revealed increased levels of total glutathione in HE patients in the visual and the sensorimotor spectroscopic volume. They were also positively correlated with individual blood ammonia measures and some brain water content measures. Brain water content did neither exhibit group effects nor correlations with CFF, ammonia or measures of GABA, glutamine, glutamate, and myo-inositol.

MR spectroscopy of glutathione

Compared to healthy controls, HE patients had higher levels of GSx/Cr. This was true for the visual (significant only for mHE, but not for HE 1) and for the sensorimotor spectroscopic volume (significant for both HE groups).

Correlation analysis further revealed positive associations of GSx/Cr ratios (visual and sensorimotor) with blood ammonia levels. Only the sensorimotor GSx/Cr levels correlated negatively with CFF (Appendix 2, Table 2).

Chapter 8. Study 2: Covert hepatic encephalopathy: Elevated total glutathione and absence of brain water content changes

GSx/Cr further showed a negative correlation with GABA/Cr in the visual, but not in the sensorimotor MRS volume. In both regions, GSx/Cr correlated positively with Gln/Cr and negatively with ml/Cr (Appendix 2, Table 3).

Brain water content

The average brain water content in healthy controls was determined to be $71.6 \pm 1.5\%$ for white matter and $81.9 \pm 1.8\%$ for grey matter. These results were well within literature values that were previously obtained with similar MR watermapping methods [60, 97, 98], indicating the successful implementation of the acquisition and evaluation routines.

Analysis did not yield significant effects on group level for any brain water measure. In addition, brain water data did not show any correlation with blood ammonia or the CFF (Appendix 2, Table 4).

Brain water content from the thalamus, *nucleus caudatus* and visual cortex showed positive correlations with the GSx/Cr ratio from the visual spectroscopic volume. No correlations of brain water measures with any other metabolite measure (GABA, Gln, Glu, ml) were observed.

Discussion

In **Study 2**, MR spectroscopic levels of the antioxidant glutathione (GSx, reduced glutathione GSH + oxidized glutathione GSSG) in distinct brain regions were scrutinized in patients with HE. Additionally, MR brain water measures were analysed. The aim of the study was to investigate whether glutathione is altered in HE, and whether it is linked to the extent of low-grade cerebral oedema.

Elevated GSx levels were found in both HE groups and were closely associated with increased blood ammonia concentrations. Moreover, GSx levels were coupled to Gln and ml, and related to GABA levels (only in the visual cortex). Visual GSx further showed positive correlations with brain water content in thalamus, *nucleus caudatus* and visual cortex. Apart from these relationships, brain water measures were not linked to any other parameter under investigation.

Glutathione in covert HE

The observed elevation of total glutathione in HE is in line with reports of increased GSH and GSSG under ammonia challenge in cultured astrocytes [79, 130] and rodent prefrontal cortex [80, 83]. GSH elevation has been attributed to increased activity of the GSH synthesizing enzyme gamma-glutamylcystein synthetase (i.e. an adaptive response to increased oxidative stress), while the markedly higher GSSG elevation is presumably caused by consumption of ROS and simultaneous impairment of the GSSG-to-GSH recycling enzyme glutathione reductase [81]. The correlation between blood ammonia levels and GSx further supports observations of an ammonium-dose dependent increase of glutathione [80]. Administration of N-acetyl-L-cysteine, a precursor of GSH, has recently been shown to ameliorate cognitive deficits and to augment the antioxidant capacity in a rodent model of chronic HE [131]. **Study 2** therefore provides evidence that glutathione levels play a considerable role in the adaptation to excess ammonia and subsequent oxidative stress in HE patients.

An increase of GSx/Cr was not consistently found in the present analysis, i.e. it was not significant in the HE 1 group in the visual spectroscopic volume. This may suggest a similar region specificity of the glutathione defence system in HE as previously observed for neurotransmitter systems, which are differentially or even conversely affected across distinct brain areas [70, 72, 132].

The correlations between visual GSx/Cr and brain water content in the thalamus, *nucleus caudatus* and visual cortex further support the concept that brain shows spatially varying susceptibility to HE. Previous studies have reported HE-related abnormalities of oscillatory coupling [62], functional connectivity [133, 134] and tissue volume [135, 136] in the thalamus. Structural alterations of the *nucleus caudatus* showed associations with blood ammonia in an MR study of brain tissue T_1 relaxation times in HE [59]. Data of **Study 2** did, however, not reveal group effects of brain water content, or links to CFF in any of the three brain areas, and visual cortex water content was not linked to visual GABA levels, which in turn directly covaried with the CFF. Brain water content may therefore rather not directly affect visual or cognitive performance, at least in the covert stages of HE. This conclusion has also been suggested by recent experiments in the rodent model of chronic HE, which further points towards altered neurotransmission as a key player in HE [137].

Role of brain water content in covert HE

Study 2 does not provide significant evidence for a global increase of brain water content in patients with covert HE. This opposes findings of a prominent previous work by Shah and colleagues [60]. In their study, a global increase of white matter water content with HE severity was detected with a similar magnetic resonance method at 1.5 T. Moreover, Shah and colleagues showed that water content in several brain regions (most notably in the *globus pallidus*) is related to the CFF, hence proposing direct pathogenetic ramifications of low-grade cerebral oedema.

Data from **Study 2** succeeds in reproducing the average white matter water content for the mHE patient group that was reported by Shah et al. ($71.6 \pm 1.5\%$). However, it reports slightly higher values for the control group ($71.6 \pm 1.5\%$ compared to $70.9 \pm 1.0\%$), and slightly lower values for the HE 1 group ($72.1 \pm 1.3\%$ compared to $72.9 \pm 1.2\%$ in the “overt HE” group investigated by Shah et al.).

The present study included a control group with a mean age of 60.1 ± 8.7 y, i.e. controls were substantially older than the control cohort studied by Shah and colleagues (mean age 52.6 ± 9.4 y). As CFF is known to be slightly age-dependent [46], this may account for the difference of mean CFF between the control groups (**Study 2**: 41.6 ± 4.0 Hz, Shah et al.: 43.2 ± 1.9 Hz). 6 out of 16 controls in **Study 2** had a CFF below the rule-of-thumb cutoff of 39 Hz for HE delineation [46]. However, the average white matter water content in **Study 2** remained constant even after exclusion of controls with a CFF below 39 Hz, suggesting that potential control population sampling errors did not influence the average WM brain water content.

Regarding the deviation in the highest HE grade group, it is remarkable that the study by Shah and co-workers did not feature a dedicated HE 1 group. Instead, three subjects with HE grade 2 were pooled with 10 HE 1 patients into a combined “overt HE” group. Most of the significant group differences in WM water content reported by Shah et al. were observed with respect to this overt HE group. Considering that the observed HE-induced changes in water content are rather small compared to their inter-individual variance (see also Appendix 2, Table 4), it is possible that the three HE 2 patients were mainly responsible for the observed effects. Furthermore, data from **Study 2** revealed a positive correlation of age with WM water content across all participants in this work, although such a relation has not been found in a large healthy control group by Neeb et al. [98]. Strikingly, Shah et

al. did not include age as a covariate in their correlation analysis. This might imply that the putative link between WM water content and CFF is of rather indirect nature, and may instead be mediated through the underlying correlation between age and CFF.

It is further surprising that there was no association between brain water content and levels of glutamine or myo-inositol, although they are vitally involved in the ammonia metabolism process and subsequent water homeostasis. This may imply that the cellular volume and water regulation system may remain at least partly functional in covert HE, and may hence still be able to prevent the precipitation of a clearly observable cerebral oedema. The latter may instead be pronounced more severely in the course of higher-grade HE (<grade 2, overt HE according to the 2014 ISHEN guidelines [29]), and may well be responsible for the emergence of more critical symptoms in these stages. Recent rodent studies even suggest that the occurrence of lactate may be more important to the formation of brain oedema than glutamine in the first place [138, 139].

Together with these considerations, the results of **Study 2** suggest that alterations in MR measures of brain water content may have rather subtle relevance for the emergence and extent of chronic HE symptoms in the cognitive and visual domain in covert HE, i.e. HE grade <2. Similar observations have previously been made in chronic HE rats that developed motor and cognitive deficits, even without occurrence of brain oedema [137]. It should, however, be noted that MR brain water measurement is only capable of measuring free tissue water. Hence, if only the ratio between intra- and extracellular water is altered by low-grade cerebral oedema, but not the total amount of tissue water, the applied method might not be susceptible to these changes. Further studies need to elucidate to what extent oedema may form without a change of total tissue water, particularly in covert HE, but also in its overt forms.

Summary

In conclusion, **Study 2** conveys two central findings that may potentially improve the understanding of pathogenetic mechanisms in covert HE. Firstly, it is demonstrated that elevated levels of the antioxidant glutathione are found in covert HE patients, and are further associated with the extent of hyperammonemia. This suggests that glutathione is pivotally involved in the adaptation to oxidative stress in HE. Secondly, the MR water

Chapter 8. Study 2: Covert hepatic encephalopathy: Elevated total glutathione and absence of brain water content changes

imaging results of **Study 2** indicate a rather marginal impact of the putative brain water changes on disease severity in the covert stages of HE. However, some correlations with visual glutathione levels suggest that oxidative stress and cerebral oedema may be associated in a regional-dependent manner.

METHODOLOGICAL CONSIDERATIONS: WATER-SCALED QUANTIFICATION OF GABA 9

In addition to the aforementioned studies, several aspects of the underlying methods have been investigated. Specifically, water concentration referencing of MR spectroscopic GABA levels on the grounds of quantitative water maps has been proposed. The concept is briefly outlined in the following sections.

As mentioned in section 5.3.3, evaluation of MR spectroscopy experiments can yield absolute metabolite concentrations. To this end, the metabolite signal needs to be normalized by the water signal from a spectrum without preceding water suppression. Metabolite quantification is then realized based on the fractional tissue composition (grey matter, white matter and cerebrospinal fluid) of the spectroscopic volume. Standard values for the respective molar water densities within each tissue class are used to provide a concentration reference for the spectroscopic water signal in absolute units. Finally, accounting for T_1 and T_2 relaxation of both the metabolite and the water signal is needed to obtain an absolute measure of the metabolite, usually given in millimol (mM).

Study 3 proposed an extension of this quantification method for J-edited MR spectroscopy of GABA in the presence of altered brain tissue water content, as can be the case in HE. Under such circumstances, the use of standard water density values for healthy tissue may not be justified. To overcome this, **Study 3** employed a combination of data from **Study 1** and **Study 2**: The quantitative brain water maps served to provide individual water concentration measures for subsequent referencing of GABA spectra, similar to a previous suggestion for chemical shift imaging [112]. The individual T_1 maps from the water imaging routine were further used to perform individual correction for longitudinal relaxation. Resulting GABA estimates were slightly higher than concentrations calculated with the standard tissue class based approach described above. Further, they confirmed the

decrease of GABA levels in HE patients that had been reported for GABA-to-creatine-ratios in **Study 1**. The respective publication appears as Appendix 3.

Methods

The visual volume MEGA-PRESS data from **Study 1** were analysed with Gannet 2.0 [116] to yield the ratio of GABA and water peak areas. Using a custom-made MATLAB routine (The Mathworks Inc., Natick/MA, USA), each spectroscopic volume was localized in the quantitative brain water and T_1 maps, and in a high-resolution anatomical image of the brain.

Segmentation of the anatomical image into the three tissue compartments (grey matter, white matter, CSF) was then performed with the SPMv8 toolbox [140]. This step allowed determination of the fraction that each tissue class contributed to the spectroscopic volume. Using literature values for water content and relaxation behaviour of each tissue class as well as GABA relaxation [110, 141–143], these fractions were used to calculate GABA estimates according to the standard tissue-segmentation based method outlined above.

In the proposed watermap-based approach, relaxation of GABA and T_2 of water were accounted for as in the segmentation-based routine. However, the individual water concentration and T_1 values from each voxel within the spectroscopic volume were extracted from the water and T_1 maps. These values were subsequently used to allow for individual assessment of the water reference needed for GABA quantification.

Results

The proposed watermap-based quantification yielded GABA concentrations that were slightly higher than the estimates given by the classic approach solely based on tissue segmentation. For both quantification routines, GABA levels in mHE and HE 1 patients were significantly lower than in healthy controls, and showed correlations with the CFF (Appendix 3, Table 1).

Discussion

The difference between the segmentation-based and the watermap-based GABA estimates can likely be attributed to the fact that the actual measures of brain water content in the spectroscopic volume were higher than the standard literature assumptions (Appendix 3, Table 2). Additionally, the actual T_1 of white matter in the spectroscopic volume was higher than the literature value [141], potentially due to an age effect [144].

As no group differences in brain water content were observed for the particular HE data (see **Study 2** for a detailed discussion), an impact of the choice of methods on the observation of effects between HE patients and healthy controls was not evident. However, more severe brain water alterations may become a critical issue in water-referenced GABA estimation, especially if comparison with the healthy brain is needed. In these cases, the proposed watermap-based quantification approach may be a helpful tool to account for brain water alterations.

Summary

Study 3 demonstrated that GABA estimation combined with individual water concentration referencing is feasible. The proposed quantification scheme may be useful for investigation of pathologies where brain water content is markedly altered (e.g. higher HE grades), as assumption of standard literature values for the healthy brain would bias GABA estimates in these cases.

CONCLUSIONS AND OUTLOOK 10

The studies presented in this work may contribute to the understanding of several important pathogenetic mechanisms of hepatic encephalopathy, i.e. hyperammonemia, oxidative stress, and disturbed neurotransmission.

Firstly, this work elucidates the role of the inhibitory neurotransmitter GABA. Its contribution to emergence and extent of HE symptoms has been controversially debated for a long time. The results of the present work reveal a reduction of GABA levels in patients with minimal HE and HE 1, albeit only for the visual cortex, where they were further closely linked to the extent of HE severity. Considering that reduction of visual GABA is clearly evident in minimal HE, it might be worthwhile to evaluate the potential of GABA spectroscopy as a complementary parameter for clinical HE diagnosis. Definition of a cut-off GABA/Cr value, similar to the suggested CFF cut-off of 39 Hz [46] or 38 Hz [48], may aid the clinically relevant identification of patients with minimal HE. The empirical value of 0.09 for visual GABA/Cr (see Appendix 1, Fig. 4a) might be a first approximation for a cut-off, however requiring validation in larger cohorts of healthy controls and patients.

Together with previous findings from animal studies, the absence of HE-related GABA level alterations in the sensorimotor cortex strengthens the notion of regional-dependent alterations to the neurotransmitter systems [70]. Experiments with rodent models of chronic liver cirrhosis demonstrated that motor symptoms of HE are rather associated with modulations of thalamic and cerebellar GABA levels [71, 72, 145]. Investigating human HE patients in a similar way as in **Study 1**, i.e. with in vivo MR spectroscopy in thalamus and cerebellum, may be worthwhile to unveil potential interdependencies and HE-induced alterations of neurotransmitters in these regions.

The observed reduction of visual GABA levels may contribute to the symptoms of HE via modulation of oscillatory activity. While it has to be noted that a recent study by Cousijn and colleagues [146] cast doubt on the previously observed direct relation between

individual GABA concentrations and *gamma* frequencies [15, 16] in healthy controls, the considerable GABA reduction in HE patients ($\sim 20\%$) may exert a crucial influence.

In the course of the presented studies, each subject (controls and patients) also underwent measurement of their oscillatory activity with magnetoencephalography (MEG). In a first separate analysis of the control group data, an interesting novel association between GABA levels from the left sensorimotor cortex and the peak frequency of *beta* activity was revealed (please see Appendix 4 for the respective publication). In line with earlier findings, this suggests that GABAergic inhibition is involved in the genesis of *beta* rhythms in the sensorimotor system [147–150]. *Beta* and *gamma* oscillation data from both healthy controls and patients are currently being evaluated, and are likely to provide further insight into the relationship between individual GABA levels, oscillatory behaviour and HE symptom characteristics.

Despite its merits, MR spectroscopy of GABA has certain drawbacks. It can only determine the bulk tissue content of GABA molecules, regardless of their exact location (extracellular or intracellular). It can not distinguish whether the measured GABA contributes to neural activity at the time of the measurement, and it is particularly not possible to determine which receptor type (short term GABA-A or long term GABA-B) is activated. Hence, MRS can not determine current inhibitory activity *per se*. Certain protocols of transcranial magnetic stimulation (TMS) can be used as a more direct means to probe excitatory and inhibitory neurotransmission on different time scales [151]. The application of such TMS protocols to distinct brain regions of HE patients may provide valuable insight into alterations of actual GABAergic and glutamatergic activity. This may complement measures of neurotransmitter levels obtained with MRS, and observation of oscillatory activity with MEG.

The second meaningful contribution of the present work is the detection of elevated levels of the principal antioxidant glutathione in HE patients. Their direct correlations with blood ammonia levels indicate that glutathione actively participates in the reaction to hyperammonemic conditions and the subsequent oxidative stress load.

The exact pathogenetic consequences of the proposed low-grade cerebral oedema for HE severity still require investigation. While previous studies clearly indicated a functional relevance of elevated brain water content in HE, results of **Study 2** point towards a less

prominent role. However, the present work only included patients with covert HE, i.e. the less severe early disease manifestation. The alterations of glutamine and myo-inositol presumably responsible for oedema formation are, however, clearly present in covert HE as well. As MR brain water imaging may not be sensitive to changes of the ratio between intra- and extracellular water in the absence of total water change, subtle oedema formation at these stages can not be ruled out based on our data. Future experiments will need to address these issues to further disentangle the complex interaction of the pathogenetic factors across the different stages of HE.

Absence of associations between brain water content and GABA or glutamate measures further indicate that the extent of low-grade cerebral oedema does not directly affect neurotransmitter systems. Coupling of GABA and GSx may instead point towards a sensitivity of neurotransmission to oxidative stress, although potential mechanisms remain largely vague [76]. Further research on a cellular level regarding the interaction between oxidative stress, antioxidant response and neurotransmitter systems is required to enhance the understanding of the underlying molecular interplay ultimately leading to the pathological ramifications of HE.

BIBLIOGRAPHY

1. Bear MF, Connors BW & Paradiso MA. *Neurowissenschaften: Ein grundlegendes Lehrbuch für Biologie, Medizin und Psychologie* (Spektrum Akademischer Verlag, 2008).
2. Kandel E, Schwartz J & Jessell T. *Neurowissenschaften: Eine Einführung* (Spektrum Akademischer Verlag, 1995).
3. Häussinger D & Sies H. Hepatic encephalopathy: Clinical aspects and pathogenetic concept. *Archives of Biochemistry and Biophysics* 536, 97–100 (2013).
4. Timmermann L, Butz M, Gross J, Ploner M, Südmeyer M, Kircheis G, Häussinger D & Schnitzler A. Impaired cerebral oscillatory processing in hepatic encephalopathy. *Clinical Neurophysiology* 119, 265–272 (2008).
5. Butz M, May ES, Häussinger D & Schnitzler A. The slowed brain: Cortical oscillatory activity in hepatic encephalopathy. *Archives of Biochemistry and Biophysics* 536, 197–203 (2013).
6. Häussinger D & Schliess F. Pathogenetic mechanisms of hepatic encephalopathy. *Gut* 57, 1156–1165 (2008).
7. Dudel J, Menzel R & Schmidt RF. *Neurowissenschaft: vom Molekül zur Kognition* (Springer, 2001).
8. Schnitzler A & Gross J. Normal and pathological oscillatory communication in the brain. *Nature Reviews Neuroscience* 6, 285–296 (2005).
9. Ward LM. Synchronous neural oscillations and cognitive processes. *Trends in Cognitive Sciences* 7, 553–559 (2003).
10. Buzsáki G & Draguhn A. Neuronal Oscillations in Cortical Networks. *Science* 304, 1926–1929 (2004).

Bibliography

11. Buzsáki G & Wang XJ. Mechanisms of Gamma Oscillations. *Annual Review of Neuroscience* 35, 203–225 (2012).
12. Gross J, Kujala J, Hämäläinen M, Timmermann L, Schnitzler A & Salmelin R. Dynamic imaging of coherent sources: Studying neural interactions in the human brain. *Proceedings of the National Academy of Sciences of the United States of America* 98, 694–699 (2001).
13. Wang XJ & Buzsáki G. Gamma Oscillation by Synaptic Inhibition in a Hippocampal Interneuronal Network Model. *The Journal of Neuroscience* 16, 6402–6413 (1996).
14. Brunel N & Wang XJ. What Determines the Frequency of Fast Network Oscillations With Irregular Neural Discharges? I. Synaptic Dynamics and Excitation-Inhibition Balance. *Journal of Neurophysiology* 90, 415–430 (2003).
15. Gaetz W, Edgar JC, Wang DJ & Roberts TPL. Relating MEG measured motor cortical oscillations to resting γ -Aminobutyric acid (GABA) concentration. *NeuroImage* 55, 616–621 (2011).
16. Muthukumaraswamy SD, Edden RAE, Jones DK, Swettenham JB & Singh KD. Resting GABA concentration predicts peak gamma frequency and fMRI amplitude in response to visual stimulation in humans. *Proceedings of the National Academy of Sciences of the United States of America* 106, 8356–8361 (2009).
17. Dringen R. Metabolism and functions of glutathione in brain. *Progress in Neurobiology* 62, 649–671 (2000).
18. Dringen R, Gutterer JM & Hirrlinger J. Glutathione metabolism in brain. *European Journal of Biochemistry* 267, 4912–4916 (2000).
19. Forman HJ, Zhang H & Rinna A. Glutathione: Overview of its protective roles, measurement, and biosynthesis. *Molecular aspects of medicine* 30, 1–12 (2009).
20. Meister A. Glutathione metabolism and its selective modification. *Journal of Biological Chemistry* 263, 17205–17208 (1988).
21. Drukarch B, Schepens E, Jongenelen CAM, Stoof JC & Langeveld CH. Astrocyte-mediated enhancement of neuronal survival is abolished by glutathione deficiency. *Brain Research* 770, 123–130 (1997).

22. Drukarch B, Schepens E, Stoof JC, Langeveld CH & Van Muiswinkel FL. Astrocyte-Enhanced Neuronal Survival is Mediated by Scavenging of Extracellular Reactive Oxygen Species. *Free Radical Biology and Medicine* 25, 217–220 (1998).
23. Schulz JB, Lindenau J, Seyfried J & Dichgans J. Glutathione, oxidative stress and neurodegeneration. *European Journal of Biochemistry* 267, 4904–4911 (2000).
24. Häussinger D & Blei AT. in *The Oxford Textbook of Hepatology* (eds Rodes J, Benhamou JP, Blei AT, Reichen J & Rizzetto M) 728–760 (Blackwell, Oxford, 2007).
25. Ferenci P, Lockwood A, Mullen K, Tarter R, Weissenborn K & Blei AT. Hepatic encephalopathy—Definition, nomenclature, diagnosis, and quantification: Final report of the Working Party at the 11th World Congresses of Gastroenterology, Vienna, 1998. *Hepatology* 35, 716–721 (2002).
26. Butz M, Timmermann L, Braun M, Groiss SJ, Wojtecki L, Ostrowski S, Krause H, Pollok B, Gross J, Südmeyer M, Kircheis G, Häussinger D & Schnitzler A. Motor impairment in liver cirrhosis without and with minimal hepatic encephalopathy. *Acta Neurologica Scandinavica* 122, 27–35 (2010).
27. Poordad FF. Review article: the burden of hepatic encephalopathy. *Alimentary Pharmacology & Therapeutics* 25, 3–9 (2007).
28. Bajaj JS, Cordoba J, Mullen KD, Amodio P, Shawcross DL, Butterworth RF & Morgan MY. Review article: the design of clinical trials in hepatic encephalopathy – an International Society for Hepatic Encephalopathy and Nitrogen Metabolism (ISHEN) consensus statement. *Alimentary Pharmacology & Therapeutics* 33, 739–747 (2011).
29. Vilstrup H, Amodio P, Bajaj J, Cordoba J, Ferenci P, Mullen KD, Weissenborn K & Wong P. Hepatic encephalopathy in chronic liver disease: 2014 Practice Guideline by the American Association for the Study Of Liver Diseases and the European Association for the Study of the Liver. *Hepatology* 60, 715–735 (2014).
30. Felipo V. Hepatic encephalopathy: effects of liver failure on brain function. *Nature Reviews Neuroscience* 14, 851–858 (2013).

Bibliography

31. Rikkers L, Jenko P, Rudman D & Freides D. Subclinical hepatic encephalopathy: detection, prevalence, and relationship to nitrogen metabolism. *Gastroenterology* 75, 462–469 (1978).
32. Schomerus H & Hamster W. Neuropsychological Aspects of Portal-Systemic Encephalopathy. *Metabolic Brain Disease* 13, 361–377 (1998).
33. Weissenborn K, Ennen JC, Schomerus H, Rückert N & Hecker H. Neuropsychological characterization of hepatic encephalopathy. *Journal of Hepatology* 34, 768–773 (2001).
34. Amodio P, Campagna F, Olianas S, Iannizzi P, Mapelli D, Penzo M, Angeli P & Gatta A. Detection of minimal hepatic encephalopathy: Normalization and optimization of the Psychometric Hepatic Encephalopathy Score. A neuropsychological and quantified EEG study. *Journal of Hepatology* 49, 346–353 (2008).
35. Amodio P, Del Piccolo F, Marchetti P, Angeli P, Iemmolo R, Caregaro L, Merkel C, Gerunda G & Gatta A. Clinical features and survival of cirrhotic patients with subclinical cognitive alterations detected by the number connection test and computerized psychometric tests. *Hepatology* 29, 1662–1667 (1999).
36. Lauridsen MM, Thiele M, Kimer N & Vilstrup H. The continuous reaction times method for diagnosing, grading, and monitoring minimal/covert hepatic encephalopathy. *Metabolic Brain Disease* 28, 231–234 (2013).
37. Bajaj JS, Thacker LR, Heuman DM, Fuchs M, Sterling RK, Sanyal AJ, Puri P, Siddiqui MS, Stravitz RT, Bouneva I, Luketic V, Noble N, White MB, Monteith P, Unser A & Wade JB. The Stroop smartphone application is a short and valid method to screen for minimal hepatic encephalopathy. *Hepatology* 58, 1122–1132 (2013).
38. Kircheis G, Fleig WE, Görtelmeyer R, Grafe S & Häussinger D. Assessment of low-grade hepatic encephalopathy: A critical analysis. *Journal of Hepatology* 47, 642–650 (2007).
39. Agrawal S, Umapathy S & Dhiman RK. Minimal Hepatic Encephalopathy Impairs Quality of Life. *Journal of Clinical and Experimental Hepatology* 5, Supplement 1, S42–S48 (2015).

40. Romero-Gomez M, Boza F, Garcia-Valdecasas MS, Garciaa E & Aguilar-Reina J. Subclinical hepatic encephalopathy predicts the development of overt hepatic encephalopathy. *Am J Gastroenterol* 96, 2718–2723 (2001).
41. Stewart CA, Malinchoc M, Kim WR & Kamath PS. Hepatic encephalopathy as a predictor of survival in patients with end-stage liver disease. *Liver Transplantation* 13, 1366–1371 (2007).
42. Prasad S, Dhiman RK, Duseja A, Chawla YK, Sharma A & Agarwal R. Lactulose improves cognitive functions and health-related quality of life in patients with cirrhosis who have minimal hepatic encephalopathy. *Hepatology* 45, 549–559 (2007).
43. Bajaj JS, Wade JB, Gibson DP, Heuman DM, Thacker LR, Sterling RK, Stravitz RT, Luketic V, Fuchs M, White MB, Bell DE, Gilles H, Morton K, Noble N, Puri P & Sanyal AJ. The Multi-Dimensional Burden of Cirrhosis and Hepatic Encephalopathy on Patients and Caregivers. *The American Journal of Gastroenterology* 106, 1646–1653 (2011).
44. Kircheis G, Knoche A, Hilger N, Manhart F, Schnitzler A, Schulze H & Häussinger D. Hepatic Encephalopathy and Fitness to Drive. *Gastroenterology* 137, 1706–1715.e9 (2009).
45. Kircheis G, Hilger N & Häussinger D. Value of Critical Flicker Frequency and Psychometric Hepatic Encephalopathy Score in Diagnosis of Low-Grade Hepatic Encephalopathy. *Gastroenterology* 146, 961–969 (2014).
46. Kircheis G, Wettstein M, Timmermann L, Schnitzler A & Häussinger D. Critical flicker frequency for quantification of low-grade hepatic encephalopathy. *Hepatology* 35, 357–366 (2002).
47. Sharma P, Sharma BC, Puri V & Sarin SK. Critical flicker frequency: Diagnostic tool for minimal hepatic encephalopathy. *Journal of Hepatology* 47, 67–73 (2007).
48. Romero-Gómez M, Córdoba J, Jover R, del Olmo JA, Ramírez M, Rey R, de Madaria E, Montoliu C, Nuñez D, Flavia M, Compañy L, Rodrigo JM & Felipe V. Value of the critical flicker frequency in patients with minimal hepatic encephalopathy. *Hepatology* 45, 879–885 (2007).

Bibliography

49. Torlot FJ, McPhail MJW & Taylor-Robinson SD. Meta-analysis: the diagnostic accuracy of critical flicker frequency in minimal hepatic encephalopathy. *Alimentary Pharmacology & Therapeutics* 37, 527–536 (2013).
50. Shawcross D & Jalan R. The pathophysiologic basis of hepatic encephalopathy: central role for ammonia and inflammation. *Cellular and Molecular Life Sciences CMLS* 62, 2295–2304 (2005).
51. Butterworth RF. Hepatic encephalopathy: A central neuroinflammatory disorder? *Hepatology* 53, 1372–1376 (2011).
52. Görg B, Schliess F & Häussinger D. Osmotic and oxidative/nitrosative stress in ammonia toxicity and hepatic encephalopathy. *Archives of Biochemistry and Biophysics* 536, 158–163 (2013).
53. Häussinger D, Laubenberger J, Vom Dahl S, Ernst T, Bayer S, Langer M, Gerok W & Hennig J. Proton magnetic resonance spectroscopy studies on human brain Myo-inositol in hypo-osmolality and hepatic encephalopathy. *Gastroenterology* 107, 1475–1480 (1994).
54. Shawcross DL, Balata S, Damink SWMO, Hayes PC, Wardlaw J, Marshall I, Deutz NEP, Williams R & Jalan R. Low myo-inositol and high glutamine levels in brain are associated with neuropsychological deterioration after induced hyperammonemia. *American Journal of Physiology - Gastrointestinal and Liver Physiology* 287, G503–G509 (2004).
55. Miese F, Kircheis G, Wittsack HJ, Wenserski F, Hemker J, Mödder U, Häussinger D & Cohnen M. 1H-MR Spectroscopy, Magnetization Transfer, and Diffusion-Weighted Imaging in Alcoholic and Nonalcoholic Patients with Cirrhosis with Hepatic Encephalopathy. *American Journal of Neuroradiology* 27, 1019–1026 (2006).
56. Binesh N, Huda A, Thomas MA, Wyckoff N, Bugbee M, Han S, Rasgon N, Davanzo P, Sayre J, Guze B, Martin P & Fawzy F. Hepatic encephalopathy: a neurochemical, neuroanatomical, and neuropsychological study. *Journal of Applied Clinical Medical Physics / American College of Medical Physics* 7, 86–96 (2006).
57. Häussinger D, Kircheis G, Fischer R, Schliess F & Dahl Sv. Hepatic encephalopathy in chronic liver disease: a clinical manifestation of astrocyte swelling and low-grade cerebral edema? *Journal of Hepatology* 32, 1035–1038 (2000).

58. Häussinger D. Low grade cerebral edema and the pathogenesis of hepatic encephalopathy in cirrhosis. *Hepatology* 43, 1187–1190 (2006).
59. Shah NJ, Neeb H, Zaitsev M, Steinhoff S, Kircheis G, Amunts K, Häussinger D & Zilles K. Quantitative T1 mapping of hepatic encephalopathy using magnetic resonance imaging. *Hepatology* 38, 1219–1226 (2003).
60. Shah NJ, Neeb H, Kircheis G, Engels P, Häussinger D & Zilles K. Quantitative cerebral water content mapping in hepatic encephalopathy. *NeuroImage* 41, 706–717 (2008).
61. Alonso J, Córdoba J & Rovira A. Brain Magnetic Resonance in Hepatic Encephalopathy. *Seminars in Ultrasound, CT and MRI* 35, 136–152 (2014).
62. Timmermann L, Gross J, Butz M, Kircheis G, Häussinger D & Schnitzler A. Mini-asterixis in hepatic encephalopathy induced by pathologic thalamo-motor-cortical coupling. *Neurology* 61, 689–692 (2003).
63. Timmermann L, Gross J, Butz M, Kircheis G, Häussinger D & Schnitzler A. Pathological oscillatory coupling within the human motor system in different tremor syndromes as revealed by magnetoencephalography. *Neurology & clinical neurophysiology: NCN* 2004, 26 (2004).
64. Kahlbrock N, Butz M, May ES, Brenner M, Kircheis G, Häussinger D & Schnitzler A. Lowered frequency and impaired modulation of gamma band oscillations in a bimodal attention task are associated with reduced critical flicker frequency. *NeuroImage* 61, 216–227 (2012).
65. May ES, Butz M, Kahlbrock N, Brenner M, Hoogenboom N, Kircheis G, Häussinger D & Schnitzler A. Hepatic encephalopathy is associated with slowed and delayed stimulus-associated somatosensory alpha activity. *Clinical Neurophysiology* 125, 2427–2435 (2014).
66. Timmermann L, Butz M, Gross J, Kircheis G, Häussinger D & Schnitzler A. Neural Synchronization in Hepatic Encephalopathy. *Metabolic Brain Disease* 20, 337–346 (2005).
67. Schafer DF & Jones EA. Hepatic encephalopathy and the gamma-aminobutyric-acid neurotransmitter system. *The Lancet* 319, 18–20 (1982).

Bibliography

68. Palomero-Gallagher N & Zilles K. Neurotransmitter receptor alterations in hepatic encephalopathy: A review. *Archives of Biochemistry and Biophysics* 536, 109–121 (2013).
69. Sergeeva OA. GABAergic transmission in hepatic encephalopathy. *Archives of Biochemistry and Biophysics* 536, 122–130 (2013).
70. Llansola M, Montoliu C, Agusti A, Hernandez-Rabaza V, Cabrera-Pastor A, Gomez-Gimenez B, Malaguarnera M, Dadsetan S, Belghiti M, Garcia-Garcia R, Balzano T, Taoro L & Felipo V. Interplay between glutamatergic and GABAergic neurotransmission alterations in cognitive and motor impairment in minimal hepatic encephalopathy. *Neurochemistry International*. doi:10.1016/j.neuint.2014.10.011 (2014).
71. Cauli O, Llansola M, Erceg S & Felipo V. Hypolocomotion in rats with chronic liver failure is due to increased glutamate and activation of metabotropic glutamate receptors in substantia nigra. *Journal of Hepatology* 45, 654–661 (2006).
72. Cauli O, Mansouri MT, Agusti A & Felipo V. Hyperammonemia Increases GABAergic Tone in the Cerebellum but Decreases It in the Rat Cortex. *Gastroenterology* 136, 1359–1367.e2 (2009).
73. Norenberg MD, Jayakumar AR & Rao KVR. Oxidative Stress in the Pathogenesis of Hepatic Encephalopathy. *Metabolic Brain Disease* 19, 313–329 (2004).
74. Görg B, Qvarthava N, Bidmon HJ, Palomero-Gallagher N, Kircheis G, Zilles K & Häussinger D. Oxidative stress markers in the brain of patients with cirrhosis and hepatic encephalopathy. *Hepatology* 52, 256–265 (2010).
75. Schliess F, Görg B & Häussinger D. Pathogenetic interplay between osmotic and oxidative stress: the hepatic encephalopathy paradigm. *Biological Chemistry* 387, 1363–1370 (2006).
76. Häussinger D & Görg B. Interaction of oxidative stress, astrocyte swelling and cerebral ammonia toxicity. *Current Opinion in Clinical Nutrition and Metabolic Care* 13, 87–92 (2010).
77. Bosoi CR, Yang X, Huynh J, Parent-Robitaille C, Jiang W, Tremblay M & Rose CF. Systemic oxidative stress is implicated in the pathogenesis of brain edema in rats with chronic liver failure. *Free Radical Biology and Medicine* 52, 1228–1235 (2012).

78. Bosoi CR, Tremblay M & Rose CF. Induction of systemic oxidative stress leads to brain oedema in portacaval shunted rats. *Liver International* 34, 1322–1329 (2014).
79. Murthy CRK, Bender AS, Dombro RS, Bai G & Norenberg MD. Elevation of glutathione levels by ammonium ions in primary cultures of rat astrocytes. *Neurochemistry International* 37, 255–268 (2000).
80. Wegrzynowicz M, Hilgier W, Dybel A, Oja SS, Saransaari P & Albrecht J. Upregulation of cerebral cortical glutathione synthesis by ammonia in vivo and in cultured glial cells: The role of cystine uptake. *Neurochemistry International* 50, 883–889 (2007).
81. Sathyaikumar KV, Swapna I, Reddy PVB, Murthy CRK, Gupta AD, Senthil Kumaran B & Reddanna P. Fulminant Hepatic Failure in Rats Induces Oxidative Stress Differentially in Cerebral Cortex, Cerebellum and Pons Medulla. *Neurochemical Research* 32, 517–524 (2007).
82. Klejman A, Wegrzynowicz M, Szatmari EM, Mioduszezewska B, Hetman M & Albrecht J. Mechanisms of ammonia-induced cell death in rat cortical neurons: Roles of NMDA receptors and glutathione. *Neurochemistry International* 47, 51–57 (2005).
83. Hilgier W, Wegrzynowicz M, Ruszkiewicz J, Oja SS, Saransaari P & Albrecht J. Direct Exposure to Ammonia and Hyperammonemia Increase the Extracellular Accumulation and Degradation of Astroglia-Derived Glutathione in the Rat Prefrontal Cortex. *Toxicological Sciences* 117, 163–168 (2010).
84. Zeeman P. The Effect of Magnetisation on the Nature of Light Emitted by a Substance. *Nature* 55, 347 (1897).
85. Gerlach W & Stern O. Der experimentelle Nachweis der Richtungsquantelung im Magnetfeld. *Zeitschrift für Physik* 9, 349–352 (1922).
86. Rabi II, Zacharias JR, Millman S & Kusch P. A New Method of Measuring Nuclear Magnetic Moment. *Physical Review* 53, 318–318 (1938).
87. Purcell EM, Torrey HC & Pound RV. Resonance Absorption by Nuclear Magnetic Moments in a Solid. *Physical Review* 69, 37–38 (1946).
88. Bloch F. Nuclear Induction. *Physical Review* 70, 460–474 (1946).
89. Lauterbur PC. Image Formation by Induced Local Interactions: Examples Employing Nuclear Magnetic Resonance. *Nature* 242, 190–191 (1973).

Bibliography

90. Mansfield P & Grannell PK. NMR 'diffraction' in solids? *Journal of Physics C: Solid State Physics* 6, L422 (1973).
91. Garroway AN, Grannell PK & Mansfield P. Image formation in NMR by a selective irradiative process. *Journal of Physics C: Solid State Physics* 7, L457 (1974).
92. Haacke EM, Brown RW, Thompson MR & Venkatesan R. *Magnetic Resonance Imaging: Physical Principles and Sequence Design* (Wiley, 1999).
93. Hahn EL. Spin Echoes. *Physical Review* 80, 580–594 (1950).
94. Carr HY & Purcell EM. Effects of Diffusion on Free Precession in Nuclear Magnetic Resonance Experiments. *Physical Review* 94, 630–638 (1954).
95. Mansfield P. Multi-planar image formation using NMR spin echoes. *Journal of Physics C: Solid State Physics* 10, L55 (1977).
96. Neeb H, Zilles K & Shah N. A new method for fast quantitative mapping of absolute water content in vivo. *NeuroImage* 31, 1156–1168 (2006).
97. Neeb H, Ermer V, Stocker T & Shah N. Fast quantitative mapping of absolute water content with full brain coverage. *NeuroImage* 42, 1094–1109 (2008).
98. Neeb H, Zilles K & Shah NJ. Fully-automated detection of cerebral water content changes: Study of age- and gender-related H₂O patterns with quantitative MRI. *NeuroImage* 29, 910–922 (2006).
99. Mandal PK. In vivo proton magnetic resonance spectroscopic signal processing for the absolute quantitation of brain metabolites. *European Journal of Radiology* 81, e653–e664 (2012).
100. Friebolin H. *Ein- und zweidimensionale NMR-Spektroskopie* (Wiley, 2006).
101. Bottomley PA. Spatial Localization in NMR Spectroscopy in Vivo. *Annals of the New York Academy of Sciences* 508, 333–348 (1987).
102. Frahm J, Merboldt KD & Hänicke W. Localized proton spectroscopy using stimulated echoes. *Journal of Magnetic Resonance (1969)* 72, 502–508 (1987).
103. Pouillet JB, Sima DM & Van Huffel S. MRS signal quantitation: A review of time- and frequency-domain methods. *Journal of Magnetic Resonance* 195, 134–144 (2008).

104. Naressi A, Couturier C, Devos JM, Janssen M, Mangeat C, Beer Rd & Graveron-Demilly D. Java-based graphical user interface for the MRUI quantitation package. *Magnetic Resonance Materials in Physics, Biology and Medicine* 12, 141–152 (2001).
105. Wilson M, Reynolds G, Kauppinen RA, Arvanitis TN & Peet AC. A constrained least-squares approach to the automated quantitation of in vivo ¹H magnetic resonance spectroscopy data. *Magnetic Resonance in Medicine* 65, 1–12 (2011).
106. Provencher SW. Estimation of metabolite concentrations from localized in vivo proton NMR spectra. *Magnetic Resonance in Medicine* 30, 672–679 (1993).
107. Provencher SW. Automatic quantitation of localized in vivo ¹H spectra with LCModel. *NMR in Biomedicine* 14, 260–264 (2001).
108. Helms G. The principles of quantification applied to in vivo proton MR spectroscopy. *European Journal of Radiology. Clinical ¹H MR Spectroscopy* 67, 218–229 (2008).
109. Jansen JFA, Backes WH, Nicolay K & Kooi ME. ¹H MR Spectroscopy of the Brain: Absolute Quantification of Metabolites. *Radiology* 240, 318–332 (2006).
110. Gussew A, Erdtel M, Hiepe P, Rzanny R & Reichenbach JR. Absolute quantitation of brain metabolites with respect to heterogeneous tissue compositions in ¹H-MR spectroscopic volumes. *Magnetic Resonance Materials in Physics, Biology and Medicine* 25, 321–333 (2012).
111. Gasparovic C, Song T, Devier D, Bockholt HJ, Caprihan A, Mullins PG, Posse S, Jung RE & Morrison LA. Use of tissue water as a concentration reference for proton spectroscopic imaging. *Magnetic Resonance in Medicine* 55, 1219–1226 (2006).
112. Gasparovic C, Neeb H, Feis D, Damaraju E, Chen H, Doty M, South D, Mullins P, Bockholt H & Shah N. Quantitative spectroscopic imaging with in situ measurements of tissue water T₁, T₂, and density. *Magnetic Resonance in Medicine* 62, 583–590 (2009).
113. Mescher M, Merkle H, Kirsch J, Garwood M & Gruetter R. Simultaneous in vivo spectral editing and water suppression. *NMR in Biomedicine* 11, 266–272 (1998).
114. Rothman DL, Petroff OA, Behar KL & Mattson RH. Localized ¹H NMR measurements of gamma-aminobutyric acid in human brain in vivo. *Proceedings of the National Academy of Sciences of the United States of America* 90, 5662–5666 (1993).

Bibliography

115. Mullins PG, McGonigle DJ, O’Gorman RL, Puts NAJ, Vidyasagar R, Evans CJ & Edden RAE. Current practice in the use of MEGA-PRESS spectroscopy for the detection of GABA. *NeuroImage* 86, 43–52 (2014).
116. Edden RA, Puts NA, Harris AD, Barker PB & Evans CJ. Gannet: A batch-processing tool for the quantitative analysis of gamma-aminobutyric acid–edited MR spectroscopy spectra. *Journal of Magnetic Resonance Imaging* 40, 1445–1452 (2014).
117. Henry PG, Dautry C, Hantraye P & Bloch G. Brain GABA editing without macromolecule contamination. *Magnetic Resonance in Medicine* 45, 517–520 (2001).
118. Bhattacharyya PK. Macromolecule contamination in GABA editing using MEGA-PRESS should be properly accounted for. *NeuroImage* 84, 1111–1112 (2014).
119. Murdoch JB & Dydak U. *Modeling MEGA-PRESS macromolecules for a better grasp of GABA* in *Proc. Intl. Soc. Magn. Reson. Med.* 19 (Montreal, 2011), 1394.
120. Edden RAE, Puts NAJ & Barker PB. Macromolecule-suppressed GABA-edited magnetic resonance spectroscopy at 3T. *Magnetic Resonance in Medicine* 68, 657–661 (2012).
121. Harris AD, Puts NA, Barker PB & Edden RA. Spectral-editing measurements of GABA in the human brain with and without macromolecule suppression. *Magnetic Resonance in Medicine*. doi:10.1002/mrm.25549 (2014).
122. Yousry TA, Schmid UD, Alkadhi H, Schmidt D, Peraud A, Buettner A & Winkler P. Localization of the motor hand area to a knob on the precentral gyrus. A new landmark. *Brain* 120, 141–157 (1997).
123. Behar KL, Rothman DL, Petersen KF, Hooten M, Delaney R, Petroff OA, Shulman GI, Navarro V, Petrakis IL, Charney DS & Krystal JH. Preliminary Evidence of Low Cortical GABA Levels in Localized 1H-MR Spectra of Alcohol-Dependent and Hepatic Encephalopathy Patients. *American Journal of Psychiatry* 156, 952–954 (1999).
124. Terhune DB, Russo S, Near J, Stagg CJ & Kadosh RC. GABA Predicts Time Perception. *The Journal of Neuroscience* 34, 4364–4370 (2014).

125. Edden RAE, Muthukumaraswamy SD, Freeman TCA & Singh KD. Orientation Discrimination Performance Is Predicted by GABA Concentration and Gamma Oscillation Frequency in Human Primary Visual Cortex. *The Journal of Neuroscience* 29, 15721–15726 (2009).
126. Sandberg K, Blicher JU, Dong MY, Rees G, Near J & Kanai R. Occipital GABA correlates with cognitive failures in daily life. *NeuroImage* 87, 55–60 (2014).
127. Cauli O, Rodrigo R, Llansola M, Montoliu C, Monfort P, Piedrafita B, Mlilil Ne, Boix J, Agustí A & Felipo V. Glutamatergic and gabaergic neurotransmission and neuronal circuits in hepatic encephalopathy. *Metabolic Brain Disease* 24, 69–80 (2008).
128. Laubenberger J, Haussinger D, Bayer S, Gufler H, Hennig J & Langer M. Proton magnetic resonance spectroscopy of the brain in symptomatic and asymptomatic patients with liver cirrhosis. *Gastroenterology* 112, 1610–1616 (1997).
129. Chavarria L, Alonso J, García-Martínez R, Simón-Talero M, Ventura-Cots M, Ramírez C, Torrens M, Vargas V, Rovira A & Córdoba J. Brain magnetic resonance spectroscopy in episodic hepatic encephalopathy. *Journal of Cerebral Blood Flow & Metabolism* 33, 272–277 (2013).
130. Murthy C, Rama Rao K, Bai G & Norenberg MD. Ammonia-induced production of free radicals in primary cultures of rat astrocytes. *Journal of Neuroscience Research* 66, 282–288 (2001).
131. Dhanda S, Kaur S & Sandhir R. Preventive effect of N-acetyl-L-cysteine on oxidative stress and cognitive impairment in hepatic encephalopathy following bile duct ligation. *Free Radical Biology and Medicine* 56, 204–215 (2013).
132. Oeltzschner G, Butz M, Baumgarten TJ, Hoogenboom N, Wittsack HJ & Schnitzler A. Low visual cortex GABA levels in hepatic encephalopathy: links to blood ammonia, critical flicker frequency, and brain osmolytes. *Metabolic Brain Disease*. doi:10.1007/s11011-015-9729-2 (2015).
133. Qi R, Zhang LJ, Zhong J, Zhang Z, Ni L, Zheng G & Lu GM. Disrupted thalamic resting-state functional connectivity in patients with minimal hepatic encephalopathy. *European Journal of Radiology* 82, 850–856 (2013).

Bibliography

134. Qi R, Zhang LJ, Chen HJ, Zhong J, Luo S, Ke J, Xu Q, Kong X, Liu C & Lu GM. Role of local and distant functional connectivity density in the development of minimal hepatic encephalopathy. *Scientific Reports* 5. doi:10.1038/srep13720 (2015).
135. Qi R, Zhang LJ, Zhong J, Zhu T, Zhang Z, Xu C, Zheng G & Lu GM. Grey and white matter abnormalities in minimal hepatic encephalopathy: a study combining voxel-based morphometry and tract-based spatial statistics. *European Radiology* 23, 3370–3378 (2013).
136. Tao R, Zhang J, You Z, Wei L, Fan Y, Cui J & Wang J. The thalamus in cirrhotic patients with and without hepatic encephalopathy: A volumetric MRI study. *European Journal of Radiology* 82, e715–e720 (2013).
137. Cauli O, Llansola M, Agustí A, Rodrigo R, Hernández-Rabaza V, Rodrigues TB, López-Larrubia P, Cerdán S & Felipo V. Cerebral oedema is not responsible for motor or cognitive deficits in rats with hepatic encephalopathy. *Liver International* 34, 379–387 (2014).
138. Bosoi CR, Zwingmann C, Marin H, Parent-Robitaille C, Huynh J, Tremblay M & Rose CF. Increased brain lactate is central to the development of brain edema in rats with chronic liver disease. *Journal of Hepatology* 60, 554–560 (2014).
139. Bosoi CR & Rose CF. Elevated cerebral lactate: Implications in the pathogenesis of hepatic encephalopathy. *Metabolic Brain Disease* 29, 919–925 (2014).
140. Friston KJ. *Statistical parametric mapping the analysis of functional brain images* (Elsevier/Academic Press, Amsterdam; Boston, 2007).
141. Wansapura JP, Holland SK, Dunn RS & Ball WS. NMR relaxation times in the human brain at 3.0 tesla. *Journal of Magnetic Resonance Imaging* 9, 531–538 (1999).
142. Edden RA, Intrapromkul J, Zhu H, Cheng Y & Barker PB. Measuring T2 in vivo with J-difference editing: Application to GABA at 3 tesla. *Journal of Magnetic Resonance Imaging* 35, 229–234 (2012).
143. Puts NA, Barker PB & Edden RA. Measuring the longitudinal relaxation time of GABA in vivo at 3 tesla. *Journal of Magnetic Resonance Imaging* 37, 999–1003 (2013).

144. Cho S, Jones D, Reddick WE, Ogg RJ & Steen RG. Establishing norms for age-related changes in proton T1 of human brain tissue in vivo. *Magnetic Resonance Imaging* 15, 1133–1143 (1997).
145. Cauli O, Mlili N, Llansola M & Felipo V. Motor activity is modulated via different neuronal circuits in rats with chronic liver failure than in normal rats. *European Journal of Neuroscience* 25, 2112–2122 (2007).
146. Cousijn H, Haegens S, Wallis G, Near J, Stokes MG, Harrison PJ & Nobre AC. Resting GABA and glutamate concentrations do not predict visual gamma frequency or amplitude. *Proceedings of the National Academy of Sciences of the United States of America* 111, 9301–9306 (2014).
147. Jensen O, Goel P, Kopell N, Pohja M, Hari R & Ermentrout B. On the human sensorimotor-cortex beta rhythm: Sources and modeling. *NeuroImage* 26, 347–355 (2005).
148. Hall SD, Barnes GR, Furlong PL, Seri S & Hillebrand A. Neuronal network pharmacodynamics of GABAergic modulation in the human cortex determined using pharmaco-magnetoencephalography. *Human Brain Mapping* 31, 581–594 (2010).
149. Hall SD, Stanford IM, Yamawaki N, McAllister CJ, Rönqvist KC, Woodhall GL & Furlong PL. The role of GABAergic modulation in motor function related neuronal network activity. *NeuroImage* 56, 1506–1510 (2011).
150. Muthukumaraswamy SD, Myers JFM, Wilson SJ, Nutt DJ, Lingford-Hughes A, Singh KD & Hamandi K. The effects of elevated endogenous GABA levels on movement-related network oscillations. *NeuroImage* 66, 36–41 (2013).
151. Stagg CJ, Bestmann S, Constantinescu AO, Moreno Moreno L, Allman C, Mекle R, Woolrich M, Near J, Johansen-Berg H & Rothwell JC. Relationship between physiological measures of excitability and levels of glutamate and GABA in the human motor cortex. *The Journal of Physiology* 589, 5845–5855 (2011).

RELEVANT PUBLICATIONS

The present work is based on:

Publication 1:

Oeltzschner G, Butz M, Baumgarten TJ, Hoogenboom N, Wittsack HJ, Schnitzler A. Low visual cortex GABA levels in hepatic encephalopathy: links to blood ammonia, critical flicker frequency, and brain osmolytes. *Metabolic Brain Disease* 2015 (in press). DOI 10.1007/s11011-015-9729-2

Reprinted as Appendix 1 from *Metabolic Brain Disease* with permission from Springer. Original publication can be found online at <http://link.springer.com/article/10.1007/s11011-015-9729-2>.

Impact factor (2014): 2.638

Personal contribution: 80% (Data acquisition, data analysis, interpretation of results, manuscript drafting)

Publication 2:

Oeltzschner G, Butz M, Wickrath F, Wittsack HJ, Schnitzler A. Covert hepatic encephalopathy: Elevated total glutathione and absence of brain water content changes. *Metabolic Brain Disease* 2015 (accepted for publication). The manuscript is included as Appendix 2.

Personal contribution: 80% (Data acquisition, data analysis, interpretation of results,

manuscript drafting)

Publication 3:

Oeltzschner G, Schnitzler A, Wickrath F, Wittsack HJ (2015) Use of quantitative brain water imaging as concentration reference for J-edited MR spectroscopy of GABA. Magnetic Resonance Imaging 2015 (submitted). The manuscript is included as Appendix 3.

Personal contribution: 80% (Design of analysis scheme, data acquisition, data analysis, interpretation of results, manuscript drafting)

Other aspects are taken from:

Publication 4:

Baumgarten TJ, Oeltzschner G, Hoogenboom N, Wittsack HJ, Schnitzler A, Lange J. Beta peak frequencies at rest correlated with endogenous GABA/Cr concentrations in the left sensorimotor cortex. PLoS One 2015 (under review). The manuscript is included as Appendix 4.

Personal contribution: 20% (Spectroscopy data acquisition, spectroscopy data analysis, manuscript revision)

Low visual cortex GABA levels in hepatic encephalopathy: links to blood ammonia, critical flicker frequency, and brain osmolytes

Georg Oeltzschner^{1,2} · Markus Butz¹ · Thomas J. Baumgarten¹ · Nienke Hoogenboom¹ · Hans-Jörg Wittsack² · Alfons Schnitzler¹

Received: 31 March 2015 / Accepted: 3 September 2015
© Springer Science+Business Media New York 2015

Abstract The pathogenesis of hepatic encephalopathy (HE) is not fully understood yet. Hyperammonemia due to liver failure and subsequent disturbance of cerebral osmolytic balance is thought to play a pivotal role in the emergence of HE. The aim of this in-vivo MR spectroscopy study was to investigate the levels of γ -aminobutyric acid (GABA) and its correlations with clinical symptoms of HE, blood ammonia, critical flicker frequency, and osmolytic levels. Thirty patients with minimal HE or HE1 and 16 age-matched healthy controls underwent graduation of HE according to the *West-Haven* criteria and including the critical flicker frequency (CFF), neuropsychometric testing and blood testing. Edited proton magnetic resonance spectroscopy (¹H MRS) was used to non-invasively measure the concentrations of GABA, glutamate (Glu), glutamine (Gln), and myo-inositol (mI) - all normalized to creatine (Cr) - in visual and sensorimotor cortex. GABA/Cr in the visual area was significantly decreased in mHE and HE1 patients and correlated both to the CFF ($r = 0.401$, $P = 0.013$) and blood ammonia levels ($r = -0.434$, $P = 0.006$). Visual GABA/Cr was also strongly linked to mI/Cr ($r = 0.720$, $P < 0.001$) and Gln/Cr ($r = -0.699$, $P < 0.001$). No group differences or correlations were found for GABA/Cr in the sensorimotor area. Hepatic encephalopathy is

associated with a regional specific decrease of GABA levels in the visual cortex, while no changes were revealed for the sensorimotor cortex. Correlations of visual GABA/Cr with CFF, blood ammonia, and osmolytic regulators mI and Gln indicate that decreased visual GABA levels might contribute to HE symptoms, most likely as a consequence of hyperammonemia.

Keywords Hepatic encephalopathy · MR spectroscopy · γ -aminobutyric acid · Ammonia · Critical flicker frequency · MEGA-PRESS

Abbreviations

| | |
|------------|---|
| HE | hepatic encephalopathy |
| CFF | critical flicker frequency |
| MRS | magnetic resonance spectroscopy |
| GABA | γ -aminobutyric acid |
| Glu | glutamate |
| Gln | glutamine |
| mI | myo-inositol |
| Cr | creatine |
| MEGA-PRESS | Mescher-Garwood point resolved spectroscopy |
| TR | repetition time |
| TE | echo time |
| FoV | field of view |
| CRLB | Cramér-Rao lower bounds |
| MM | macromolecules |
| GM | gray matter |
| WM | white matter |
| CSF | cerebrospinal fluid |
| MEG | magnetoencephalography |

✉ Georg Oeltzschner
georg.oeltzschner@med.uni-duesseldorf.de

¹ Institute of Clinical Neuroscience and Medical Psychology, Medical Faculty, Heinrich Heine University Düsseldorf, Universitätsstr. 1, D-40225 Düsseldorf, Germany

² Medical Faculty, Department of Diagnostic and Interventional Radiology, University Düsseldorf, D-40225 Düsseldorf, Germany

Introduction

Hepatic encephalopathy (HE) is a common complication in patients with liver cirrhosis. Its clinical manifestation comprises impairments of cognitive, behavioral, and motor functions. Symptoms fluctuate with disease severity, and the severest states of HE lead to somnolence, stupor, and even coma (Butterworth 2000; Ferenci et al. 2002; Felipo 2013).

The pathogenesis of HE is considered to be of multifactorial nature (Häussinger and Sies 2013). The intrusion of ammonia through the blood brain barrier sets off a multitude of reactions including inflammation and oxidative stress. Metabolisation of ammonia by glutamine synthetase (GS) in the astrocytes leads to increased glutamine (Gln) concentrations, resulting in an osmotic imbalance, which is believed to be partially countered by a depletion of osmolytes such as myo-inositol (mI). This has led to the proposal of subsequent astrocyte swelling and the formation of low-grade cerebral edema (Häussinger and Schliess 2008).

Elevated glutamine and decreased myo-inositol levels as a consequence of hyperammonemia were consistently observed with magnetic resonance spectroscopy (MRS) (Häussinger et al. 1994; Laubenberger et al. 1997; Shawcross et al. 2004). The degree of these Gln and mI abnormalities was linked to blood ammonia levels, HE severity and changes in diffusion properties of tissue water (Thomas et al. 1998; Binesh et al. 2006; Miese et al. 2006; Mardini et al. 2011). Using quantitative water mapping, small increases of white matter water content with increasing HE severity were demonstrated (Shah et al. 2008). Ultimately, a complex interaction of these processes is thought to induce alterations in synaptic plasticity and pathological abnormalities in the oscillatory brain networks that have been observed in context with the various functional deficits in HE patients (for reviews see Timmermann et al. 2003; Butz et al. 2013). Currently, it is unclear how the hyperammonemia-induced osmolyte depletion and subsequent edema formation could affect brain oscillations. A possible pathway for the development of abnormal oscillatory behavior is via disturbed neurotransmitter homeostasis (Llansola et al. 2014). An example for this is the inhibitory neurotransmitter γ -aminobutyric acid (GABA), as GABA resting concentrations have been shown to be linked with cortical oscillations both in the motor (Gaetz et al. 2011) and the visual cortex (Muthukumaraswamy et al. 2009). However, investigation of GABA in HE yielded largely controversial outcome so far. Already more than thirty years ago gut-derived GABA was proposed to increase the GABAergic tone in the HE brain (Schafer and Jones 1982). Subsequent research analysed GABA synthesis regulation, receptor alterations, and pharmacological intervention in states of hyperammonemia, but the incoherent results did not lead to a consistent concept of the role of GABA in the pathophysiology of HE (Palomero-Gallagher and Zilles 2013). Recent animal works speak against

the notion of a generalized increased GABAergic tone in HE, and instead point towards a rather regionally selective nature of interdependent alterations in GABAergic and glutamatergic systems (for a review see Sergeeva 2013; Llansola et al. 2014). For example, hypokinesia in rats with portocaval shunting was linked to increased GABA levels in the ventromedial thalamus as a consequence of excessive mGluR1 activation in the *substantia nigra* (Cauli et al. 2008). In similar experiments, the GABAergic tone was found to be decreased in prefrontal cortex, but increased in the cerebellum of hyperammonemic rodents, contributing to cognitive impairment (Cauli et al. 2009).

All in all, more work needs to be done to illuminate function and pattern of the pathophysiological contribution of GABA in HE.

The aim of the present study was to investigate the levels of GABA in different brain regions and to reveal potential links between these, glutamate levels, HE severity, blood ammonia levels, and brain osmolytes, i.e. glutamine, and myo-inositol. To this end, edited MR spectroscopy for GABA detection was performed in a cohort of clinically well characterized HE patients with varying disease grades and healthy controls.

Material and methods

The study was performed conforming to the principles of the Declaration of Helsinki and approved by the local ethics committee (study number 3644). All recruited subjects participated after giving their full prior written informed consent.

Participants and grading

Thirty patients with hepatic encephalopathy and 16 controls were enrolled. Necessary inclusion criteria for patients were clinically confirmed liver cirrhosis and diagnosis of minimal HE or HE1 as defined by *West-Haven* criteria (see below). Healthy controls were recruited to age-match the patient groups. Exclusion criteria for both patients and controls were severe internal, neurological or psychiatric diseases other than HE, use of psychoactive substances, blood clotting dysfunction and peripheral or retinal neuropathy. If alcohol abuse was part of the medical history, the subject had to remain abstinent for ≥ 4 weeks prior to inclusion.

HE severity grading was done by a combination of the *West-Haven* criteria (Ferenci et al. 2002) and the critical flicker frequency (CFF). The CFF was used as an additional parameter as it was shown to be a reliable parameter for the graduation and monitoring of HE accounting for the continuous nature of HE (Kircheis et al. 2002, 2014). To this end, the participants underwent standard blood examination including ammonia.

Two subjects (1 mHE, 1 HE1) had to be excluded due to alcohol intake. One subject initially classified as HE1 had to

be excluded due to imprecise patient files. Information on the remaining study population is summarized in Table 1.

Assessment of HE severity according to the *West-Haven* criteria (Ferenci et al. 2002; Kircheis et al. 2002) included psychometric testing and a clinical assessment of the mental state and consciousness by an experienced clinician. Computer-based neuropsychological tests from the Vienna Test System (Dr. Schuhfried GmbH, Mödling, Austria) consisted of five test batteries and reported a range of 22 age-validated scores (calculated as percentage rank values from comparison with an age-matched control cohort) reflecting cognitive and motor performance. Higher scores indicated better performance. When a parameter value was found to be more aberrant than one standard deviation from the mean of a large control cohort, it was considered *abnormal*. If patients did not exhibit clinical symptoms of manifest HE, but showed more than 2 abnormal psychometric test results, they were classified as minimal HE (mHE) (Kircheis et al. 2002). Ten scores were selected for detailed analysis, including cognitive (“COG1”: time to reject a geometric shape not matching control shapes; “COG2”: time to confirm a geometric shape matching control shapes), fine motor performance (line following test: “LVT1”: time per item; “LVT2”: overall score), motor precision/speed (“MLS1”: hand steadiness/tremor; “MLS2”: arm/hand precision; “MLS3”: arm/hand speed; “MLS4”: finger tapping speed), and reaction performance (“WRT1”: reaction time; “WRT2”: motor reaction time).

MR measurements

Measurements were carried out on a clinical 3 T whole-body MRI scanner (Siemens MAGNETOM Trio A TIM System, Siemens Healthcare AG, Erlangen, Germany) using a 12-channel head matrix coil.

MR spectroscopy

MRS volumes were placed in different anatomical locations as depicted in Fig. 1. One spectroscopic volume was placed in the central occipital lobe and carefully aligned to include as much of the visual area as possible. The caudal boundary of the volume was aligned along the *cerebellar tentorium*. In

addition, in both hemispheres one volume each was centered on an anatomical region known as the “*hand knob*” (Yousry et al. 1997), a prominent feature of the *praecentral gyrus* that can be recognized with ease from transversal planning images. If centered at this landmark, the spectroscopic volume spans across the *central sulcus* to include both sensory and motor cortices, at the level of hand motor cortex (Hone-Blanchet et al. 2015). In all cases, special care was taken during placement of the volume to include as much cortical volume as possible and, on the other hand, avoid unwanted lipid contamination of the spectra from the skull.

After T_1 -weighted planning sequences and localizing the target volumes, MEGA-PRESS (Mescher et al. 1998) spectra were acquired (number of excitations = 192, TR = 1500 ms, TE = 68 ms, V = 3x3x3 cm³, bandwidth = 1200 Hz, 1024 data points). Spectral editing was conducted by J-refocusing pulses irradiated at 1.9 ppm and 7.5 ppm using Gaussian pulses with a bandwidth of 44 Hz.

Structural MRI

For segmentation purposes, a high-resolution 3D anatomical transversal T_1 -weighted magnetization prepared gradient echo (MP RAGE) scan was performed (TR/TE = 1950/4.6 ms, FoV 256 × 192 mm, 256 × 192 matrix, slice thickness 1 mm, 176 slices).

Data processing

Evaluation of MRS data

MEGA-PRESS data were exported from the scanner in raw TWIX and Siemens RDA file format. Processing of TWIX data from the difference spectra was performed with the freely available MATLAB-based tool GANNET 2.0 (Edden et al. 2014) and included frequency and phase correction of the single acquisitions and Gaussian fitting of the 3 ppm GABA resonance (Fig. 2). The GABA-to-creatine ratio (GABA/Cr) was subsequently used for further analysis.

Spectra from the unedited MEGA-PRESS scan (*OFF* resonance) were analyzed with LCModel version 6.3 (Provencher 2001) to yield ratios of the following metabolites with respect to creatine: glutamine (Gln/Cr), glutamate (Glu/Cr), and myo-inositol (mI/Cr). The linear decomposition of an example signal into its spectral components is depicted in Fig. 3. The variance of the metabolite estimates was provided as CRLB (Cramér-Rao lower bounds).

Metabolite-to-creatine ratios for the sensorimotor area were obtained by averaging the results from the right and left hemisphere. If MRS evaluation was only successful for one side, the estimate from this side was used for further analysis.

Table 1 Controls and patient population after exclusion. * = Significantly different from mHE ($P < 0.01$) and from controls ($P < 0.001$) with non-parametric Kruskal-Wallis analysis for independent sampling

| | Sex (M/F) | Age [y] | CFF [Hz] |
|-----------------------|-----------|------------|-------------|
| Controls ($n = 16$) | 7/9 | 60.1 ± 8.7 | 41.6 ± 4.0 |
| mHE ($n = 13$) | 8/5 | 55.7 ± 8.5 | 39.4 ± 3.2 |
| HE1 ($n = 14$) | 10/4 | 61.6 ± 7.6 | 34.5* ± 3.1 |

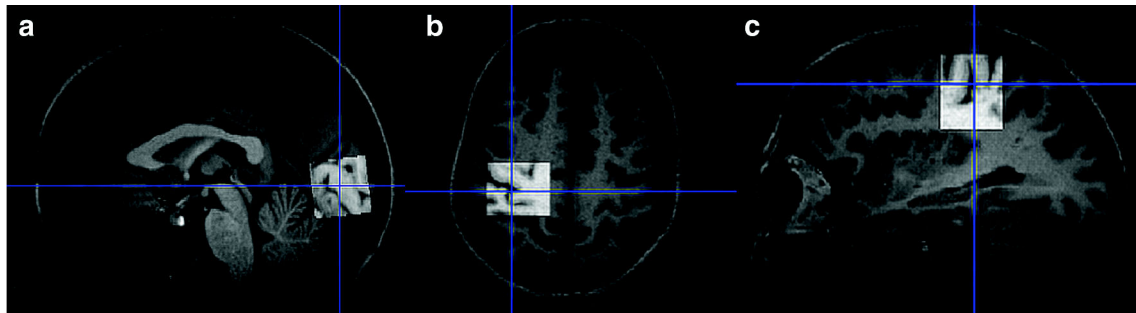


Fig. 1 T₁-weighted MRI scan of the brain. Exemplary localisation of the visual spectroscopic volume in the sagittal plane (a), placement of the left sensorimotor spectroscopic volume, centered on the hand knob, in the axial (b) and sagittal (c) planes

Evaluation of structural data

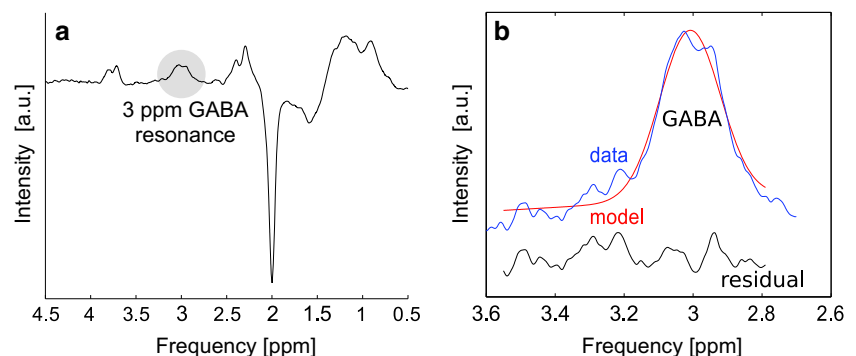
The ‘New Segment’ routine of SPM8 (<http://www.fil.ion.ucl.ac.uk/spm/>) was used to segment the MP RAGE scan into gray matter (GM), white matter (WM) and cerebrospinal fluid (CSF). The MR spectroscopic volumes were co-registered to the MP RAGE scan with a custom made MATLAB (The Mathworks Inc., Natick/MA) routine (Dr. Nia Goulden, Dr. Paul Mullins, Bangor University, <http://biu.bangor.ac.uk/projects.php.en>, modified by the authors to work with Siemens file format). It transformed the volume parameters into a binary mask that was used to calculate the fractions of GM, WM, and CSF in the respective spectroscopic volume.

Statistical evaluation

Differences of metabolite levels and psychometric scores between the participant groups (controls, mHE, and HE1) were investigated by non-parametric Kruskal-Wallis one way analyses of variance for independent samples. If group differences were discovered, post-hoc tests were automatically performed to yield Dunn-Bonferroni adjusted *P* values. Group differences were considered significant for *P* < 0.05.

Relationships between CFF and metabolite levels were assessed with partial two-tailed correlation analyses, including correction for age. Relationships between metabolite levels and blood ammonia were assessed with bivariate two-tailed Spearman’s rank correlation analyses. Again, correlations were considered significant for *P* < 0.05.

Fig. 2 GANNET output of a difference spectrum from a healthy control (a). The gray-circled area of the 3 ppm GABA resonance is shown in (b), including the Gaussian fitting, the result of which is subsequently used for further analysis



Relationships between metabolite levels and psychometric scores were also assessed with bivariate two-tailed Spearman’s rank correlation analyses.

To investigate the interplay of metabolites, bivariate two-tailed Spearman’s rank correlation analysis was performed for GABA/Cr, Gln/Cr, Glu/Cr, and mI/Cr. This was done separately for the sensorimotor and the visual MRS volume.

All correlation analyses included a false discovery rate (FDR) correction at $\alpha = 0.05$.

All statistical computations were performed using IBM SPSS Statistics for Windows, Version 22.0 (IBM Corp., Armonk, NY, USA).

Results

From a total of 43 participants (16 controls, 13 mHE, 14 HE1), visual GABA/Cr estimates could be obtained in all but 4 individuals. In these 4 participants, visual GABA/Cr estimates could not be obtained due to noisy or distorted spectra or cancellation of the measurements (2 controls, 2 mHE). Sensorimotor GABA/Cr estimates were obtained in all but 3 subjects (2 controls, 1 mHE). In eight subjects (4 controls, 2 mHE, 2 HE1), the sensorimotor GABA/Cr estimate of only one hemisphere was used for further analysis. Results from the unedited visual spectra could not be obtained from 3 subjects (2 controls, 1 mHE). Unedited sensorimotor spectra could not be analysed in one control subject. In one subject

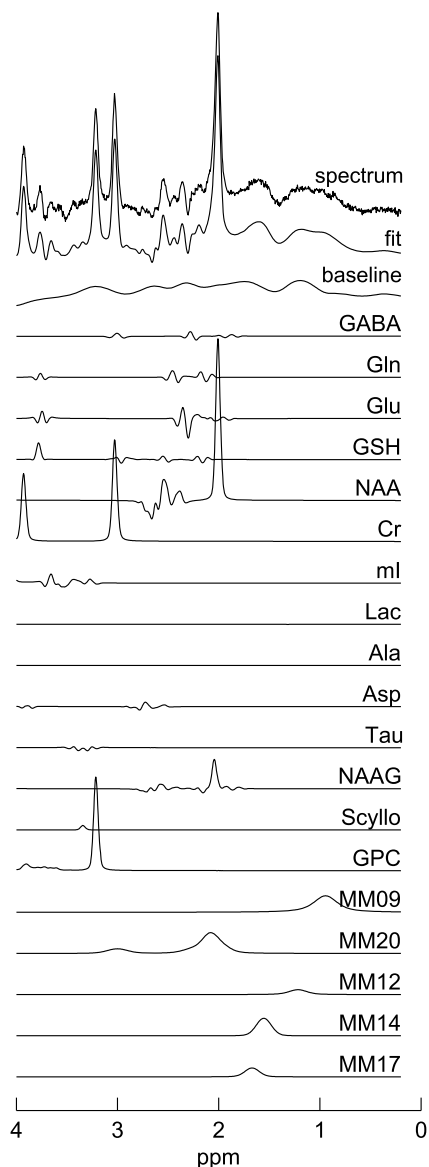


Fig. 3 LCModel decomposition of an unedited (OFF resonance) spectrum

(mHE), the unedited sensorimotor spectra of only one hemisphere were used for further analysis.

Group results and correlations with CFF and blood ammonia are summarized in Table 2. No significant differences between males and females were observed in any parameter.

GABA

Visual GABA/Cr ratios were reduced in the mHE ($P = 0.017$) and the HE1 group ($P = 0.001$) compared to controls (Fig. 4a), but no difference was found between mHE and HE1 ($P = 1.000$). Additionally, a positive correlation of visual GABA/Cr with CFF ($r = 0.401$, $P = 0.013$, Fig. 4b) and a negative correlation with blood ammonia ($r = -0.434$, $P = 0.006$) were observed.

No group differences (Fig. 4c) or correlations (Fig. 4d) could be revealed for the sensorimotor GABA/Cr levels.

Glutamate

Levels of Glu/Cr did not exhibit significant differences in mHE or HE1 compared to controls or correlations with CFF or blood ammonia. This was valid for both the visual and the sensorimotor areas.

Glutamine

Visual and sensorimotor Gln/Cr levels were elevated in the mHE and HE1 groups, but not differing between the two HE groups. There were negative correlations of Gln/Cr with CFF (visual: $r = -0.497$, $P = 0.001$, sensorimotor: $r = -0.505$, $P = 0.001$) and positive correlations with blood ammonia (visual: $r = 0.429$, $P = 0.006$, sensorimotor: $r = 0.632$, $P < 0.001$).

myo-inositol

mI/Cr levels in the visual and sensorimotor areas were decreased in the mHE and HE1 groups compared to the control group, yet did not exhibit differences between mHE and HE1. A positive correlation of mI/Cr with CFF (visual: $r = 0.473$, $P = 0.002$, sensorimotor: $r = 0.516$, $P = 0.001$) and a negative correlation with blood ammonia (visual: $r = -0.456$, $P = 0.004$, sensorimotor: $r = -0.505$, $P = 0.001$) were observed.

Cross correlations of metabolites

Our analysis of the visual metabolite concentrations yielded several important findings (Table 3):

GABA/Cr was positively correlated with mI/Cr and negatively correlated with Gln/Cr, but not correlated with Glu/Cr. mI/Cr and Gln/Cr furthermore showed a negative correlation with each other. mI/Cr and Glu/Cr were positively correlated.

In the sensorimotor MRS volume, there were no respective correlations between GABA/Cr and mI/Cr ($r = 0.083$, $P = 0.622$) or Gln/Cr ($r = -0.029$, $P = 0.862$). Glu/Cr was not correlated with any other metabolite. mI/Cr was positively correlated to Gln/Cr ($r = -0.757$, $P < 0.001$).

Psychometric testing

Results of the group analysis and correlation analysis of the psychometric test scores are shown in Table 4.

Differences between the control group and both patient groups could be observed for the cognitive scores COG1 and COG2. The line following scores LVT1 and LVT2, the finger tapping speed score MLS4, and the motor reaction time score WRT2 were different between HE1 patients and controls only.

Table 2 Results of MR spectroscopy in hepatic encephalopathy. Asterisks indicate significant differences from controls (* = $P < 0.05$, ** = $P < 0.01$, *** = $P < 0.001$). The two patient groups were not different in any of the comparisons. Bold figures indicate significant correlations

| | Controls mean (+/- SD) | HE patients mean (+/- SD) | | Correlation with CFF [Hz] | | Correlation with blood ammonia [$\mu\text{g/dl}$] | |
|---------------------|---------------------------|------------------------------|------------------|------------------------------|--------------|--|------------------|
| | | mHE | HE1 | <i>r</i> | <i>P</i> | <i>r</i> | <i>P</i> |
| Visual | | | | | | | |
| GABA/Cr | 0.107 (0.011) | 0.089* (0.026) | 0.082** (0.011) | 0.401 | 0.013 | -0.434 | 0.006 |
| Glu/Cr | 0.687 (0.107) | 0.661 (0.104) | 0.608 (0.121) | 0.183 | 0.265 | -0.016 | 0.924 |
| Gln/Cr | 0.235 (0.077) | 0.493* (0.248) | 0.558** (0.321) | -0.497 | 0.001 | 0.429 | 0.006 |
| mI/Cr | 0.811 (0.132) | 0.554* (0.152) | 0.464*** (0.223) | 0.473 | 0.002 | -0.456 | 0.004 |
| Sensorimotor | | | | | | | |
| GABA/Cr | 0.0952 (0.011) | 0.0921 (0.015) | 0.0943 (0.014) | -0.184 | 0.263 | -0.095 | 0.564 |
| Glu/Cr | 0.717 (0.071) | 0.752 (0.135) | 0.739 (0.123) | 0.153 | 0.340 | 0.112 | 0.486 |
| Gln/Cr | 0.124 (0.053) | 0.463** (0.275) | 0.562*** (0.360) | -0.505 | 0.001 | 0.632 | <0.001 |
| mI/Cr | 0.930 (0.163) | 0.574** (0.161) | 0.536*** (0.239) | 0.516 | 0.001 | -0.505 | 0.001 |

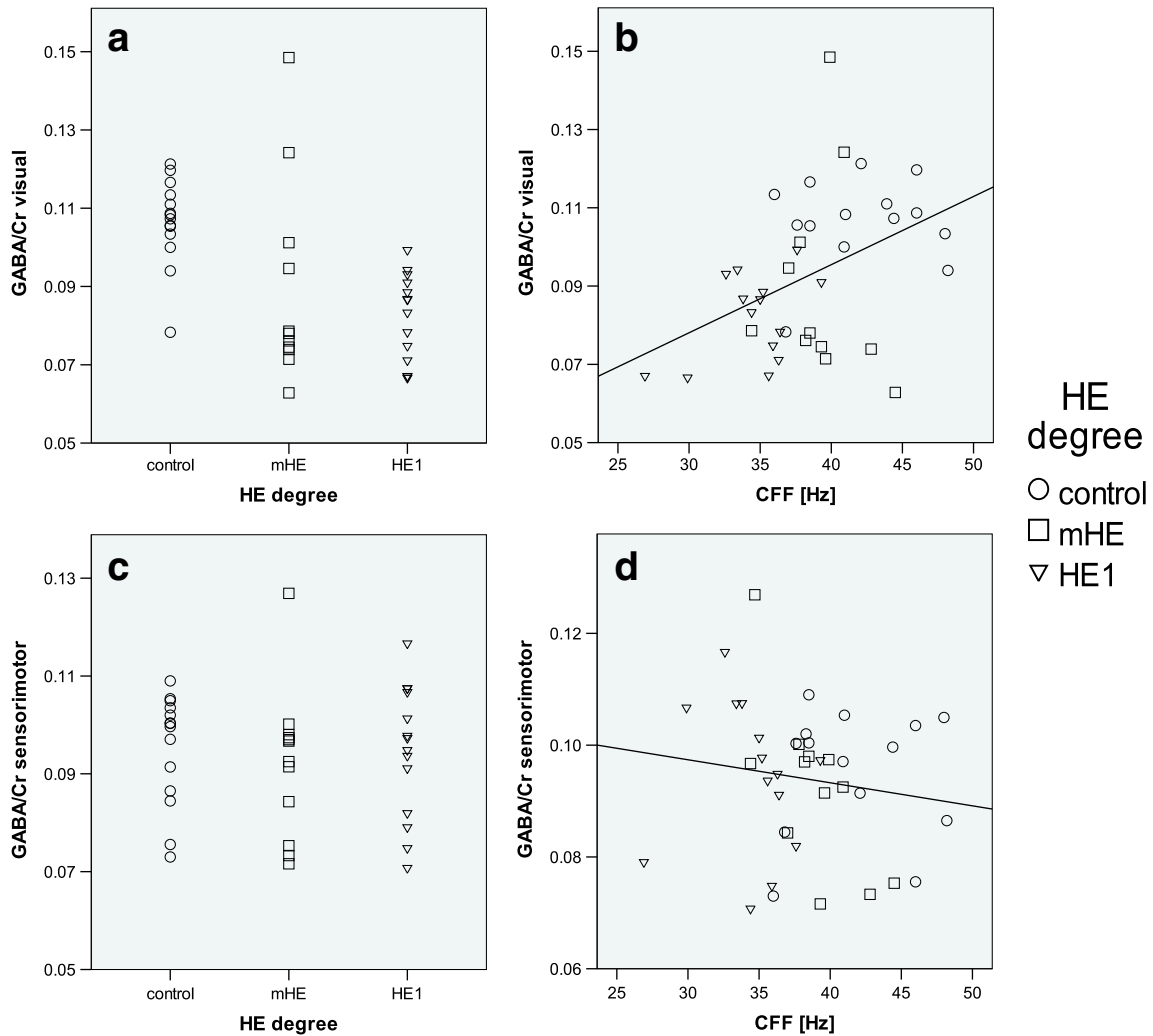


Fig. 4 GABA/Cr group differences in visual (a) and sensorimotor (c) areas and correlations of CFF and GABA/Cr in visual (b) and sensorimotor (d) areas. Group differences and correlations were significant for (a) and (b), but not for (c) and (d)

Table 3 Results of cross correlations for the visual MRS volume. Bold figures indicate significant correlations (FDR corrected at $P < 0.05$)

| | GABA/Cr | mI/Cr | Gln/Cr | Glu/Cr |
|---------|---|-------|--|--------------------------------------|
| GABA/Cr | r = 0.720 P < 0.001 | | r = -0.699 P < 0.001 | $r = 0.189$ $P = 0.270$ |
| mI/Cr | | | r = -0.751 P < 0.001 | r = 0.415 P = 0.009 |
| Gln/Cr | | | | $r = -0.288$ $P = 0.079$ |
| Glu/Cr | | | | |

Data also revealed correlations of visual GABA/Cr with COG1 scores. Additionally, Gln/Cr and mI/Cr correlated with several scores both for the visual and for the sensorimotor volume.

Discussion

In the present in-vivo MR spectroscopy study, we applied edited proton magnetic resonance spectroscopy to investigate

the link between hepatic encephalopathy and blood ammonia levels, neurotransmitter concentrations, and osmolyte concentrations. Our results show reduced visual GABA/Cr both in mHE patients and in HE1 patients. The GABA/Cr ratio is also correlated with CFF, blood ammonia, concentration of myo-inositol and glutamine as well as psychometric parameters.

MR spectroscopy of GABA in HE

Our data demonstrate that GABA/Cr in the visual area is significantly decreased already in early stages of hepatic encephalopathy, i.e. mHE and HE1. This finding tallies with preliminary results from a previous study (Behar et al. 1999) which reported low cortical GABA + homocarnosine in the occipital brain. However, only four HE subjects were included in this study and a graduation of HE severity was missing. Our result of decreased GABA/Cr in visual cortex is also in line with experiments showing an increase of GABAergic tone in the cerebellum, but a decrease in the cortex in a rodent model of HE (Cauli et al. 2009). Moreover, previous studies using localized 2D correlation spectroscopy (L-COSY) at 1.5 T also gave evidence for regionally selective changes in GABA

Table 4 Results of psychometric score analysis (COG1: time to reject a geometric shape not matching control shapes; COG2: time to confirm a geometric shape matching control shapes; line following test: LVT1: time per item; LVT2: overall score; MLS1: hand steadiness/tremor; MLS2: arm/hand precision; MLS3: arm/hand speed; MLS4: finger tapping speed; WRT1: reaction time; WRT2: motor reaction time; VIS: visual MRS

volume; SMOT: sensorimotor MRS volume). Asterisks indicate significant differences from controls (* = $P < 0.05$, ** = $P < 0.01$, *** = $P < 0.001$, Dunn-Bonferroni corrected). The two patient groups were not different in any of the comparisons. Bold figures indicate significant correlations ($P < 0.05$, Benjamini-Hochberg FDR corrected)

| | Differences to control group | | GABA/Cr | | Glu/Cr | | Gln/Cr | | mI/Cr | |
|------|------------------------------|-----------|--------------|--------|--------|--------|------------------|------------------|------------------|------------------|
| | Adjusted P values | | r | P | r | P | r | P | r | P |
| | mHE | HE1 | VIS | SMOT | VIS | SMOT | VIS | SMOT | VIS | SMOT |
| COG1 | 0.008** | <0.001*** | 0.437 | 0.155 | 0.210 | 0.038 | -0.588 | -0.509 | 0.523 | 0.435 |
| | | | 0.006 | 0.339 | 0.192 | 0.811 | <0.001 | 0.001 | 0.001 | 0.004 |
| COG2 | 0.029* | 0.015* | 0.328 | 0.212 | 0.103 | 0.124 | -0.533 | -0.442 | 0.459 | 0.367 |
| | | | 0.044 | 0.189 | 0.525 | 0.435 | <0.001 | 0.003 | 0.003 | 0.017 |
| LVT1 | 0.124 | 0.016* | 0.376 | 0.083 | 0.178 | 0.111 | -0.496 | -0.437 | 0.388 | 0.311 |
| | | | 0.020 | 0.609 | 0.272 | 0.485 | 0.001 | 0.004 | 0.013 | 0.045 |
| LVT2 | 0.215 | 0.038* | 0.319 | 0.202 | 0.172 | 0.027 | -0.403 | -0.390 | 0.288 | 0.229 |
| | | | 0.051 | 0.212 | 0.289 | 0.863 | 0.010 | 0.011 | 0.071 | 0.145 |
| MLS1 | - | - | 0.185 | -0.208 | 0.162 | 0.040 | -0.121 | -0.217 | 0.080 | 0.045 |
| | | | 0.266 | 0.198 | 0.319 | 0.800 | 0.456 | 0.168 | 0.624 | 0.777 |
| MLS2 | - | - | 0.149 | -0.058 | 0.258 | 0.075 | -0.253 | -0.382 | 0.354 | 0.319 |
| | | | 0.371 | 0.723 | 0.108 | 0.637 | 0.115 | 0.013 | 0.025 | 0.040 |
| MLS3 | - | - | 0.112 | 0.045 | 0.157 | -0.016 | -0.175 | -0.325 | 0.267 | 0.228 |
| | | | 0.501 | 0.782 | 0.334 | 0.921 | 0.280 | 0.036 | 0.096 | 0.146 |
| MLS4 | 0.811 | 0.007** | 0.185 | -0.083 | 0.171 | -0.162 | -0.446 | -0.472 | 0.343 | 0.319 |
| | | | 0.266 | 0.613 | 0.293 | 0.306 | 0.004 | 0.002 | 0.030 | 0.040 |
| WRT1 | - | - | 0.263 | 0.139 | 0.351 | 0.146 | -0.420 | -0.238 | 0.402 | 0.334 |
| | | | 0.111 | 0.392 | 0.026 | 0.355 | 0.007 | 0.128 | 0.010 | 0.031 |
| WRT2 | 0.142 | 0.018* | 0.336 | 0.133 | 0.187 | -0.116 | -0.610 | -0.556 | 0.572 | 0.525 |
| | | | 0.039 | 0.414 | 0.247 | 0.463 | <0.001 | <0.001 | <0.001 | <0.001 |

levels by reporting no significant difference of GABA/Cr between minimal HE and healthy controls in the anterior cingulate gyrus (Binesh et al. 2005) as well as the frontal lobe and the occipital lobe (Singhal et al. 2010). Compared to our data, these studies suffered from a very high variability of the measured GABA/Cr values with a standard deviation of >70 % of the group mean in the mHE group in the work of (Singhal et al. 2010). While studying a comparable number of individuals, the high variability might explain why group differences were not observed in these studies.

The present study found strong correlations of GABA/Cr with mI/Cr and Gln/Cr. Furthermore, our data demonstrate correlations of visual GABA/Cr with the CFF and blood ammonia levels. Elevated occipital GABA levels have been previously associated with improved visual orientation discrimination performance (Edden et al. 2009) and contracted time perception of visual intervals (Terhune et al. 2014). In line with these findings, the correlation we report between visual GABA and the CFF suggests that modulation of neural activity by resting GABA concentration is crucial for the individual ability to discern quickly oscillating stimuli. The potential mechanisms are difficult to relate to either specific inhibitory neurotransmission or GABAergic tone in general, as localized MRS is not capable of separating extra- and intrasynaptic GABA pools.

The correlation of visual GABA/Cr and COG1 test scores is concordant with earlier results showing that low visual GABA levels are associated with higher self-reported cognitive failure rates in daily life (Sandberg et al. 2014).

Slowing of oscillatory brain activity in the *gamma* band, as measured with magnetoencephalography (MEG), has been shown to be a feature of HE and to be correlated with the individual CFF (Kahlbrock et al. 2012). In turn, the peak *gamma* frequency has been found to be positively correlated to the resting GABA concentration in the visual area of healthy subjects (Muthukumaraswamy et al. 2009). While these relations would render decreased GABA levels in HE highly plausible, the direct link between peak *gamma* frequency and GABA could not be replicated in a recent study and therefore remains vague (Cousijn et al. 2014).

It is noteworthy that – in contrast to the visual area – our data do not show a correlation between osmolytes and neurotransmitters in the sensorimotor areas. This might indicate that GABAergic tone regulation is either regional-specifically or not even at all coupled to the osmolytic adaptation to hyperammonemia. Furthermore, our results do not reveal a significant change in sensorimotor GABA/Cr compared to controls or correlations with blood ammonia or CFF. Given that HE also slows down oscillatory brain activity in the *beta* band in motor relevant regions (for a review see Butz et al. 2013) and following a proposed link of GABA concentration and motor oscillations (Gaetz et al. 2011), a global decrease of GABA could be expected. In the rodent model, however, it

was shown that HE motor symptoms like hypokinesia might be mediated by alterations of GABA levels in the ventromedial thalamus, ultimately leading to a modulation of cortical glutamate release (Cauli et al. 2008). In fact, the region-sensitive character of changes in extracellular GABA has been shown earlier (Cauli et al. 2009). Finally, taking into account that GABA levels are linked to osmolytes in the visual, but not in the sensorimotor area, our results lend additional support to the conclusion that HE-induced changes in GABAergic tone are regional specific.

An alternative explanation for our negative findings might be that tissue composition effects of the spectroscopic volumes obscured the detection of potential HE-induced changes of the sensorimotor GABA/Cr ratio. The average fractional gray matter volume (27 %) of the sensorimotor area volume is about half the average fractional gray matter volume (57 %) of the visual area volume. Given that GABA concentration is around two-fold higher in GM than WM (Jensen et al. 2005), one might argue that HE-induced changes in GABA/Cr will not be as prominent in white matter dominated volumes, if mainly the neuronal population in gray matter is affected. However, similar MRS volume positions proved to be sensitive to changes in sensorimotor GABA numerous times (for review see Puts and Edden 2012). The correlations of mI/Cr and Gln/Cr with CFF, blood ammonia, and psychometric test results further suggest that hyperammonemic regulation is indeed a global phenomenon in HE, but its subsequent effects on GABA levels again strongly depend on the specific brain region.

MR spectroscopy of other metabolites

Our data coincide with results from several previous studies that demonstrated elevated concentrations of glutamine and decreased levels of myo-inositol in HE (Miese et al. 2006; Chavarria et al. 2013; Alonso et al. 2014). Our analyses yield strong correlations of those metabolites with the CFF, the blood ammonia levels and psychometric test scores, further adding to the importance of recognizing the continuative nature of HE severity progression. Their substantial mutual correlation also underlines the close interaction in the osmolytic regulation.

Interestingly, our results reveal no significant alterations of glutamate levels in HE, albeit it may be linked to the HE-relevant osmolytic actor myo-inositol. Integrating these findings with literature is difficult, as most earlier studies reported combined Glu + Gln levels as Glx.

Limitations

It must be noted that ¹H-MRS levels of GABA represent the overall amount of GABA in the selected tissue volume, regardless of its functional role and prevalence in the extra- or

intracellular space. As GABAergic neurotransmission arises mainly from extracellular GABA, MRS GABA levels do not necessarily reflect the actual degree of inhibitory activity in itself. It is thought that they are markers of the GABAergic tone (Stagg et al. 2011; Rae 2013). In disease, this interpretation has to be handled with caution. As an example, receptor densities or release and uptake mechanisms – all contributing to the GABAergic tone – can be severely altered in HE.

Another potential shortcoming of this study is the implementation of a “classic” spectral editing pulse scheme. With an editing pulse bandwidth of 44 Hz, GABA editing at 1.9 ppm will inevitably co-edit macromolecular (MM) resonances at 1.7 ppm, leading to a contamination of the 3 ppm peak area. Workarounds do exist, but require additional measurements or affect signal-to-noise (Mullins et al. 2014). The fraction of the peak occupied by MM signal is therefore often assumed to be constant, attributing differences in the peak area mainly to differences in GABA concentration. It should be noted, however, that recent work showed that this assumption needs to be handled with care, as MM contribution may vary across brain regions and subjects (Harris et al. 2014).

Last but not least, it is arguable whether separation of glutamine and glutamate in 68 ms PRESS spectra at 3 T is sufficient. Wijtenburg et al. showed that the coefficient of variation of Glu estimation for a 72 ms STEAM sequence (13.8 %) – comparable to our 68 ms PRESS – was acceptable with CRLBs <8 % (Wijtenburg and Knight-Scott 2011). In our study, the LCModel fits of visual Glu yielded CRLBs as low as 12.6 ± 4.9 % (Gln: 17.2 ± 15.0 %), suggesting that separate quantification is reasonable. The higher average Gln variability was mainly driven by the control group that exhibited comparably low Gln concentrations and, accordingly, higher CRLBs.

Conclusions

In this study, we investigated the relationships between GABA, glutamate, glutamine and myo-inositol with HE severity and blood ammonia levels. For both mHE and HE1, data indicate decreased visual levels, which are furthermore correlated to blood ammonia levels, CFF, and brain osmolytes myo-inositol and glutamine. No such outcome could be demonstrated for the sensorimotor area. This may be seen as evidence for a regional specificity of alterations in GABAergic tone in HE.

Acknowledgments The authors would like to express their thanks to Dr. James Murdoch (Toshiba Medical Research Institute USA) for the LCModel basis set and useful discussion on spectral evaluation, Nur-Deniz Füllenbach and Dr. Gerald Kircheis (Department of Gastroenterology, Hepatology and Infectiology, University Hospital Düsseldorf) for help with patient recruitment and psychometric grading, and Erika Rädisch (Department of Diagnostic and Interventional Radiology, University Hospital Düsseldorf) for support with MR measurements.

Funding This work was supported by the Sonderforschungsbereich (SFB) 974 of the Deutsche Forschungsgemeinschaft (DFG).

Conflict of interest The authors declare that they have no conflict of interest.

References

- Alonso J, Córdoba J, Rovira A (2014) Brain magnetic resonance in hepatic encephalopathy. *Semin. Ultrasound CT MRI* 35:136–152
- Behar KL, Rothman DL, Petersen KF, Hooten M, Delaney R, Petroff OAC, Shulman GI, Navarro V, Petrakis IL, Charney DS, et al. (1999) Preliminary evidence of low cortical GABA levels in localized 1 H-MR spectra of alcohol-dependent and hepatic encephalopathy patients. *Am J Psychiatry* 156:952–954
- Binesh N, Huda A, Bugbee M, Gupta R, Rasgon N, Kumar A, Green M, Han S, Thomas MA (2005) Adding another spectral dimension to 1 H magnetic resonance spectroscopy of hepatic encephalopathy. *J Magn Reson Imaging* 21:398–405
- Binesh N, Huda A, Thomas MA, Wyckoff N, Bugbee M, Han S, Rasgon N, Davanzo P, Sayre J, Guze B, et al. (2006) Hepatic encephalopathy: a neurochemical, neuroanatomical, and neuropsychological study. *J Appl Clin Med Phys Am Coll Med Phys* 7:86–96
- Butterworth RF (2000) Complications of cirrhosis III. Hepatic encephalopathy. *J Hepatol* 32(Supplement 1):171–180
- Butz M, May ES, Häussinger D, Schnitzler A (2013) The slowed brain: cortical oscillatory activity in hepatic encephalopathy. *Arch Biochem Biophys* 536:197–203
- Cauli O, Rodrigo R, Llansola M, Montoliu C, Monfort P, Piedrafita B, Mili N el, Boix J, Agustí A, Felipe V (2008) Glutamatergic and gabaergic neurotransmission and neuronal circuits in hepatic encephalopathy. *Metab Brain Dis* 24:69–80
- Cauli O, Mansouri MT, Agustí A, Felipe V (2009) Hyperammonemia increases GABAergic tone in the cerebellum but decreases it in the rat cortex. *Gastroenterology* 136:1359–1367
- Chavarria L, Alonso J, García-Martínez R, Simón-Talero M, Ventura-Cots M, Ramírez C, Torrens M, Vargas V, Rovira A, Córdoba J (2013) Brain magnetic resonance spectroscopy in episodic hepatic encephalopathy. *J Cereb Blood Flow Metab* 33:272–277
- Cousijn H, Haegens S, Wallis G, Near J, Stokes MG, Harrison PJ, Nobre AC (2014) Resting GABA and glutamate concentrations do not predict visual gamma frequency or amplitude. *Proc Natl Acad Sci U S A* 111:9301–9306
- Edden RAE, Muthukumaraswamy SD, Freeman TCA, Singh KD (2009) Orientation discrimination performance is predicted by GABA concentration and gamma oscillation frequency in human primary visual cortex. *J Neurosci*. 29:15721–15726
- Edden RAE, Puts NAJ, Harris AD, Barker PB, Evans CJ (2014) Gannet: a batch-processing tool for the quantitative analysis of gamma-aminobutyric acid-edited MR spectroscopy spectra. *J Magn Reson Imaging* 40:1445–1452
- Felipo V (2013) Hepatic encephalopathy: effects of liver failure on brain function. *Nat Rev Neurosci* 14:851–858
- Ferenci P, Lockwood A, Mullen K, Tarter R, Weissenborn K, Blei AT (2002) Hepatic encephalopathy—definition, nomenclature, diagnosis, and quantification: final report of the working party at the 11th world congresses of gastroenterology, Vienna, 1998. *Hepatology* 35:716–721
- Gaetz W, Edgar JC, Wang DJ, Roberts TPL (2011) Relating MEG measured motor cortical oscillations to resting γ -aminobutyric acid (GABA) concentration. *NeuroImage* 55:616–621
- Harris AD, Puts NAJ, Barker PB, Edden RAE (2014) Spectral-editing measurements of GABA in the human brain with and without

- macromolecule suppression. *Magn Reson Med* Published Online: December 17, 2014. doi:10.1002/mrm.25549
- Häussinger D, Schliess F (2008) Pathogenetic mechanisms of hepatic encephalopathy. *Gut* 57:1156–1165
- Häussinger D, Sies H (2013) Hepatic encephalopathy: clinical aspects and pathogenetic concept. *Arch Biochem Biophys* 536:97–100
- Häussinger D, Laubenberg J, Vom Dahl S, Ernst T, Bayer S, Langer M, Gerok W, Hennig J (1994) Proton magnetic resonance spectroscopy studies on human brain Myo-inositol in hypo-osmolarity and hepatic encephalopathy. *Gastroenterology* 107:1475–1480
- Hone-Blanchet A, Salas RE, Celnik P, Kalloo A, Schar M, Puts NAJ, Harris AD, Barker PB, Fecteau S, Earley CJ, et al. (2015) Co-registration of magnetic resonance spectroscopy and transcranial magnetic stimulation. *J Neurosci Methods* 242:52–57
- Jensen JE, Frederick BB, Renshaw PF (2005) Grey and white matter GABA level differences in the human brain using two-dimensional J-Resolved spectroscopic Imaging *NMR Biomed* 18:570–576
- Kahlbrock N, Butz M, May ES, Brenner M, Kircheis G, Häussinger D, Schnitzler A (2012) Lowered frequency and impaired modulation of gamma band oscillations in a bimodal attention task are associated with reduced critical flicker frequency. *NeuroImage* 61:216–227
- Kircheis G, Wettstein M, Timmermann L, Schnitzler A, Häussinger D (2002) Critical flicker frequency for quantification of low-grade hepatic encephalopathy. *Hepatology* 35:357–366
- Kircheis G, Hilger N, Häussinger D (2014) Value of critical flicker frequency and psychometric hepatic encephalopathy score in diagnosis of low-grade hepatic encephalopathy. *Gastroenterology* 146:961–969
- Laubenberg J, Häussinger D, Bayer S, Gufler H, Hennig J, Langer M (1997) Proton magnetic resonance spectroscopy of the brain in symptomatic and asymptomatic patients with liver cirrhosis. *Gastroenterology* 112:1610–1616
- Llansola M, Montoliu C, Agustí A, Hernandez-Rabaza V, Cabrera-Pastor A, Gomez-Gimenez B, Malaguenera M, Dadsetan S, Belghiti M, Garcia-Garcia R, et al. (2014) Interplay between glutamatergic and GABAergic neurotransmission alterations in cognitive and motor impairment in minimal hepatic encephalopathy. *Neurochem Int*. doi:10.1016/j.neuint.2014.10.011
- Mardini H, Smith FE, Record CO, Blamire AM (2011) Magnetic resonance quantification of water and metabolites in the brain of cirrhotics following induced hyperammonaemia. *J Hepatol* 54:1154–1160
- Mescher M, Merkle H, Kirsch J, Garwood M, Gruetter R (1998) Simultaneous in vivo spectral editing and water suppression. *NMR Biomed* 11:266–272
- Miese F, Kircheis G, Wittsack HJ, Wenserski F, Hemker J, Mödder U, Häussinger D, Cohnen M (2006) 1 H-MR spectroscopy, magnetization transfer, and diffusion-weighted imaging in alcoholic and non-alcoholic patients with cirrhosis with hepatic encephalopathy. *Am J Neuroradiol* 27:1019–1026
- Mullins PG, McGonigle DJ, O’Gorman RL, Puts NAJ, Vidyasagar R, Evans CJ, Edden RAE (2014) Current practice in the use of MEGA-PRESS spectroscopy for the detection of GABA. *NeuroImage* 86: 43–52
- Muthukumaraswamy SD, Edden RAE, Jones DK, Swettenham JB, Singh KD (2009) Resting GABA concentration predicts peak gamma frequency and fMRI amplitude in response to visual stimulation in humans. *Proc Natl Acad Sci* 106:8356–8361
- Palomero-Gallagher N, Zilles K (2013) Neurotransmitter receptor alterations in hepatic encephalopathy: a review. *Arch Biochem Biophys* 536:109–121
- Provencher SW (2001) Automatic quantitation of localized in vivo 1H spectra with LCModel. *NMR Biomed* 14:260–264
- Puts NAJ, Edden RAE (2012) In vivo magnetic resonance spectroscopy of GABA: a methodological review. *Prog Nucl Magn Reson Spectrosc* 60:29–41
- Rae CD (2013) A guide to the metabolic pathways and function of metabolites observed in human brain 1 H magnetic resonance spectra. *Neurochem Res* 39:1–36
- Sandberg K, Blicher JU, Dong MY, Rees G, Near J, Kanai R (2014) Occipital GABA correlates with cognitive failures in daily life. *NeuroImage* 87:55–60
- Schafer DF, Jones EA (1982) Hepatic encephalopathy and the gamma-aminobutyric-acid neurotransmitter system. *Lancet* 319:18–20
- Sergeeva OA (2013) GABAergic transmission in hepatic encephalopathy. *Arch Biochem Biophys* 536:122–130
- Shah NJ, Neeb H, Kircheis G, Engels P, Häussinger D, Zilles K (2008) Quantitative cerebral water content mapping in hepatic encephalopathy. *NeuroImage* 41:706–717
- Shawcross DL, Balata S, Damink SWMO, Hayes PC, Wardlaw J, Marshall I, Deutz NEP, Williams R, Jalan R (2004) Low myo-inositol and high glutamine levels in brain are associated with neuropsychological deterioration after induced hyperammonemia. *Am J Physiol - Gastrointest Liver Physiol* 287:G503–G509
- Singhal A, Nagarajan R, Hinkin CH, Kumar R, Sayre J, Elderkin-Thompson V, Huda A, Gupta RK, Han S-H, Thomas MA (2010) Two-dimensional MR spectroscopy of minimal hepatic encephalopathy and neuropsychological correlates in vivo. *J Magn Reson Imaging* 32:35–43
- Stagg CJ, Bachtar V, Johansen-Berg H (2011) What are we measuring with GABA magnetic resonance Spectroscopy? *Commun Integr Biol* 4:573–575
- Terhune DB, Russo S, Near J, Stagg CJ, Kadosh RC (2014) GABA predicts time perception. *J Neurosci* 34:4364–4370
- Thomas MA, Huda A, Guze B, Curran J, Bugbee M, Fairbanks L, Ke Y, Oshiro T, Martin P, Fawzy F (1998) Cerebral 1 H MR spectroscopy and neuropsychologic status of patients with hepatic encephalopathy. *Am J Roentgenol* 171:1123–1130
- Timmermann L, Gross J, Butz M, Kircheis G, Häussinger D, Schnitzler A (2003) Mini-asterix in hepatic encephalopathy induced by pathologic thalamo-motor-cortical coupling. *Neurology* 61:689–692
- Wijtenburg SA, Knight-Scott J (2011) Very short echo time improves the precision of glutamate detection at 3 T in 1 H magnetic resonance spectroscopy. *J Magn Reson Imaging* 34:645–652
- Yousry TA, Schmid UD, Alkadhi H, Schmidt D, Peraud A, Buettner A, Winkler P (1997) Localization of the motor hand area to a knob on the precentral gyrus. A new Landmark *Brain* 120:141–157

Covert hepatic encephalopathy: Elevated total glutathione and absence of brain water content changes

Georg Oeltzschner^{1,2,*}, Markus Butz, PhD¹,

Frithjof Wickrath², Hans-Jörg Wittsack, PhD², Alfons Schnitzler, MD¹

¹ Institute of Clinical Neuroscience and Medical Psychology,

Medical Faculty, Heinrich-Heine-University Düsseldorf, D-40225 Düsseldorf, Germany

² Department of Diagnostic and Interventional Radiology,

Medical Faculty, Heinrich-Heine-University Düsseldorf, D-40225 Düsseldorf, Germany

* Corresponding author.

Address: Institute of Clinical Neuroscience and Medical Psychology,

Medical Faculty, Heinrich-Heine-University Düsseldorf,

Universitätsstr. 1, D-40225 Düsseldorf, Germany.

Tel.: +49 211 81 08609.

E-mail: georg.oeltzschner@med.uni-duesseldorf.de

Keywords: Hepatic encephalopathy; MR spectroscopy; glutathione; ammonia;
brain water content

Abbreviations: HE, hepatic encephalopathy; GSx, total glutathione; GSH, reduced glutathione; GSSG, oxidized glutathione; OS, oxidative stress; CFF, critical flicker frequency; MRS, magnetic resonance spectroscopy; GABA, γ -aminobutyric acid; Glu, glutamate; Gln, glutamine; mI, myo-inositol; Cr, creatine; MEGA-PRESS; Mescher-Garwood point resolved spectroscopy; TR, repetition time; TE, echo time; FoV, field of view; CRLB, Cramér-Rao lower bounds; GM, grey matter; WM, white matter; CSF, cerebrospinal fluid.

Abstract

Introduction: Recent pathophysiological models suggest that oxidative stress and hyperammonemia lead to a mild brain oedema in hepatic encephalopathy (HE). Glutathione (GSx) is a major cellular antioxidant and known to be involved in the interception of both. The aim of this work was to study total glutathione levels in covert HE (minimal HE and HE grade 1) and to investigate their relationship with local brain water content, levels of glutamine (Gln), myo-inositol (mI), neurotransmitter levels, critical flicker frequency (CFF), and blood ammonia.

Materials and methods: Proton magnetic resonance spectroscopy (^1H MRS) data were analysed from visual and sensorimotor cortices of thirty patients with covert HE and 16 age-matched healthy controls. Total glutathione levels (GSx/Cr) were quantified with respect to creatine. Furthermore, quantitative MRI brain water content measures were evaluated. Data were tested for links with the CFF and blood ammonia.

Results: GSx/Cr was elevated in the visual (mHE) and sensorimotor (mHE, HE 1) MRS volumes and correlated with blood ammonia levels (both $P < 0.001$). It was further linked to Gln/Cr and mI/Cr ($P < 0.01$ in visual, $P < 0.001$ in sensorimotor) and to GABA/Cr ($P < 0.01$ in visual). Visual GSx/Cr correlated with brain water content in the thalamus, *nucleus caudatus*, and visual cortex ($P < 0.01$). Brain water measures did neither show group effects nor correlations with CFF or blood ammonia.

Conclusions: Elevated total glutathione levels in covert HE (< HE 2) correlate with blood ammonia and may be a regional-specific reaction to hyperammonemia and oxidative stress. Brain water content is locally linked to visual glutathione levels, but appears not to be associated with changes of clinical parameters. This might suggest that cerebral oedema is only be marginally responsible for the symptoms of covert HE.

1. Introduction

Hepatic encephalopathy (HE) is a neuropsychiatric complication that frequently accompanies liver cirrhosis. Symptoms include impairment of cognitive, behavioural, and motor functions. Their severity varies, beginning with subtle changes in neuropsychometric test scores, i.e. the so-called *minimal HE* (mHE). *Overt HE* – delineated by the West-Haven criteria (Ferenci et al. 2002) – reflects an increasing deterioration of the mental state from *HE 1* up to somnolence, stupor, and even hepatic coma (*HE 4*) (Butterworth 2000; Felipo 2013). Recently, a revised classification has been suggested to meet the substantial subjectivity in the assessment of clinical symptoms – most importantly the change of mental state – more appropriately, as especially the discrimination of minimal HE and HE 1 was not deemed satisfactory (Bajaj et al. 2011; Waghray et al. 2015). Rather than classifying patients as either minimal HE (without change of mental state) or overt HE (with change of mental state), the term *covert HE* was coined to define patients who present neuropsychometric changes, but do not exhibit clear clinical features of HE such as disorientation and motor symptoms like asterixis (Bajaj et al. 2011). According to the revised classification, *covert HE* comprises the mHE and HE 1 groups, and stands opposed to *overt HE* with clear exhibitions of the clinical symptoms (HE 2 – HE 4).

The common thread in the complex and multi-factorial model of HE pathogenesis is ammonia. With the liver increasingly losing its filter function, the blood ammonia level rises. Finally, ammonia accumulates in the brain and triggers oxidative stress (OS), inflammation, and numerous other alterations regarding protein synthesis, receptor and transporter activity and metabolic pathways (Häussinger and Schliess 2008). In

addition, a global slowing of neural oscillations was described and suggested to underlie the global functional deficits in HE patients (Butz et al. 2013).

A low-grade cerebral oedema is believed to act as a mediator towards these functional impairments. Detoxification of ammonia in the astrocytes by glutamine synthetase (GS) causes glutamine (Gln) accumulation. This results in an osmotic gradient that may be partially balanced by release of myo-inositol (mI) from the astrocytes, but will induce cell swelling with increasing osmolyte depletion (Häussinger and Sies 2013). Both Gln increase and mI decrease have been consistently observed with magnetic resonance spectroscopy and linked to blood ammonia, HE severity, and diffusion parameters (Laubenberger et al. 1997; Miese et al. 2006). Using quantitative water mapping, small increases of white matter water content with increasing HE severity were demonstrated (Shah et al. 2008).

In a rodent model of chronic HE, cerebral oedema have recently been shown not to be elicited by either OS or hyperammonemia alone, but by synergistic effects of both (Bosoi et al. 2014a). A compound that is vitally involved in the adaptation to both OS and hyperammonemia is reduced glutathione (GSH), the most abundant antioxidant in the human brain. This tripeptide is capable of scavenging reactive oxygen species and thus decreasing OS (Bains and Shaw 1997). In the process, it converts to its oxidized form (GSSG) which can be recycled back for the replenishment of GSH by glutathione reductase to sustain the antioxidant potential of the cell. *In vitro* ammonia challenge experiments showed an increase of total glutathione levels (GSH+GSSG, henceforth labelled *GSt*) and stimulation of glutathione synthesis (Murthy et al. 2000; Wegrzynowicz et al. 2007) in cultured astrocytes, but total glutathione decrease and cell death in cultured neurons (Klejman et al. 2005). *In vivo* data from rodents showed that

hyperammonemia is associated with an increased glutathione synthesis and boosts export from the astrocytes to the extracellular space. This mechanism helps defending the otherwise unprotected neurons (Hilgier et al. 2010). Elevated total glutathione was also demonstrated *in vivo* in rodent cortex, cerebellum, and medulla after induced acute liver failure (Sathyaikumar et al. 2007). In summary, glutathione is involved in the regulation and interception of the deleterious effects of oxidative stress and hyperammonemia. As both are prerequisites for the precipitation of cerebral oedema, total glutathione levels might be directly related to emergence, extent, and impact of brain water disturbances in HE.

Glutathione can be noninvasively detected and quantified *in vivo* with magnetic resonance spectroscopy (MRS) (Terpstra et al. 2002). Though optimized detection protocols do exist (Terpstra et al. 2003), it has been shown that reliable GSH levels can also be obtained from unedited subspectra of J-edited MEGA-PRESS acquisitions (Michels et al. 2014). These can provide sufficient signal-to-noise ratio, as they require comparably large MRS volumes for their routine use in quantification of gamma-aminobutyric acid (GABA). This enabled us to re-analyse previously acquired GABA-focused MRS data, with attention to potential changes of total glutathione concentration in hepatic encephalopathy.

The aim of the present study was to re-analyse *in vivo* MR spectroscopy data from a population of HE patients and healthy controls, with focus on the role of total glutathione. Hence, it was intended to scrutinize whether the levels of this major antioxidant compound relate to clinical severity, ammonia load, or brain water content.

Ultimately, the role of glutathione in the regulation of hyperammonemia and oxidative stress in the pathophysiology of HE may be further elucidated.

To this end, we analysed total glutathione levels from a cohort of patients with covert hepatic encephalopathy (mHE and HE 1) and healthy controls, along with quantitative MR brain water content measures, blood ammonia, CFF, and their links to the levels of total glutathione, GABA, glutamate, glutamine, and myo-inositol.

2. Material and methods

The data under study stems from a recently acquired data set, which was analysed regarding GABA quantification previously (Oeltzschner et al. 2015). The study was performed conforming to the principles of the revised Declaration of Helsinki and approved by the local ethics committee (study number 3644). All recruited participants gave their full prior written informed consent before they participated.

2.1. Patients and healthy controls

Thirty patients with covert hepatic encephalopathy (defined as minimal HE or HE grade 1 (Bajaj et al. 2011)) and 16 healthy controls participated in this study. Patients were included if they had been diagnosed with clinically confirmed liver cirrhosis and minimal HE (Kircheis et al. 2002) or HE of grade 1. Healthy controls were enrolled in a third group to age-match the two patient groups.

Patients and controls were excluded if they suffered from any severe internal, neurological or psychiatric diseases other than HE, peripheral or retinal neuropathy, or reported use of psychoactive substances. Participants with reported alcohol dependency

in their medical history needed to remain abstinent for at least 4 weeks prior before the study. Additional exclusion criteria were pregnancy and blood clotting dysfunction.

2.2 HE grading

HE severity was categorized according to the *West-Haven* criteria with psychometric testing and a clinical assessment of the mental state and consciousness by an experienced clinician including the assessment of the critical flicker frequency (CFF). The CFF was assessed as it has been demonstrated by several groups to be a reliable complementary parameter for the diagnosis and monitoring of HE severity. It allows indexing HE severity in a fine-graded manner accounting for the continuous nature of HE progression (Kircheis et al. 2002; Romero-Gómez et al. 2007; Sharma et al. 2007; Torlot et al. 2013). In addition, it has been shown to reflect both oscillatory brain activity in different brain regions and behavioural performance (Butz et al. 2013), e.g. motor performance (Butz et al. 2010) and somatosensory perception (Brenner et al. 2015).

For the psychometric testing, five batteries of computer-based neuropsychological tests from the Vienna Test System (Dr. Schuhfried GmbH, Mödling, Austria) were performed by each individual and revealed 22 age-validated scores reflecting cognitive and motor performance (reported as percentage ranks from comparison with age-matched control cohorts). If a parameter value deviated more than 1σ from the mean of the control cohort, it was considered *abnormal*. Patients with no clinical symptoms of manifest HE, but more than 2 abnormal psychometric scores, were classified as *mHE* (minimal HE) (Kircheis 2002). Additionally, all participants underwent standard blood tests including measurement of venous ammonia levels.

Two participants (1 mHE, 1 HE 1) were excluded after assessment due to positive blood ethanol testing on the day of recording. One participant (initially classified as HE 1) had to be excluded due to imprecise patient files. The remaining population under study is characterized in **Table 1**.

| | n | male / female | Age [y] | CFF [Hz] | Etiology of cirrhosis |
|---------------|----------|----------------------|----------------|--------------------|--|
| Contr. | 16 | 7 / 9 | 60.1 ± 8.7 | 41.6 ± 4.0 | - |
| mHE | 13 | 8 / 5 | 55.7 ± 8.5 | 39.4 ± 3.2 | 7 ALC, 4 CRYP, 1 HBV, 1 AI |
| HE 1 | 14 | 10 / 4 | 61.6 ± 7.6 | 34.5* ± 3.1 | 7 ALC, 3 CRYP, 2 NASH, 1 HCV, 1 PSC |

Table 1: Healthy control (Contr.) and patient populations. Asterisks indicate significant differences of HE 1 group from mHE and from controls (Kruskal-Wallis test, both $P < 0.001$). AI = autoimmune, ALC = alcoholic, CRYP = cryptogenic, HBV = hepatitis B virus, HCV = hepatitis C virus, NASH = non-alcoholic steatohepatitis, PSC = primary sclerosing cholangitis.

2.3. MR measurements

MR data collection was performed on a clinical 3T whole-body MRI scanner (Siemens MAGNETOM Trio A TIM System, Siemens Healthcare AG, Erlangen, Germany) with a 12-channel head matrix coil.

2.3.1. MR spectroscopy

T_1 -weighted planning sequences were used to localize MRS volumes in distinct anatomical positions (please see (Oeltzschner et al. 2015) for a detailed image). The

“visual” spectroscopic volume was placed in the central occipital lobe. One “sensorimotor” volume in each hemisphere was placed on the “*hand knob*” (Yousry et al. 1997) to include both sensory and motor cortex areas. MEGA-PRESS (Mescher et al. 1998) spectra were acquired from these volumes (no. of excitations = 192, TR = 1500 ms, TE = 68 ms, V = 3 × 3 × 3 cm³, bandwidth = 1200 Hz, 1024 data points). Gaussian (bandwidth 44 Hz) pulses irradiated at 1.9 ppm and 7.5 ppm were employed for frequency selective spectral editing.

Creatine-normalized measures of total glutathione (GSx/Cr), glutamine (Gln/Cr), glutamate (Glu/Cr), and myo-inositol (mI/Cr) were obtained with LCModel version 6.3 (Provencher 2001) by linear composition of the unedited MEGA-PRESS spectra (*OFF* resonance) into its spectral components (**Fig. 1**). Their variance was provided by LCModel as CRLB (Cramér-Rao lower bounds).

Sensorimotor data were calculated by averaging the metabolite-to-creatine ratios from both hemispheres. If acquisition was unsuccessful or evaluation failed for one side, the estimate from the remaining side was used for further analysis.

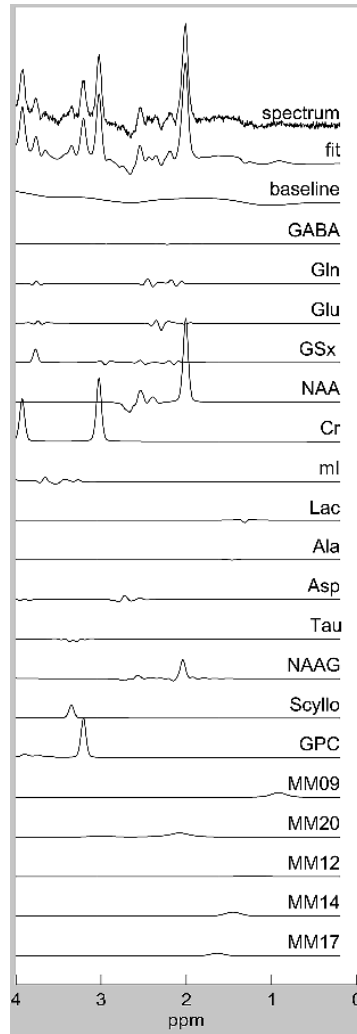


Fig. 1 Linear decomposition of an unedited (OFF resonance) MEGA-PRESS spectrum into its spectral components with LCModel. Metabolite levels were subsequently normalized to the creatine signal.

MEGA-PRESS difference spectra were processed with GANNET 2.0 (Edden et al. 2014), performing frequency and phase correction and Gaussian fitting of the 3 ppm GABA resonance to output the GABA-to-creatine ratio (GABA/Cr), which was used for further analysis.

2.3.2. Mapping of cerebral water content

Quantitative water content maps of the brain were created with an in-house developed MATLAB routine (The Mathworks Inc., Natick/MA) that has been published and applied in hepatic encephalopathy patients before (Neeb et al. 2006b; Shah et al. 2008; Neeb et al. 2008). Data acquisition included two gradient echo (GRE) sequences (FoV 256×192 mm, 256x192 matrix, slice thickness = 2 mm, gap = 1 mm, 50 slices) and three echo planar imaging (EPI) sequences (TE = 16 ms, FoV 256×192 mm, 64×48 matrix, slice thickness = 2 mm, gap = 1 mm, 50 slices): i) GRE for backwards extrapolation of the initial water magnetization (TR = 2140 ms, 8 echoes with TE = 4/9/14/19... ms); ii) GRE for T_1 mapping (TR = 638 ms, 2 echoes with TE = 4/9 ms); iii) EPI (90° flip angle); iv) EPI (30° flip angle); and v) EPI (30° flip angle, acquired with the body coil as receiver coil) to account for coil and B_1 field inhomogeneities. Transversal T_1 -weighted 3D magnetization prepared gradient echo (MP RAGE, TR / TE = 1950 / 4.6 ms, FoV 256×192 mm, 256×192 matrix, slice thickness 1 mm, 176 slices) images were acquired at the end of the measurement.

Structural data were segmented into grey matter (GM), white matter (WM), and cerebrospinal fluid (CSF) with the ‘New Segment’ tool of SPMv8.

The quantitative water maps of each participant were co-registered to the respective structural and subsequently evaluated in three different ways:

- i) Global analysis: Average water contents for GM and WM were computed across all voxels with a respective tissue probability of >0.9 to circumvent partial volume effects.
- ii) Spectroscopic volume analysis: The MR spectroscopic volume parameters were transformed into a binary mask that was subsequently co-registered to the structural with a custom-made MATLAB routine (Dr. Nia Goulden, Dr. Paul Mullins, Bangor

University, <http://biu.bangor.ac.uk/projects.php.en>, modified to process Siemens file format). Fractions of GM, WM, and CSF and their respective average water contents were calculated for each volume.

iii) Interactive ROI analysis: 10 individual regions of interest (ROI) were interactively defined in the *nucleus caudatus*, putamen, *globus pallidus*, thalamus, *corpus callosum*, *centrum semiovale*, prefrontal and occipital white matter, visual, and prefrontal cortex. The ROIs were drawn on the individual structural maps as they offer improved contrast compared to the quantitative water maps.

2.4. Statistics

All statistical computations were performed with IBM SPSS Statistics for Windows, Version 22.0 (IBM Corp., Armonk, NY, USA).

Non-parametric Kruskal-Wallis one way analysis of variance for independent samples was used to assess differences of metabolite levels, tissue fractions (GM, WM, CSF) and brain water content parameters between the participant groups (controls, mHE, and HE 1). Post-hoc tests with Dunn-Bonferroni correction for multiple comparisons were performed to give adjusted P values. Group differences were significant if adjusted $P < 0.05$.

Mutual bivariate two-tailed Spearman's rank correlation analysis was conducted to test for relations between tissue fractions (GM, WM, CSF) of the spectroscopic volumes and their metabolite or tissue-specific water content measures, including Benjamini-Hochberg false discovery rate (FDR) correction at $\alpha = 0.05$.

Partial two-tailed correlation analysis was used to investigate relationships between CFF (including correction for age) and metabolite levels. Bivariate two-tailed

Spearman's rank correlation analysis was used to discover links between metabolite levels, brain water content measures, and blood ammonia, with application of Benjamini-Hochberg false discovery rate (FDR) correction at $\alpha = 0.05$ to account for multiple comparison.

Mutual bivariate two-tailed Spearman's rank correlation analysis was performed for GSx/Cr, Gln/Cr, mI/Cr, Glu/Cr, and GABA/Cr to investigate their interdependencies (separately for the sensorimotor and visual MRS data), including Benjamini-Hochberg false discovery rate (FDR) correction at $\alpha = 0.05$.

3. Results

Out of 43 participants, metabolite-to-creatine estimates from the unedited visual spectra could be obtained in all but 3 participants (2 controls, 1 mHE). Visual GABA-to-creatine estimates were obtained in all but 4 individuals (2 controls, 2 mHE). Unedited sensorimotor spectra could not be analysed in one healthy control. Sensorimotor GABA-to-creatine estimates were obtained in all but 3 individuals (2 controls, 1 mHE). Data from only one hemisphere was used for one unedited spectrum (1 mHE) and eight GABA difference spectra (4 controls, 2 mHE, 2 HE 1).

No significant differences between males and females were observed. Moreover, no correlations of any metabolite measure with tissue volume fractions within the spectroscopic volumes were observed. Tissue fractions did not differ between controls, mHE or HE 1 groups, indicating that individual tissue composition did not influence the observation of HE-related metabolite findings.

3.1. MR spectroscopy

Results of the group analysis and correlation analysis of total glutathione (GSx/Cr) with CFF and blood ammonia are summarized in **Table 2**.

| GSx/Cr | Controls mean (+/- SD) | mHE mean (+/- SD) | HE 1 mean (+/- SD) | vs. CFF [Hz] | | vs. blood ammonia [$\mu\text{g}/\text{dl}$] | |
|--------------------------|------------------------------|----------------------------------|----------------------------------|-----------------|-------------|--|-----------------|
| | | | | <i>r</i> | <i>P</i> | <i>r</i> | <i>P</i> |
| visual | 0.199 (0.030) | 0.260* (0.071) | 0.235 (0.055) | -.276 | .089 | .578 | <.001 |
| sensori motor | 0.184 (0.028) | 0.248** (0.052) | 0.242** (0.048) | -.312 | .047 | .575 | <.001 |

Table 2: Total glutathione levels (expressed as ratios to creatine) measured with magnetic resonance spectroscopy in hepatic encephalopathy. Asterisks indicate significant differences from controls (Kruskal-Wallis test, * $P < 0.05$, ** $P < 0.01$). No significant differences were observed between mHE and HE 1 groups. Bold figures indicate significant correlations ($P < 0.05$).

3.1.2. Glutamine

Visual and sensorimotor Gln/Cr levels were significantly elevated in the mHE and HE 1 groups. Gln/Cr correlated negatively with CFF (visual: $r = -.497$, $P = .001$, sensorimotor: $r = -.505$, $P = .001$) and positively with blood ammonia (visual: $r = .429$, $P = .006$, sensorimotor: $r = .632$, $P < .001$).

3.1.3. myo-Inositol

mI/Cr levels in the visual and sensorimotor areas were decreased significantly in the mHE and HE 1 groups compared to the control group. A positive correlation of mI/Cr with CFF (visual: $r = .473$, $P = .002$, sensorimotor: $r = .516$, $P = .001$) and a negative

correlation with blood ammonia (visual: $r = -.456$, $P = .004$, sensorimotor: $r = -.505$, $P = .001$) were observed.

3.1.4. GABA

Visual GABA/Cr levels were significantly reduced in the mHE and the HE 1 group compared to controls. Additionally, visual GABA/Cr correlated positively with CFF ($r = .401$, $P = .013$) and negatively with blood ammonia ($r = -.434$, $P = .006$). No group differences or correlations could be revealed for the sensorimotor GABA/Cr levels.

3.1.5. Glutamate

Levels of Glu/Cr did not exhibit significant differences in mHE or HE 1 compared to controls or correlations with CFF or blood ammonia. This was true both for the visual and for the sensorimotor areas.

3.1.6 Cross correlations of metabolites

Cross analysis of the visual metabolite levels resulted in several findings (**Table 3**).

| | mI/Cr | Gln/Cr | GABA/Cr | Glu/Cr |
|----------------|---|--|--|--|
| GSx/Cr | $r = -.452$ $P = .004$ | $r = .493$ $P = .002$ | $r = -.451$ $P = .006$ | $r = -.047$ $P = .782$ |
| mI/Cr | | $r = -.751$ $P < .001$ | $r = .720$ $P < .001$ | $r = .415$ $P = .009$ |
| Gln/Cr | | | $r = -.699$ $P < .001$ | $r = -.288$ $P = .079$ |
| GABA/Cr | | | | $r = .189$ |

| | | | | |
|--|--|--|--|------------|
| | | | | $P = .270$ |
|--|--|--|--|------------|

Table 3: Metabolite cross-correlations in the visual MRS volume. Bold figures indicate significant correlations (after Benjamini-Hochberg false discovery rate correction).

GSx/Cr correlated negatively with mI/Cr and GABA/Cr, and positively with Gln/Cr. mI/Cr was negatively associated with Gln/Cr and Glu/Cr, and positively correlating with GABA/Cr. Gln/Cr correlated negatively with GABA/Cr.

In the sensorimotor MRS volume, GSx/Cr correlated negatively with mI/Cr ($r = -.544$, $P < .001$) and positively with Gln/Cr ($r = .726$, $P < .001$) which were in turn anticorrelated to each other ($r = -.757$, $P < .001$).

3.2. Brain water content

Three individuals (1 control, 1 mHE, 1 HE 1) cancelled the measurements before the watermapping sequences. For 12 participants (4 controls, 3 mHE, 5 HE 1), reconstruction of reliable water maps failed or yielded very noisy maps which were excluded after visual inspection.

Average brain water measures for the healthy control population were 71.6 ± 1.5 % for white matter and 81.9 ± 1.8 % for gray matter. These results are within the range of previously published values obtained with a comparable watermapping method (70.9 ± 1.1 % and 81.2 ± 1.2 % (Neeb et al. 2006b), 70.3 ± 1.4 % and 79.7 ± 2.0 % (Neeb et al. 2006a), 70.8 ± 1.2 % in WM (Shah et al. 2008)). Representative maps (healthy control no. 0573 and patient no. 582) are depicted in **Fig. 2**.

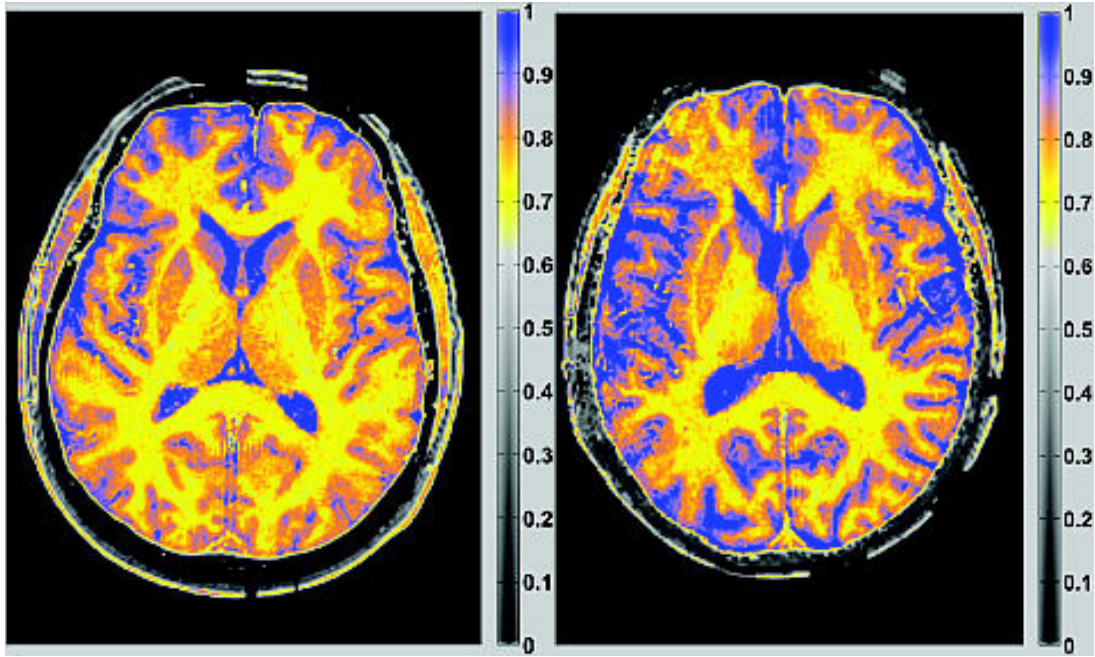


Fig. 2: Exemplary colour-coded brain water content map of a healthy control (left, female, 58 years) and HE patient (right, female, 58 years). The colour bar indicates the brain water content with respect to 100% (pure water).

Quantitative brain water content analysis did not yield any significant group effects or correlations with blood ammonia or CFF. This was true for the global, the MRS volume, and the ROI analyses (**Table 4**).

| water content (%) | Controls mean (+/- SD) | mHE mean (+/- SD) | HE 1 mean (+/- SD) | vs. CFF [Hz] | | vs. blood ammonia [$\mu\text{g}/\text{dl}$] | |
|---------------------|---------------------------|----------------------|-----------------------|--------------|----------|---|----------|
| | | | | <i>r</i> | <i>P</i> | <i>r</i> | <i>P</i> |
| global | | | | | | | |
| white matter | 71.6 (1.5) | 71.6 (1.5) | 72.1 (1.3) | .136 | .483 | .028 | .884 |
| grey matter | 81.9 (1.8) | 82.9 (1.9) | 82.6 (0.7) | .176 | .370 | .185 | .345 |
| MRS volume | | | | | | | |
| WM motor | 71.6 (1.4) | 71.4 (1.5) | 71.7 (1.2) | .220 | .261 | -.025 | .899 |
| GM motor | 83.7 (1.9) | 84.2 (2.3) | 83.3 (1.4) | .291 | .134 | -.050 | .799 |
| WM visual | 74.3 (1.4) | 75.3 (2.0) | 74.4 (1.2) | .253 | .213 | .001 | .996 |
| GM visual | 84.0 (1.8) | 85.8 (2.7) | 84.7 (1.0) | .113 | .583 | .052 | .801 |
| ROI analysis | | | | | | | |

| | | | | | | | |
|-------------------|------------|------------|------------|-------|------|-------|------|
| Nucleus caudatus | 82.2 (1.4) | 82.9 (2.5) | 82.5 (2.9) | .132 | .504 | .106 | .592 |
| Putamen | 81.8 (1.5) | 81.8 (2.3) | 81.9 (1.6) | .145 | .461 | .084 | .672 |
| Globus pallidus | 75.2 (1.7) | 75.4 (2.3) | 76.7 (1.9) | -.328 | .088 | .183 | .352 |
| Thalamus | 79.1 (1.2) | 78.8 (2.2) | 79.1 (2.0) | .030 | .878 | .214 | .275 |
| Corpus callosum | 73.7 (3.0) | 73.1 (2.3) | 73.6 (2.1) | .313 | .105 | .050 | .800 |
| Centrum semiovale | 71.7 (1.5) | 71.5 (1.6) | 71.9 (1.8) | .137 | .486 | -.020 | .918 |
| Prefrontal WM | 71.4 (1.3) | 72.3 (3.0) | 72.9 (2.8) | -.006 | .977 | -.030 | .883 |
| Occipital WM | 70.9 (1.1) | 71.5 (2.2) | 71.2 (1.7) | .264 | .175 | -.088 | .655 |
| Visual cortex | 81.6 (2.1) | 83.2 (3.4) | 81.8 (2.0) | .141 | .473 | .152 | .441 |
| Prefrontal cortex | 83.3 (1.5) | 84.0 (3.3) | 83.2 (1.8) | -.067 | .733 | -.060 | .764 |

Table 4: Results of quantitative brain water content measurement. Correlation analysis included patient and controls groups.

3.3. Correlation of brain water content and MR spectroscopy

Visual GSx/Cr correlated with thalamic ($r = .694$, $P < .001$), *nucleus caudatus* ($r = .578$, $P = .001$), and visual cortex ($r = .573$, $P = .001$) water content. No correlations of GM or WM water content in the visual MRS volume with the tissue fractions of GM, WM, or CSF were found, indicating that underlying tissue composition effects were not responsible for these observations.

Further correlations between metabolite levels and cerebral water measures were observed, but did not reach significance after correcting for multiple comparisons:

Visual GSx/Cr correlated with global GM water content ($r = .419$, $P = .030$).

Sensorimotor GABA/Cr correlated negatively with water content in the putamen ($r = -.458$, $P = .013$), global WM ($r = -.445$, $P = .015$), visual cortex ($r = -.386$, $P = .038$), and prefrontal cortex ($r = -.397$, $P = .033$). Visual GABA/Cr was not linked to any water content parameter at all. Sensorimotor Glu/Cr correlated with water content in the *corpus callosum* ($r = .391$, $P = .036$).

Water content in the *globus pallidus* was associated with visual Gln/Cr ($r = .414$, $P = .028$), sensorimotor Gln/Cr ($r = .378$, $P = .043$), and sensorimotor GSx/Cr ($r = .468$, $P = .010$).

4. Discussion

In this study, we re-evaluated proton magnetic resonance spectroscopy data from HE patients with respect to glutathione. We used these data and quantitative brain water content imaging to investigate the interrelations of blood ammonia levels, total glutathione (GSH+GSSG or GSx) levels in the brain, low-grade cerebral oedema, neurotransmitter concentrations, and clinical symptoms of covert hepatic encephalopathy (i.e. minimal HE and HE of grade 1).

To our knowledge, we report the first *in vivo* MR spectroscopic estimates of GSx/Cr as a measure of total glutathione (GSH+GSSG) in HE patients. The principal findings are an increase of GSx/Cr in patients with mHE (sensorimotor and visual areas) and HE 1 (sensorimotor), and its positive association with blood ammonia levels. Moreover, GSx/Cr is linked to measures of the osmolytic compounds glutamine (Gln/Cr) and myo-inositol (mI/Cr). Brain water content measures did not exhibit significant changes in covert HE, and showed only a few correlations with total glutathione, but not with MRS measures of other metabolites.

4.1 Increased total glutathione levels in HE

The observed elevation of total glutathione levels, tightly coupled to ammonia, tallies with several previous findings. Murthy and colleagues observed a 1.5-fold increase of GSH and a 5-fold increase of GSSG in cells and medium of cultured cortical astrocytes

that were treated with 5 mM ammonia chloride. The fraction of GSSG in total glutathione was rather small (16% in medium, <1% in cells) (Murthy et al. 2000). The effect was found to be dependent on ammonia concentration by Węgrzynowicz and colleagues who measured higher total glutathione after incubation of higher ammonium chloride doses (Węgrzynowicz et al. 2007). Experiments using the rodent models of HE reported further evidence. *In vivo* administration of ammonia raised total glutathione levels in the prefrontal cortex of rats, presumably by upregulated synthesis in astrocytes (Węgrzynowicz et al. 2007). Sathyasaikumar et al. measured increased levels of both glutathione forms. GSH elevation was attributed to increased gamma-glutamylcysteine synthetase activity. The increase in GSSG was suggested to be caused by both reactive oxygen species consumption and reduced activity of glutathione reductase, thereby impairing the recycling of oxidized to reduced glutathione (Sathyasaikumar et al. 2007). Hilgier and colleagues demonstrated increased extracellular glutathione in the rat prefrontal cortex, suggesting that excess ammonia stimulates GSH synthesis in the astrocytes, and further increases its degradation in the extracellular space. This is thought to boost the availability of GSH precursors to the neurons, effectively improving their defensive capability against ammonia neurotoxicity (Hilgier et al. 2010). Together with these findings, our data suggest that a similar activation of the glutathione defence system may be involved in the interception of hyperammonemia in patients with hepatic encephalopathy. More detailed and separate investigation of GSH and GSSG behaviour under hyperammonemia in the human brain might provide further insight.

The observed increase of visual GSx/Cr in HE 1 patients is not significant. A partial volume effect due to the higher fraction of white matter (~60%) in the sensorimotor MRS volume compared to the visual MRS volume (~30%) would imply that the interception process is majorly localized in white matter astrocytes. This is less likely, as the referenced experiments employed cultures from cortical astrocytes or investigated cortical areas in rodents. The variability in the glutathione increase may rather point towards a regional dependence of the mechanisms responsible for the reaction of the glutathione system. Similar region specific alterations have been observed for neurotransmitter systems in HE (Cauli et al. 2009; Llansola et al. 2014). Again, additional studies looking into glutathione behaviour in distinct brain regions may help clarifying the underlying mechanisms.

Further investigations into regional glutathione changes in HE might also be desirable in light of the correlations that visual GSx/Cr demonstrates with brain water content in the thalamus, *nucleus caudatus*, and visual cortex. Although all three regions did not exhibit significant group differences in brain water content or correlations with CFF and blood ammonia, they may be sensitive to oxidative stress (OS) and mediate HE-related functional impairment. Especially the thalamus is involved in the slowed oscillatory coupling within the motor system related to mini-asterixis (Timmermann et al. 2003) and shows abnormal functional connectivity in mHE (Qi et al. 2013a). Several studies could further verify increased thalamic volume in mHE, arguing that this may be a compensatory mechanism to counter the malfunctions in other brain regions (Qi et al. 2013b; Tao et al. 2013).

HE-related alterations in the *nucleus caudatus* have been less frequently observed; one study confirmed a negative correlation between its T_1 relaxation time and blood ammonia levels, potentially a combined effect of manganese deposition and ammonia (Shah et al. 2003). Functional implications of structural alterations within *nucleus caudatus* remain, however, speculative.

Water content in the visual cortex notably correlates with visual GSx/Cr, which is anticorrelated with visual GABA/Cr. As visual GABA/Cr is in turn not correlated to visual cortex water content, but to CFF (Oeltzschner et al. 2015), low-grade oedema are less likely to directly affect visual performance. This may be in line with rodent experiments, in which cognitive and motor impairment occurred even without presence of cerebral oedema and instead possibly due to altered neurotransmission (Cauli et al. 2014; Llansola et al. 2014).

Interestingly, water content in the *globus pallidus* did not exhibit correlations with the CFF (despite a trend at $P = 0.088$) or blood ammonia in our study, although it has been a promising candidate in earlier quantitative imaging studies (Shah et al. 2003; Shah et al. 2008). Future MR spectroscopic experiments in the basal ganglia regions may shed light on the subcortical interactions of ammonia, glutathione, osmolytes, and HE severity.

4.2 The role of brain water content in HE

It is debatable why the results from our experiments can only partly reproduce the relationships between disease grade, CFF, and the cerebral water content that were previously demonstrated by Shah and colleagues using a 1.5 T MR scanner (Shah et al.

2008). An influence of magnetic field strength is unlikely, as water content estimates at 1.5 T and 3 T have been shown to be consistent (Abbas et al. 2015).

First and foremost, it is striking that our WM water content results are in good agreement with the results of Shah and colleagues for the mHE (71.6 % vs. 71.6 %) patients, while they are ~0.7 percentage points higher for controls (71.6 % vs. 70.9 %) and ~0.8 percentage points lower for HE 1 (72.1 % vs. 72.9 % from the overt HE group). The study population of Shah et al. included three patients with disease grade HE 2 which were subsequently pooled with ten HE 1 patients to form an “overt HE” group following earlier terminology. The HE-related changes found in cerebral water content (global white matter: +0.4 % for HE-0, +0.8 % for mHE, +2.1 % for overt HE; globus pallidus: +0.3 % for HE-0, +0.1 % for mHE, +1.9 % for overt HE) were relatively low compared to its inter-individual variance (global white matter: 1.2 % for controls, globus pallidus: 2.2 % for controls). Since most group differences were significant for the overt HE group only, one might speculate that the three HE 2 patients strongly impacted the group averages and were responsible for the observed effects. The absence of correlations between brain water measures and CFF or blood ammonia in our study might further suggest that the actual functional involvement of subtle brain water changes is rather small within early stages (< HE 2) of chronic HE. As stated above, a similar conclusion has recently been suggested by Cauli and co-workers after showing the occurrence of motor and cognitive deficits in chronic HE rats in absence of cerebral oedema (Cauli et al. 2014). Recent rodent experiments even suggest that cerebral lactate rather than glutamine might be a more important actor in the pathogenesis of cerebral oedema in HE (Bosoi et al. 2014b; Bosoi and Rose 2014).

Regarding potential population sampling errors, it is noteworthy that 6 out of 16 of our controls showed a CFF below the value of 39 Hz which was suggested as a cut-off to identify HE (Kircheis et al. 2014). An alternative threshold of 38 Hz, however, has previously been suggested (Romero-Gómez et al. 2007). The average CFF across controls in our study was 41.6 Hz (Shah et al.: 43.2 Hz). The higher mean age of our controls (60.1 y vs. 52.6 y in Shah et al.) might account for the CFF differences as CFF is known to be age-dependent. When performing the partial correlations with CFF, we observed that white matter water content measures across all participants correlated positively with age, although WM water content has previously been demonstrated not to vary with age in a cohort of healthy volunteers (Neeb et al. 2006a). As age was not included as a covariant in the correlation analysis by Shah et al., this may indicate that increase of white matter water content with age appears in HE patients only. This could explain the correlations between CFF and white matter water content that were observed by Shah and colleagues. Yet, in our study, the average WM water content in controls did not yield lower values even after we only included controls with CFF >39 Hz into the analysis.

Finally, its comparably high inter-individual variability gives rise to the thought that individual brain water content may not be a suitable indicator for HE severity. This is noteworthy, considering that osmotic regulation plays a vital part in the pathogenesis of HE, as is suggested by the consistently observed roles of glutamine and myo-inositol. Last but not least, MR brain water imaging is a measure of free bulk tissue water, and it is not capable of discerning between extracellular and intracellular water or detecting water bound to, for instance, macromolecules. Based on our data, it is hence not possible to rule out the emergence of a low-grade cerebral oedema in covert HE or its

potential importance for HE progression. It might just be that the ratio of extracellular and intracellular water changes due to a low-grade oedema while the total amount of water content remains widely unchanged, or that the changes are subtle and below the detection threshold of the method at hand. This might be particularly the case in covert HE, but also remains to be investigated in more detail in overt HE. Considering these aspects, future studies are needed to further enlighten the role of cerebral oedema in HE. To this end, e.g. it might be valuable to design a longitudinal study approach. As HE patients are known to vary in their disease grade and degree of symptoms within weeks, repeated measurements of water content and brain metabolites could provide more detailed insight into individual short-term mechanisms of cerebral water homeostasis and the impact of low-grade oedema formation.

4.3 Glutamine and myo-inositol

HE-related increase of glutamine and simultaneous depletion of myo-inositol has been observed in numerous studies (Laubenberger et al. 1997; Shawcross et al. 2004; Miese et al. 2006). Increase of glutamine has also been reported in patients in remission from alcohol use disorder (Thoma et al. 2011) and may drive the Gln increase in cirrhosis patients. In our data, however, no differences in Gln/Cr between alcoholic and non-alcoholic HE patients (see Table 1 for etiology details) were observed. This was true for both the sensorimotor and the visual data, in the mHE group as well as in the HE 1 group, suggesting that Gln is consistently elevated in HE, regardless of its etiology.

4.4 Limitations

Importantly, the MEGA-PRESS protocol used in this study is optimized for GABA detection and quantification, but not for measuring glutathione. Nevertheless, Cramér-Rao lower bounds (CRLB) – a parameter widely seen as quality criterion for MRS experiments – for GSx/Cr were on average <10% for both the sensorimotor and the visual volume in our study. This suggests sufficient sensitivity and reliable measurability, and may result from the relatively large MRS volume providing good signal-to-noise ratio, together with the spectral fitting approach using linear combination of metabolite basis sets. Optimized MRS protocols (Terpstra et al. 2003) may be employed in the future to enhance the reliability of glutathione quantification and confirm our results.

The MRS contribution of oxidized glutathione (GSSG) is assumed to be negligible in healthy human brain under normal physiological circumstances (Terpstra et al. 2003; Terpstra et al. 2006). The previous experiments with cultured astrocytes and rodents in the HE model (Murthy et al. 2000; Sathyasaikumar et al. 2007; Wegrzynowicz et al. 2007) have shown that the magnitude of increase of GSSG was notably higher than the increase of GSH, so that this assumption may not be valid any more in HE. Therefore, an important limitation of the present study may be the inability to discern the different functional pools of total glutathione. Other than the GSH/GSSG ratio, measures of total glutathione (obtained with PRESS) may thus not reflect the total level of OS or its fraction that is actually intercepted by the glutathione system. This might be different for MRS protocols that employ J-editing techniques (Sato and Yoshioka 2006).

The sufficiency with which glutamine and glutamate can be separated from 68 ms PRESS spectra at 3T is a concern. Analysis of a similar 72 ms STEAM acquisition has

been shown to provide reasonable variability (13.8 %) and average CRLBs <8% (Wijtenburg and Knight-Scott 2011). In comparison, our LCModel fits of visual Glu yielded CRLBs as low as 12.6 ± 4.9 % (Gln: 17.2 ± 15.0 %). Considering that a CRLBs cut-off of 20% is routinely used for quality management in MRS experiments, separate quantification of Gln and Glu therefore appears feasible. The higher average Gln variability was mainly driven by the control group that exhibited comparably low Gln concentrations and accordingly higher CRLBs.

A potential source of error in the quantitative brain water content measurement originates in the interactive definition of ROIs, since it is clearly prone to additional inter-rater variability. While structures like the putamen or the *nucleus caudatus* are comparably well-defined, it is more challenging to reliably delineate areas such as the prefrontal cortex or the occipital white matter. Moreover, the areas close to the cortex boundaries may particularly suffer from partial volume effects that distort the water content estimations. However, this might add variance in the estimate of the respective regions, but should be independent of the disease grade.

5. Conclusions

In this work, we analysed MR spectroscopic data of healthy controls and patients suffering from covert HE with respect to total glutathione. GSx/Cr was significantly changed in patients, with links to concentrations of the osmolytic compounds glutamine and myo-inositol. Furthermore, it was associated with blood ammonia levels. This gives rise to the assumption that it is part of the reaction to OS induced by hyperammonemia.

Brain water content measures were neither changed in covert HE nor correlated to CFF, blood ammonia, neurotransmitter or brain osmolyte levels, suggesting that cerebral oedema have only subtle functional impact in these patients. However, few correlations with visual GSx/Cr might indicate region-specific relationships between cerebral oedema and OS.

Acknowledgements

The authors would like to thank Dr. James Murdoch (Toshiba Medical Research Institute USA) for providing the LCModel basis set, Nur-Deniz Füllenbach and Dr. Gerald Kircheis (Department of Gastroenterology, Hepatology and Infectiology, University Hospital Düsseldorf) for support with patient recruitment, psychometry, and HE grading, and Erika Rädisch (Department of Diagnostic and Interventional Radiology, University Hospital Düsseldorf) for help with MR measurements.

Funding

This work has been supported by the Sonderforschungsbereich (SFB) 974 of the Deutsche Forschungsgemeinschaft (DFG).

Conflict of interest

The authors declare that they have no conflict of interest.

References

- Abbas Z, Gras V, Möllenhoff K, et al (2015) Quantitative water content mapping at clinically relevant field strengths: A comparative study at 1.5 T and 3 T. *NeuroImage* 106:404–413. doi: 10.1016/j.neuroimage.2014.11.017
- Bains JS, Shaw CA (1997) Neurodegenerative disorders in humans: the role of glutathione in oxidative stress-mediated neuronal death. *Brain Res Rev* 25:335–358. doi: 10.1016/S0165-0173(97)00045-3
- Bajaj JS, Cordoba J, Mullen KD, et al (2011) Review article: the design of clinical trials in hepatic encephalopathy – an International Society for Hepatic Encephalopathy and Nitrogen Metabolism (ISHEN) consensus statement. *Aliment Pharmacol Ther* 33:739–747. doi: 10.1111/j.1365-2036.2011.04590.x
- Bosoi CR, Rose CF (2014) Elevated cerebral lactate: Implications in the pathogenesis of hepatic encephalopathy. *Metab Brain Dis* 29:919–925. doi: 10.1007/s11011-014-9573-9
- Bosoi CR, Tremblay M, Rose CF (2014a) Induction of systemic oxidative stress leads to brain oedema in portacaval shunted rats. *Liver Int* 34:1322–1329. doi: 10.1111/liv.12414
- Bosoi CR, Zwingmann C, Marin H, et al (2014b) Increased brain lactate is central to the development of brain edema in rats with chronic liver disease. *J Hepatol* 60:554–560. doi: 10.1016/j.jhep.2013.10.011
- Brenner M, Butz M, May ES, et al (2015) Patients with manifest hepatic encephalopathy can reveal impaired thermal perception. *Acta Neurol Scand* 132:156–163. doi: 10.1111/ane.12376
- Butterworth RF (2000) Complications of cirrhosis III. Hepatic encephalopathy. *J Hepatol* 32, Supplement 1:171–180. doi: 10.1016/S0168-8278(00)80424-9
- Butz M, May ES, Häussinger D, Schnitzler A (2013) The slowed brain: Cortical oscillatory activity in hepatic encephalopathy. *Arch Biochem Biophys* 536:197–203. doi: 10.1016/j.abb.2013.04.004
- Butz M, Timmermann L, Braun M, et al (2010) Motor impairment in liver cirrhosis without and with minimal hepatic encephalopathy. *Acta Neurol Scand* 122:27–35. doi: 10.1111/j.1600-0404.2009.01246.x
- Cauli O, Llansola M, Agustí A, et al (2014) Cerebral oedema is not responsible for motor or cognitive deficits in rats with hepatic encephalopathy. *Liver Int* 34:379–387. doi: 10.1111/liv.12258
- Cauli O, Mansouri MT, Agusti A, Felipo V (2009) Hyperammonemia Increases GABAergic Tone in the Cerebellum but Decreases It in the Rat Cortex. *Gastroenterology* 136:1359–1367.e2. doi: 10.1053/j.gastro.2008.12.057

- Edden RAE, Puts NAJ, Harris AD, et al (2014) Gannet: A batch-processing tool for the quantitative analysis of gamma-aminobutyric acid-edited MR spectroscopy spectra. *J Magn Reson Imaging* 40:1445–1452. doi: 10.1002/jmri.24478
- Felipo V (2013) Hepatic encephalopathy: effects of liver failure on brain function. *Nat Rev Neurosci* 14:851–858. doi: 10.1038/nrn3587
- Ferenci P, Lockwood A, Mullen K, et al (2002) Hepatic encephalopathy—Definition, nomenclature, diagnosis, and quantification: Final report of the Working Party at the 11th World Congresses of Gastroenterology, Vienna, 1998. *Hepatology* 35:716–721. doi: 10.1053/jhep.2002.31250
- Häussinger D, Schliess F (2008) Pathogenetic mechanisms of hepatic encephalopathy. *Gut* 57:1156–1165. doi: 10.1136/gut.2007.122176
- Häussinger D, Sies H (2013) Hepatic encephalopathy: Clinical aspects and pathogenetic concept. *Arch Biochem Biophys* 536:97–100. doi: 10.1016/j.abb.2013.04.013
- Hilgier W, Węgrzynowicz M, Ruszkiewicz J, et al (2010) Direct Exposure to Ammonia and Hyperammonemia Increase the Extracellular Accumulation and Degradation of Astroglia-Derived Glutathione in the Rat Prefrontal Cortex. *Toxicol Sci* 117:163–168. doi: 10.1093/toxsci/kfq171
- Kircheis G, Hilger N, Häussinger D (2014) Value of Critical Flicker Frequency and Psychometric Hepatic Encephalopathy Score in Diagnosis of Low-Grade Hepatic Encephalopathy. *Gastroenterology* 146:961–969. doi: 10.1053/j.gastro.2013.12.026
- Kircheis G, Wettstein M, Timmermann L, et al (2002) Critical flicker frequency for quantification of low-grade hepatic encephalopathy. *Hepatology* 35:357–366. doi: 10.1053/jhep.2002.30957
- Klejman A, Węgrzynowicz M, Szatmari EM, et al (2005) Mechanisms of ammonia-induced cell death in rat cortical neurons: Roles of NMDA receptors and glutathione. *Neurochem Int* 47:51–57. doi: 10.1016/j.neuint.2005.04.006
- Laubenberger J, Häussinger D, Bayer S, et al (1997) Proton magnetic resonance spectroscopy of the brain in symptomatic and asymptomatic patients with liver cirrhosis. *Gastroenterology* 112:1610–1616. doi: 10.1016/S0016-5085(97)70043-X
- Llansola M, Montoliu C, Agusti A, et al (2014) Interplay between glutamatergic and GABAergic neurotransmission alterations in cognitive and motor impairment in minimal hepatic encephalopathy. *Neurochem Int* 88:15–19. doi: 10.1016/j.neuint.2014.10.011
- Mescher M, Merkle H, Kirsch J, et al (1998) Simultaneous in vivo spectral editing and water suppression. *NMR Biomed* 11:266–272. doi: 10.1002/(SICI)1099-1492(199810)11:6<266::AID-NBM530>3.0.CO;2-J

- Michels L, Schulte-Vels T, Schick M, et al (2014) Prefrontal GABA and glutathione imbalance in posttraumatic stress disorder: Preliminary findings. *Psychiatry Res Neuroimaging* 224:288–295. doi: 10.1016/j.psychresns.2014.09.007
- Miese F, Kircheis G, Wittsack HJ, et al (2006) 1H-MR Spectroscopy, Magnetization Transfer, and Diffusion-Weighted Imaging in Alcoholic and Nonalcoholic Patients with Cirrhosis with Hepatic Encephalopathy. *Am J Neuroradiol* 27:1019–1026.
- Murthy CRK, Bender AS, Dombro RS, et al (2000) Elevation of glutathione levels by ammonium ions in primary cultures of rat astrocytes. *Neurochem Int* 37:255–268. doi: 10.1016/S0197-0186(00)00028-0
- Neeb H, Ermer V, Stocker T, Shah NJ (2008) Fast quantitative mapping of absolute water content with full brain coverage. *NeuroImage* 42:1094–1109. doi: 10.1016/j.neuroimage.2008.03.060
- Neeb H, Zilles K, Shah NJ (2006a) A new method for fast quantitative mapping of absolute water content in vivo. *NeuroImage* 31:1156–1168. doi: 10.1016/j.neuroimage.2005.12.063
- Neeb H, Zilles K, Shah NJ (2006b) Fully-automated detection of cerebral water content changes: Study of age- and gender-related H₂O patterns with quantitative MRI. *NeuroImage* 29:910–922. doi: 10.1016/j.neuroimage.2005.08.062
- Oeltzschner G, Butz M, Baumgarten TJ, et al (2015) Low visual cortex GABA levels in hepatic encephalopathy: links to blood ammonia, critical flicker frequency, and brain osmolytes. *Metab Brain Dis*. doi: 10.1007/s11011-015-9729-2
- Provencher SW (2001) Automatic quantitation of localized in vivo 1H spectra with LCModel. *NMR Biomed* 14:260–264. doi: 10.1002/nbm.698
- Qi R, Zhang LJ, Zhong J, et al (2013a) Disrupted thalamic resting-state functional connectivity in patients with minimal hepatic encephalopathy. *Eur J Radiol* 82:850–856. doi: 10.1016/j.ejrad.2012.12.016
- Qi R, Zhang LJ, Zhong J, et al (2013b) Grey and white matter abnormalities in minimal hepatic encephalopathy: a study combining voxel-based morphometry and tract-based spatial statistics. *Eur Radiol* 23:3370–3378. doi: 10.1007/s00330-013-2963-2
- Romero-Gómez M, Córdoba J, Jover R, et al (2007) Value of the critical flicker frequency in patients with minimal hepatic encephalopathy. *Hepatology* 45:879–885. doi: 10.1002/hep.21586
- Sathyasaikumar KV, Swapna I, Reddy PVB, et al (2007) Fulminant Hepatic Failure in Rats Induces Oxidative Stress Differentially in Cerebral Cortex, Cerebellum and Pons Medulla. *Neurochem Res* 32:517–524. doi: 10.1007/s11064-006-9265-x

- Satoh T, Yoshioka Y (2006) Contribution of reduced and oxidized glutathione to signals detected by magnetic resonance spectroscopy as indicators of local brain redox state. *Neurosci Res* 55:34–39. doi: 10.1016/j.neures.2006.01.002
- Shah NJ, Neeb H, Kircheis G, et al (2008) Quantitative cerebral water content mapping in hepatic encephalopathy. *NeuroImage* 41:706–717. doi: 10.1016/j.neuroimage.2008.02.057
- Shah NJ, Neeb H, Zaitsev M, et al (2003) Quantitative T1 mapping of hepatic encephalopathy using magnetic resonance imaging. *Hepatology* 38:1219–1226. doi: 10.1053/jhep.2003.50477
- Sharma P, Sharma BC, Puri V, Sarin SK (2007) Critical flicker frequency: Diagnostic tool for minimal hepatic encephalopathy. *J Hepatol* 47:67–73. doi: 10.1016/j.jhep.2007.02.022
- Shawcross DL, Balata S, Damink SWMO, et al (2004) Low myo-inositol and high glutamine levels in brain are associated with neuropsychological deterioration after induced hyperammonemia. *Am J Physiol - Gastrointest Liver Physiol* 287:G503–G509. doi: 10.1152/ajpgi.00104.2004
- Tao R, Zhang J, You Z, et al (2013) The thalamus in cirrhotic patients with and without hepatic encephalopathy: A volumetric MRI study. *Eur J Radiol* 82:e715–e720. doi: 10.1016/j.ejrad.2013.07.029
- Terpstra M, Henry P-G, Gruetter R (2003) Measurement of reduced glutathione (GSH) in human brain using LCModel analysis of difference-edited spectra. *Magn Reson Med* 50:19–23. doi: 10.1002/mrm.10499
- Terpstra M, Marjanska M, Henry P-G, et al (2006) Detection of an antioxidant profile in the human brain in vivo via double editing with MEGA-PRESS. *Magn Reson Med* 56:1192–1199. doi: 10.1002/mrm.21086
- Terpstra M, Ugurbil K, Gruetter R (2002) Direct in vivo measurement of human cerebral GABA concentration using MEGA-editing at 7 Tesla. *Magn Reson Med* 47:1009–1012. doi: 10.1002/mrm.10146
- Thoma R, Mullins P, Ruhl D, et al (2011) Perturbation of the Glutamate–Glutamine System in Alcohol Dependence and Remission. *Neuropsychopharmacology* 36:1359–1365. doi: 10.1038/npp.2011.20
- Timmermann L, Gross J, Butz M, et al (2003) Mini-asterixis in hepatic encephalopathy induced by pathologic thalamo-motor-cortical coupling. *Neurology* 61:689–692. doi: 10.1212/01.WNL.0000078816.05164.B1
- Torlot FJ, McPhail MJW, Taylor-Robinson SD (2013) Meta-analysis: the diagnostic accuracy of critical flicker frequency in minimal hepatic encephalopathy. *Aliment Pharmacol Ther* 37:527–536. doi: 10.1111/apt.12199

- Waghray A, Waghray N, Mullen K (2015) Management of Covert Hepatic Encephalopathy. *J Clin Exp Hepatol* 5, Supplement 1:S75–S81. doi: 10.1016/j.jceh.2014.02.007
- Węgrzynowicz M, Hilgier W, Dybel A, et al (2007) Upregulation of cerebral cortical glutathione synthesis by ammonia in vivo and in cultured glial cells: The role of cystine uptake. *Neurochem Int* 50:883–889. doi: 10.1016/j.neuint.2006.12.003
- Wijtenburg SA, Knight-Scott J (2011) Very short echo time improves the precision of glutamate detection at 3T in 1H magnetic resonance spectroscopy. *J Magn Reson Imaging* 34:645–652. doi: 10.1002/jmri.22638
- Yousry TA, Schmid UD, Alkadhi H, et al (1997) Localization of the motor hand area to a knob on the precentral gyrus. A new landmark. *Brain* 120:141–157. doi: 10.1093/brain/120.1.141

**Use of quantitative brain water imaging as concentration reference for
J-edited MR spectroscopy of GABA**

Georg Oeltzschner^{1,2,*}, Alfons Schnitzler, MD¹,
Frithjof Wickrath², Hans-Jörg Wittsack, PhD²

¹ Institute of Clinical Neuroscience and Medical Psychology, Medical Faculty,
Heinrich-Heine-University Düsseldorf, Düsseldorf, Germany

² Department of Diagnostic and Interventional Radiology, University Dusseldorf,
Medical Faculty, D-40225 Düsseldorf, Germany

* Corresponding author. *Address:* Institute of Clinical Neuroscience and Medical
Psychology, Medical Faculty, Heinrich-Heine-University Düsseldorf, Universitätsstr. 1,
D-40225 Düsseldorf, Germany. *Tel.:* +49 211 81 08609. *E-mail:*
georg.oeltzschner@med.uni-duesseldorf.de

Grant Support: Collaborative Research Centre (Sonderforschungsbereich) SFB 974
of the German Research Foundation (Deutsche Forschungsgemeinschaft)

Keywords: GABA, ¹H-MRS, MEGA-PRESS, water reference,
quantification, MRS analysis

Running Title: Watermap analysis of GABA spectroscopy

ABSTRACT

PURPOSE: To determine quantitative water-scaled in vivo concentrations of γ -aminobutyric acid (GABA) by obtaining the water reference concentration from individual water maps.

METHODS: Water-scaled GABA estimates for localized J-edited MR spectroscopy experiments can be computed using standard values for tissue-specific water content and relaxation times. Water content and relaxation may, however, be altered in pathology. This work re-analysed data from a recent study in healthy controls and patients with minimal (mHE) or grade I (HE 1) hepatic encephalopathy, a disease associated with slight elevation of brain water content. J-edited MR spectroscopy data were combined with quantitative brain water measures which provided individual water concentration references and T_1 relaxation times. Resulting GABA estimates were compared to concentrations obtained using standard tissue-specific water content and relaxation values.

RESULTS: Occipital GABA concentrations obtained from individual water and T_1 maps were 1.64 ± 0.35 mM in controls, and significantly higher ($P < 0.01$) than in mHE (1.15 ± 0.28 mM) and HE 1 patients (1.18 ± 0.09 mM). Results from the tissue-dependent approach (1.58 ± 0.30 mM (controls), 1.10 ± 0.27 mM (mHE) and 1.12 ± 0.12 mM (HE 1)) were slightly lower ($P < 0.05$ in each group).

CONCLUSION: Water-scaled in vivo GABA estimates can be obtained with individual water concentration and T_1 relaxation mapping. This approach may be useful for studying GABA levels in pathologies with substantial brain water content or relaxation changes.

1. INTRODUCTION

γ -aminobutyric acid (GABA) is the primary inhibitory neurotransmitter in the human brain. Magnetic resonance spectroscopy (MRS) is the only technique to non-invasively measure cerebral GABA in vivo and has therefore gained a lot of research interest [1–3]. In single-voxel proton magnetic resonance spectroscopy (^1H -MRS) at field strengths of 1.5 to 3 T, J-resolved spectral editing sequences are required to isolate the GABA resonance that is otherwise obstructed by peaks like creatine. MEGA-PRESS [4,5] is one of the frequently used editing schemes amongst others [6,7].

GABA concentration from MRS is currently almost exclusively reported in two ways: either it is normalized to other metabolites such as N-acetylaspartate (NAA) or creatine (Cr), or it is scaled to a water-unsuppressed spectrum and then provided in absolute measures (mM), based on assumptions of tissue specific molar water concentrations [1]. Particularly for water-scaled concentration estimation, data comparison across research sites, scanner platforms, and sequence implementations can be difficult, as the quantification routines are not uniform. Reported water-scaled GABA concentration for the healthy brain may range from 1.1 mM [8] to 2.5 mM [9], depending on the assumptions made. More importantly, the concentration estimates may be biased in pathologies where the water concentration in brain tissue might deviate from the assumptions, such as hepatic encephalopathy [10].

Both MEGA-PRESS spectra and brain water content data have been acquired from healthy controls and patients with hepatic encephalopathy (HE) in the course of a recent study [11]. HE comprises impairment of cerebral functions as a consequence of liver damage. Its severity can be classified from grade I to IV, complemented by the term *minimal HE (mHE)* to describe patients with subtle symptoms only measurable with

psychometric testing [12]. HE is believed to be associated with a low-grade cerebral oedema due to disturbed cell volume regulation [13]. Previous investigations in HE patients showed mildly increased MR brain water content measures in white matter [10] and decreased T_1 values in certain regions within the basal ganglia [14].

HE is therefore a suitable model to examine to what extent such alterations might affect water-scaled MR spectroscopic GABA concentrations. Hence, the goal of the present work was the employment of individual brain water content data to serve as subject-specific concentration reference for water-scaling, including individual T_1 relaxation correction [15,16]. A similar approach has previously been suggested by Gasparovic et al. for metabolite quantification in chemical shift imaging experiments [17]. To examine the impact of putative brain water and T_1 alterations in pathology, the obtained values were compared to GABA concentrations calculated using standard tissue-specific water concentration and relaxation values.

2. MATERIAL AND METHODS

2.1 Determination of GABA concentrations

For water-scaled spectroscopy experiments, the concentration of a metabolite $[M]$ can be calculated according to

$$[M] = \frac{S_M}{S_{H_2O}} \cdot [H_2O] \cdot \frac{2}{H_M} \cdot C_{ref} \quad [1.1]$$

S_M and S_{H_2O} are the peak areas of the metabolite and water (including accounting for the averaging over the acquisitions), $[H_2O]$ denotes the concentration of MR visible water (55.5 mol/L for pure water), H_M is the number of signal giving metabolite protons (2 in the γ methylene group of GABA at 3 ppm), and C_{ref} is a term accounting for the water densities used for referencing, their relaxation properties and the relaxation behaviour of the target metabolite.

2.1.1 Water-scaling and relaxation correction

Treatment of the water reference determination varies largely across studies. In its general form

$$C_{ref} = \frac{f_{H_2O} \times R_{H_2O}}{R_M} \quad [1.2]$$

f_{H_2O} denotes the assumed or measured tissue water content (with 1 being pure water).

R_{H_2O} and R_M contain the relaxation, according to $R_y = \exp\left(-\frac{TE}{T_{2,y}}\right) \times \left(1 - \exp\left(-\frac{TR}{T_{1,y}}\right)\right)$.

2.1.2 Spectral editing specific modifications

In case of spectral editing, Eq. [1.1] needs to be modified by an additional factor C_{edit} . It contains acquisition specific corrections treating (i) macromolecular contamination and

(ii) editing efficiency, and is calculated by $C_{edit} = \frac{MM_{cor}}{eff}$.

Regarding (i), editing techniques suffer from GABA peak contamination with co-edited macromolecule resonances. Different approaches have been introduced to work around the MM problem (MM nulling [18,19] or MM-symmetric editing [6]). In many cases the presence of MM contamination is simply accepted and explicitly acknowledged, with the corresponding peak area often being termed “GABA+” (for GABA + MM).

In the present study, the macromolecular contribution to the GABA+ peak was assumed to be 55% since the classic editing scheme (pulses at 1.9 and 7.5 ppm) was used [1].

MM_{cor} was therefore set to 0.45 in this work.

Regarding (ii), the editing efficiency indicates how much of the signal intensity of the 3 ppm GABA resonance is conserved in the difference spectrum. Ideally, the normalized peak intensities within the triplet are 1-2-1 (with editing, ON resonance) and (-1)-2-(-1) (without editing, OFF resonance). Hence, they follow a 2-0-2 pattern in the ideal difference spectrum. As ON and OFF are subtracted and not averaged, accounting for the “number of acquisitions” (ON and OFF = 2, DIFF = 1) results in the ideal value of 0.5 for eff . In practice, imperfect editing leads to contribution of the central peak [20], altering eff . In the present work, eff was measured as described previously [18,21,22], by comparing PRESS and MEGA-PRESS spectra from a phantom containing GABA and glycine (pH = 7.0, concentration = 100 mM/L each) according to

$$eff = \left(\frac{I_{GABA,PRESS}}{I_{Gly,PRESS}} \right) \bigg/ \left(\frac{I_{GABA,MEGA-PRESS,(ON-OFF)}}{I_{Gly,MEGA-PRESS,(ON+OFF)}} \right),$$

containing the intensities of the GABA

multiplet and the glycine singlet from the respective scans. The experimental value for eff was determined to be 0.63, exceeding the ideal value of 0.5 due to presence of the residual central peak [22].

2.1.3 Methods of GABA quantification

We designed two different quantification routines: **Segmentation** and **Watermap**.

The **Segmentation** approach is based on tissue class segmentation of anatomical images into grey matter (GM), white matter (WM), and cerebrospinal fluid (CSF). C_{ref} can be written as

$$C_{ref} = \frac{f_{GM} \times R_{H_2O,GM} + f_{WM} \times R_{H_2O,WM} + f_{CSF} \times R_{H_2O,CSF}}{R_{GABA} \cdot (1 - f_{vol_CSF})} \quad [1.3]$$

f_i describes fractional water densities. C_{ref} is calculated pixel-wise using

$$f_i = \frac{f_{vol_i} \cdot WD_i}{f_{vol_GM} \cdot WD_{GM} + f_{vol_WM} \cdot WD_{WM} + f_{vol_CSF} \cdot WD_{CSF}} \quad [1.4]$$

where f_{vol_i} is the tissue class probability, and WD_i is its assumed relative water density.

A similar approach has been described and used before [21,23,24]. In this work, GABA concentrations were calculated assuming the relative water densities in WM, GM, and CSF to be $WD_{WM} = 0.70$, $WD_{GM} = 0.80$ and $WD_{CSF} = 0.99$ [16,25]. Tissue specific values for water T_1 relaxation times were used: $T_{1,GM} = 1331$ ms, $T_{1,WM} = 832$ ms, $T_{2,GM} = 110$ ms, $T_{2,WM} = 79.6$ ms [26], $T_{1,CSF} = 4160$ ms and $T_{2,CSF} = 500$ ms [27]. As CSF contains negligible amounts of metabolites, partial volume correction is applied by dividing the complete term by the sum of non-CSF tissue fractions (GM+WM).

The **Watermap** approach has been originally suggested for chemical shift imaging [17].

Instead of assuming relative water densities for each tissue class (WD_i), it is based on

the additional acquisition of several multi gradient echo and EPI images as previously proposed [16]. This procedure yields a quantitative water and T_1 map, providing individual tissue-specific water intensities and T_1 for each high-resolution pixel inside

the spectroscopic volume. Eq. [1.4] thus becomes $f_y = \frac{\sum_i f_{vol,y}(i) \times WD_{Watermap}(i) \cdot R(i)}{\sum_i WD_{Watermap}(i)}$,

already including the relaxation terms. In this term, $WD_{Watermap}$ denotes the water density as measured by the watermapping technique. To ensure the correct relaxation correction, $WD_{Watermap}$ is attributed to the tissue fraction y by multiplying it pixel-wise with the tissue class probability $f_{vol,y}$, and the result is subsequently normalized by the sum of the water densities over all i pixels within the MRS volume [17]. Additionally, relaxation correction is conducted pixel-wise in this step by extracting the individual T_1 values of water from the high-resolution T_1 map and assuming the other relaxation parameters as in the **Segmentation** method. CSF partial volume correction is also applied.

For both methods, R_{GABA} is calculated tissue-independently with $T_{1,GABA} = 1310$ ms [28] and $T_{2,GABA} = 88$ ms [29].

2.2 Subjects and data acquisition

2.2.1 Participants

Data used in this work has been previously acquired in the course of a clinical study that included healthy controls and patients with hepatic encephalopathy (HE). Datasets included measurements of the critical flicker frequency (CFF), an experimental indicator of visual performance that is suitable to describe HE severity on a continuous scale [30–32].

The original study included 16 healthy controls and 27 HE patients of varying severity (13 with minimal HE, 14 with HE of grade 1). For details regarding inclusion and exclusion criteria, HE severity grading and CFF measurement, please see the original publication [11].

All participants underwent examination after giving their full written informed consent. The study was approved by local ethics committee (study number 3644) in accordance to the Declaration of Helsinki. All measurements were carried out on a clinical 3T whole-body MRI scanner (Siemens MAGNETOM Trio A TIM System, Siemens Healthcare AG, Erlangen, Germany) using a 12-channel head matrix coil.

2.2.2 Spectroscopic measurements

MEGA-PRESS spectra (TR = 1500 ms, TE = 68 ms, V = 27 mL, bandwidth = 1200 Hz, 1024 data points) were acquired from the central occipital lobe. Spectral editing was performed by 44 Hz broad Gaussian editing pulses irradiated at 1.9 ppm and 7.5 ppm. The acquisition included water-suppressed (96 MEGA-PRESS iterations) and non-suppressed (8 MEGA-PRESS iterations) spectra for the water reference. Manual tuning of the automatic second order 3D shim was performed to lower the width of the unsuppressed water peak (FWHM) to <15 Hz.

2.2.3 Watermapping procedure

The acquisition of the watermap consisted of five sequences and is briefly outlined in the following (for details, please refer to the original work of Neeb and colleagues [16]). First, a multi gradient echo sequence to determine the proton density was carried out (TR = 2140 ms, eight echoes with TE = 4/9/14/19... ms, flip angle 40°, FoV 256×192

mm², 256×192 matrix, slice thickness = 2 mm, gap = 1 mm, 50 slices). It was followed by another gradient echo sequence to map T_1 relaxation for the correction of saturation effects (TR = 638 ms, two echoes with TE = 4/9 ms, flip angle 70°, FoV 256×192 mm², 256×192 matrix, slice thickness = 2 mm, gap = 1 mm, 50 slices). 30 s waiting time for full relaxation were allowed before the upcoming echo planar imaging (EPI) with 90° flip angle, followed by another 30 s of waiting and the second EPI with 30° flip angle. Results allowed for the calculation of and correction for B_1 field inhomogeneities. After another 30 s of relaxation, another EPI with 30° flip angle followed, with data acquired by the body coil, allowing for the correction of receiving head coil inhomogeneities. All three EPI scans were acquired with TE = 16 ms, FoV 256×192 mm², 64×48 matrix, slice thickness = 2 mm, gap = 1 mm, and 50 slices. Total acquisition time for these five sequences was roughly 11 minutes.

2.2.4 Anatomical scan

For segmentation purposes, a high-resolution 3D anatomical transversal T_1 -weighted magnetization prepared gradient echo (MP RAGE) scan was performed at the end of the experiment (TR / TE = 1950 / 4.6 ms, FoV 256×192 mm², 512×384 matrix, slice thickness = 1 mm, 176 slices).

2.3 Postprocessing

2.3.1 Spectral postprocessing

GABA difference spectra were processed with Gannet 2.0 [33], including frequency and phase correction. Gannet 2.0 performs Gaussian fitting of the GABA+ resonance and mixed Gaussian-Lorentzian modelling of the water signal. For the present work, its

default corrections for macromolecule contamination, relaxation and editing efficiency were removed from the original code to obtain the pure ratio of GABA+ and water peak areas.

2.3.2 Image processing pipeline

The five images from the watermap acquisition protocol were processed with an in-house written MATLAB (The Mathworks Inc., Natick/MA) program to calculate individual quantitative maps of brain water content, T_1 and T_2^* . Exemplary maps from a healthy control are shown in **Fig. 1**.

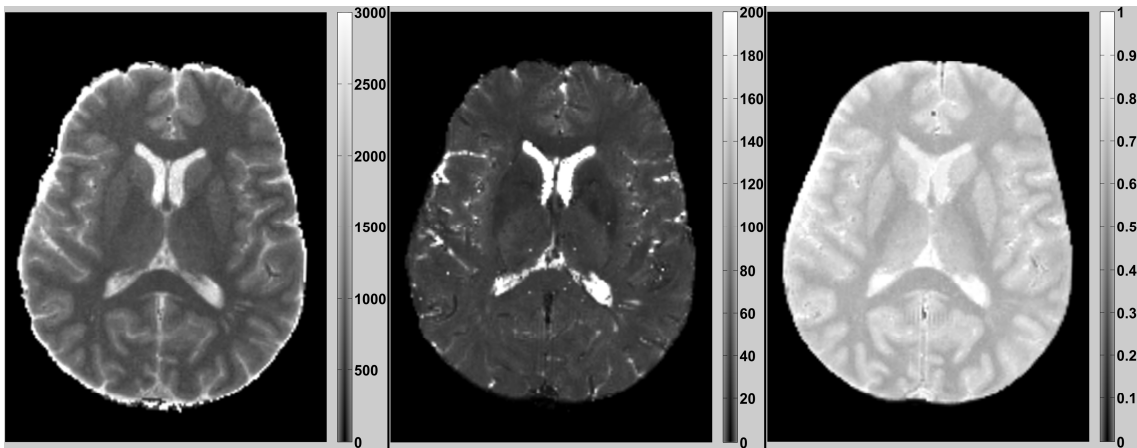


Figure 1: T1, T2* and water content maps from a healthy control (subject no. 573). T1 and T2* maps are expressed in milliseconds (ms). The water content map is scaled to 100% water content (1.0).

The ‘New Segment’ routine of SPM v8 [34] was employed to segment the anatomical scan into GM, WM and CSF tissue probability maps which were subsequently coregistered to the watermap.

MRS volume information were read from the raw file header with a custom made MATLAB routine (Dr. Nia Goulden, Dr. Paul Mullins, Bangor University,

<http://biu.bangor.ac.uk/projects.php.en>, modified by the authors to work with Siemens file format). This routine also transformed the volume parameters into a binary mask. It was used to calculate the fractions of the three tissue classes (GM, WM, and CSF), the tissue-specific average water content, and the corresponding tissue-specific T_1 values from the water, T_1 and tissue probability maps.

2.4 Statistical evaluation

All statistical calculations were conducted with IBM SPSS Statistics for Windows, Version 22.0 (IBM Corp., Armonk, NY, USA).

Group differences between the healthy control, mHE and HE 1 groups were assessed with one-way ANOVA (after confirming normal distribution using Shapiro-Wilk testing), including post-hoc testing yielding Dunn-Bonferroni corrected P values. Group effects were considered significant for $P < 0.05$. Correlations of GABA estimates with the critical flicker frequency (CFF) were examined using partial two-tailed correlation analysis (age as control variable, significant for $P < 0.05$).

The differences of GABA concentration estimates between the **Watermap** and **Segmentation** routines were tested for statistical significance. Repeated measures one-way ANOVA (after confirming normal distribution using Shapiro-Wilk testing) was conducted for all complete datasets. Bonferroni correction for multiple testing was performed with a single test significance level of $\alpha = 0.05$.

Extreme outliers, as identified by SPSS boxplot analysis, were removed prior to further analysis.

3. RESULTS

Complete datasets (MEGA-PRESS spectra from the occipital cortex, quantitative brain water maps and anatomical scans) could be obtained from 10 controls, 10 mHE and 10 HE 1 patients. Due to measurement cancellation, noisy or distorted spectra or severe artefacts in the watermap reconstructions (assessed by visual inspection), 6 control datasets, 3 mHE datasets and 4 HE 1 datasets were discarded prior to analysis.

3.1 GABA estimates

Results of GABA estimation are listed in **Table 1**. Occipital GABA concentrations obtained with the **Watermap** method in controls were significantly higher ($P < 0.01$) than in mHE and HE 1 patients. No difference was noted between the HE groups.

Respective results from the **Segmentation** approach in healthy controls were significantly ($P < 0.01$) higher than in the mHE and HE 1 groups. Within each group, they were slightly lower than the **Watermap** estimates ($P = 0.03$ in controls, $P = 0.014$ in mHE, $P = 0.002$ in HE 1).

Both measures of GABA levels correlated positively with the critical flicker frequency. The normalized difference between the two methods increased from controls over mHE to HE 1, but this result was not significant.

| | Controls | minimal HE | HE 1 | Correlation with CFF |
|---|----------------|------------------|------------------|------------------------|
| Watermap | 1.64 ± 0.35 mM | 1.15 ± 0.28 mM * | 1.18 ± 0.09 mM * | $r = 0.511, P = 0.009$ |
| Segmentation | 1.58 ± 0.30 mM | 1.10 ± 0.27 mM * | 1.12 ± 0.12 mM * | $r = 0.522, P = 0.007$ |
| Normalized difference (Watermap – Segmentation) / Segmentation | 3.6 ± 4.1 % | 4.7 ± 4.1 % | 5.9 ± 4.3 % | - |

Table 1: GABA estimates according to the **Watermap** and **Segmentation** routines, and normalized difference measures. Asterisks mark significant differences from the control group (ANOVA, $P < 0.01$). No significant differences between mHE and HE 1 groups were noted.

3.2 Water content and relaxation times

Global water content within GM and WM, as well as tissue-specific GM and WM water content and T_1 and T_2^* relaxation times are summarized in **Table 2**. No significant alterations of brain water content measures could be determined between the groups in this particular study. T_1 of white matter in the MRS volume was significantly lower in HE 1 patients compared to healthy controls ($P = 0.031$).

| | | Controls | minimal HE | HE 1 |
|----------------------|----|---------------|--------------|---------------|
| Global water content | GM | 82.6 ± 1.2 % | 82.7 ± 2.0 % | 82.6 ± 0.7 % |
| | WM | 71.8 ± 1.5 % | 71.4 ± 1.3 % | 71.7 ± 1.1 % |
| MRS volume | | | | |
| Water content | GM | 84.0 ± 1.8 % | 85.2 ± 2.1 % | 84.7 ± 1.0 % |
| | WM | 74.3 ± 1.4 % | 74.8 ± 1.5 % | 74.4 ± 1.2 % |
| T_1 | GM | 1369 ± 102 ms | 1355 ± 65 ms | 1343 ± 88 ms |
| | WM | 1004 ± 33 ms | 971 ± 28 ms | 944 ± 64 ms * |
| T_2^* | GM | 56 ± 6 ms | 58 ± 4 ms | 58 ± 10 ms |
| | WM | 51 ± 3 ms | 50 ± 4 ms | 50 ± 4 ms |

Table 2: Estimates of water content and relaxation times obtained with the **Watermap** routine. Asterisks mark significant differences from the control group (ANOVA, $P < 0.05$).

4. DISCUSSION

The present work estimates in vivo GABA concentrations from J-edited MR spectroscopy, combined with individual quantitative water referencing and T_1 relaxation correction. GABA estimates were computed for three groups: healthy controls, patients with minimal HE, and patients of HE grade 1. GABA levels were compared to estimates calculated with standard tissue-segmentation based evaluation.

Tissue-specific global water content measures are within the range of previously published values for cohorts of comparable age [16,25], suggesting successful implementation of the MR brain water mapping method.

4.1 Literature consistency of GABA levels in healthy brain

The occipital GABA concentrations ([GABA]) for healthy controls that were obtained with individual **Watermap** quantification and the **Segmentation** routine are well inside the range of recently published literature. Several studies used quantification similar to the **Segmentation** method. Mon et al. calculated [GABA] = 1.50 ± 0.36 mM (parieto-occipital cortex) [35], Gao et al. measured [GABA] = 1.65 ± 0.29 mM and 1.28 ± 0.31 mM (left and right auditory cortex) [36]. Liu et al. reported [GABA] = 1.43 ± 0.11 mM (anterior cingulate cortex) [24]. Foerster et al. determined [GABA] = 1.72 ± 0.34 mM [37] (motor cortex). Despite varying assumptions regarding mean tissue water content and relaxation, our results are within the range of these values.

4.2 GABA levels in hepatic encephalopathy

Water-scaled GABA estimates from the occipital area were significantly reduced in patients with minimal HE and HE 1, and correlated with the individual critical flicker

frequency. Thereby, this work confirms the findings of the original evaluation of the data, where creatine had been used as an internal reference [11].

It is noteworthy that the putative HE-related changes of brain water content reported by Shah et al. [10] were not found in this particular study. The inter-individual variance of brain water content is comparably large with respect to the water increase found by Shah et al. Hence, the small control sample sizes in both studies (9 in the present study vs. 7 in the study by Shah and colleagues) may critically bias the group mean values. Further, three patients with HE grade 2 were included in the study by Shah and colleagues, potentially increasing the mean water content value within the “overt HE” group they investigated.

4.3 Differences between Watermap and Segmentation method

Actual measures of water content within the MRS volume were slightly higher than the assumed standard tissue-specific values, and were therefore likely mainly responsible for the observed small differences in GABA estimates between the **Watermap** and the **Segmentation** method.

This effect was overlapped by a notable deviation of white matter T_1 from the standard value of 832 ± 10 ms [26] for all three groups in the present study, with the highest deviation in the control group. Considering the lower mean age in the study by Wansapura et al. (~37 y compared to 59 y in the present work), this T_1 increase might be due to an age effect [38]. White matter decrease of T_1 in HE was previously observed, albeit not for occipital white matter [14]. Average T_1 in grey matter was consistent with the values reported by Wansapura et al. (1331 ± 13 ms, [26]).

While HE-induced alterations in T_2^* -weighted images were reported [39], T_2^* did not differ between the groups in this study. This does not rule out variations of T_2 which may in turn influence the water reference signal, but would not be corrected for by the **Watermap** method. In fact, T_2 alterations have been reported in mHE, however not in occipital white matter [40].

Quantification patterns did not notably differ in their relative standard deviation (Controls: Watermap 21.3 % vs. Segmentation 18.9 %, mHE: Watermap 24.3 % vs. Segmentation 24.5 %, HE 1: Watermap 7.6 % vs. Segmentation 10.7 %). Potential sources of variance introduced by the **Watermap** method arise from the estimation of brain water content and T_1 , but the systematic errors are rather small. According to Neeb et al., the underlying technique bears systematic errors of <1% and random errors of ~2-3% across the whole brain [16]. T_1 estimation with a variable flip angle method, as was used here, exhibits an error of ~2% [41].

4.4 Limitations

While the impact of the water reference has been treated in this work and the editing efficiency can be attained by phantom measurements, two main issues of GABA quantification remain challenging: relaxation and the extent of macromolecular contribution to the GABA+ signal.

A drawback of the implemented watermapping technique is its use of gradient echo imaging. This has the disadvantage of producing a T_2^* map instead of a T_2 map. T_2 mapping may be included in future experiments using additional multi spin echo images [17]. Due to time concerns, it was not included in the protocol designed for this specific clinical study. In future studies, however, T_2 measurement should be included to enable

a more individual relaxation correction of the water signal and further improve GABA quantification.

Secondly, the described **Watermap** method is not able to account for possible individual or pathological changes of the GABA relaxation times. Pathological abnormalities in the relaxation behaviour of NAA, Cr and Cho have rarely been investigated, but were actually observed in patients with bipolar disorder and schizophrenia [42,43]. Individual measurement of GABA relaxation is possible [28,44], but time-consuming. Future studies will need to address regional or tissue specific variations of GABA relaxation in pathology.

Further, the influence of macromolecules on GABA quantification remains delicate. In this study, no attempt of individual accounting for MM was undertaken, i.e. the obtained GABA measurements directly scaled with GABA+ (see Section 2.1.2).

Regional dependence, grey/white matter distribution or pathology may increase the variance of the MM contribution to the GABA+ area [45]. If it cannot be avoided at all by using MM suppression techniques (lower signal to noise ratio) or MM-nulling scans (additional scan time), accounting for MM contribution needs to be explicitly acknowledged when performing GABA quantification [46].

4.5 Conclusions and Outlook

In this work, it was demonstrated that GABA estimation from edited MR spectroscopy, based on individual brain water content mapping and T_1 relaxation, is feasible. The observed differences to standard tissue-specific estimation are comparably small, but significant. If substantial alterations of brain water content or relaxation times are not expected, the standard tissue-segmentation based approach can still be expected to

provide comparable results. For this particular study, both methods for GABA estimation confirmed the previously observed group difference between healthy control subjects and patients with covert (i.e. low-grade) HE.

The **Watermap** method may therefore be useful for future MR spectroscopic measurements of GABA in pathologies where larger alterations of brain water content or relaxation behaviour are expected (e.g. higher grades of hepatic encephalopathy, multiple sclerosis lesions, tumour etc. [47]). This is especially true if comparison with the healthy brain is targeted, and computation of individual GABA levels is desirable (e.g. for correlation with individual clinical or behavioural parameters).

To further improve individual GABA quantification, more research regarding macromolecular influence and metabolite relaxation times in healthy and pathological tissue is needed.

Acknowledgements

This work was supported by the Sonderforschungsbereich (SFB) 974 of the Deutsche Forschungsgemeinschaft (DFG). The authors would like to thank Erika Rädisch for help with the measurements, Dr. Markus Butz (Heinrich Heine University Düsseldorf) for helpful discussions and comments on the manuscript, and Dr. Keith Heberlein (Siemens Medical Solutions) for technical support.

REFERENCES

- [1] Mullins PG, McGonigle DJ, O’Gorman RL, Puts NAJ, Vidyasagar R, Evans CJ, et al. Current practice in the use of MEGA-PRESS spectroscopy for the detection of GABA. *NeuroImage* 2014;86:43–52. doi:10.1016/j.neuroimage.2012.12.004.
- [2] Puts NAJ, Edden RAE. In vivo magnetic resonance spectroscopy of GABA: A methodological review. *Prog Nucl Magn Reson Spectrosc* 2012;60:29–41. doi:10.1016/j.pnmrs.2011.06.001.
- [3] O’Gorman RL, Michels L, Edden RA, Murdoch JB, Martin E. In vivo detection of GABA and glutamate with MEGA-PRESS: Reproducibility and gender effects. *J Magn Reson Imaging* 2011;33:1262–7. doi:10.1002/jmri.22520.
- [4] Mescher M, Merkle H, Kirsch J, Garwood M, Gruetter R. Simultaneous in vivo spectral editing and water suppression. *NMR Biomed* 1998;11:266–72. doi:10.1002/(SICI)1099-1492(199810)11:6<266::AID-NBM530>3.0.CO;2-J.
- [5] Rothman DL, Petroff OA, Behar KL, Mattson RH. Localized ¹H NMR measurements of gamma-aminobutyric acid in human brain in vivo. *Proc Natl Acad Sci* 1993;90:5662–6.
- [6] Henry P-G, Dautry C, Hantraye P, Bloch G. Brain GABA editing without macromolecule contamination. *Magn Reson Med* 2001;45:517–20. doi:10.1002/1522-2594(200103)45:3<517::AID-MRM1068>3.0.CO;2-6.
- [7] Near J, Simpson R, Cowen P, Jezzard P. Efficient γ -aminobutyric acid editing at 3T without macromolecule contamination: MEGA-SPECIAL. *NMR Biomed* 2011;24:1277–85. doi:10.1002/nbm.1688.
- [8] Evans CJ, McGonigle DJ, Edden RAE. Diurnal stability of γ -aminobutyric acid concentration in visual and sensorimotor cortex. *J Magn Reson Imaging* 2010;31:204–9. doi:10.1002/jmri.21996.
- [9] Chowdhury FA, O’Gorman RL, Nashef L, Elwes RD, Edden RA, Murdoch JB, et al. Investigation of glutamine and GABA levels in patients with idiopathic generalized epilepsy using MEGAPRESS. *J Magn Reson Imaging* 2015;41:694–9. doi:10.1002/jmri.24611.
- [10] Shah NJ, Neeb H, Kircheis G, Engels P, Häussinger D, Zilles K. Quantitative cerebral water content mapping in hepatic encephalopathy. *NeuroImage* 2008;41:706–17. doi:10.1016/j.neuroimage.2008.02.057.
- [11] Oeltzschner G, Butz M, Baumgarten TJ, Hoogenboom N, Wittsack H-J, Schnitzler A. Low visual cortex GABA levels in hepatic encephalopathy: links to blood ammonia, critical flicker frequency, and brain osmolytes. *Metab Brain Dis* 2015. doi:10.1007/s11011-015-9729-2.
- [12] Vilstrup H, Amodio P, Bajaj J, Cordoba J, Ferenci P, Mullen KD, et al. Hepatic encephalopathy in chronic liver disease: 2014 Practice Guideline by the American Association for the Study Of Liver Diseases and the European Association for the Study of the Liver. *Hepatology* 2014;60:715–35. doi:10.1002/hep.27210.
- [13] Häussinger D, Schliess F. Pathogenetic mechanisms of hepatic encephalopathy. *Gut* 2008;57:1156–65. doi:10.1136/gut.2007.122176.
- [14] Shah NJ, Neeb H, Zaitsev M, Steinhoff S, Kircheis G, Amunts K, et al. Quantitative T1 mapping of hepatic encephalopathy using magnetic resonance imaging. *Hepatology* 2003;38:1219–26. doi:10.1053/jhep.2003.50477.

- [15] Neeb H, Zilles K, Shah NJ. A new method for fast quantitative mapping of absolute water content in vivo. *NeuroImage* 2006;31:1156–68. doi:10.1016/j.neuroimage.2005.12.063.
- [16] Neeb H, Ermer V, Stocker T, Shah NJ. Fast quantitative mapping of absolute water content with full brain coverage. *NeuroImage* 2008;42:1094–109. doi:10.1016/j.neuroimage.2008.03.060.
- [17] Gasparovic C, Neeb H, Feis D l., Damaraju E, Chen H, Doty M j., et al. Quantitative spectroscopic imaging with in situ measurements of tissue water T1, T2, and density. *Magn Reson Med* 2009;62:583–90. doi:10.1002/mrm.22060.
- [18] Terpstra M, Ugurbil K, Gruetter R. Direct in vivo measurement of human cerebral GABA concentration using MEGA-editing at 7 Tesla. *Magn Reson Med* 2002;47:1009–12. doi:10.1002/mrm.10146.
- [19] Behar KL, Rothman DL, Spencer DD, Petroff OAC. Analysis of macromolecule resonances in 1H NMR spectra of human brain. *Magn Reson Med* 1994;32:294–302. doi:10.1002/mrm.1910320304.
- [20] Near J, Evans CJ, Puts NAJ, Barker PB, Edden RAE. J-difference editing of gamma-aminobutyric acid (GABA): Simulated and experimental multiplet patterns. *Magn Reson Med* 2013;70:1183–91. doi:10.1002/mrm.24572.
- [21] Bhattacharyya PK, Phillips MD, Stone LA, Bermel RA, Lowe MJ. Sensorimotor Cortex Gamma-Aminobutyric Acid Concentration Correlates with Impaired Performance in Patients with MS. *Am J Neuroradiol* 2013. doi:10.3174/ajnr.A3483.
- [22] Oeltzschner G, Bhattacharyya PK. Editing efficiency for macromolecule-suppressed and unsuppressed J-edited GABA spectroscopy. *Proc Intl Soc Magn Reson Med*, vol. 23, Toronto: 2015, p. 1394.
- [23] Bhattacharyya PK, Phillips MD, Stone LA, Lowe MJ. In vivo magnetic resonance spectroscopy measurement of gray-matter and white-matter gamma-aminobutyric acid concentration in sensorimotor cortex using a motion-controlled MEGA point-resolved spectroscopy sequence. *Magn Reson Imaging* 2011;29:374–9. doi:10.1016/j.mri.2010.10.009.
- [24] Liu B, Wang G, Gao D, Gao F, Zhao B, Qiao M, et al. Alterations of GABA and glutamate–glutamine levels in premenstrual dysphoric disorder: A 3T proton magnetic resonance spectroscopy study. *Psychiatry Res Neuroimaging* 2015;231:64–70. doi:10.1016/j.psychres.2014.10.020.
- [25] Neeb H, Zilles K, Shah NJ. Fully-automated detection of cerebral water content changes: Study of age- and gender-related H2O patterns with quantitative MRI. *NeuroImage* 2006;29:910–22. doi:10.1016/j.neuroimage.2005.08.062.
- [26] Wansapura JP, Holland SK, Dunn RS, Ball WS. NMR relaxation times in the human brain at 3.0 tesla. *J Magn Reson Imaging* 1999;9:531–8. doi:10.1002/(SICI)1522-2586(199904)9:4<531::AID-JMRI4>3.0.CO;2-L.
- [27] Gussew A, Erdtel M, Hiepe P, Rzanny R, Reichenbach JR. Absolute quantitation of brain metabolites with respect to heterogeneous tissue compositions in 1H-MR spectroscopic volumes. *Magn Reson Mater Phys Biol Med* 2012;25:321–33. doi:10.1007/s10334-012-0305-z.
- [28] Puts NAJ, Barker PB, Edden RAE. Measuring the longitudinal relaxation time of GABA in vivo at 3 tesla. *J Magn Reson Imaging* 2013;37:999–1003. doi:10.1002/jmri.23817.

- [29] Edden RAE, Intrapromkul J, Zhu H, Cheng Y, Barker PB. Measuring T2 in vivo with J-difference editing: Application to GABA at 3 tesla. *J Magn Reson Imaging* 2012;35:229–34. doi:10.1002/jmri.22865.
- [30] Kircheis G, Wettstein M, Timmermann L, Schnitzler A, Häussinger D. Critical flicker frequency for quantification of low-grade hepatic encephalopathy. *Hepatology* 2002;35:357–66. doi:10.1053/jhep.2002.30957.
- [31] Kircheis G, Hilger N, Häussinger D. Value of Critical Flicker Frequency and Psychometric Hepatic Encephalopathy Score in Diagnosis of Low-Grade Hepatic Encephalopathy. *Gastroenterology* 2014;146:961–9. doi:10.1053/j.gastro.2013.12.026.
- [32] Sharma P, Sharma BC, Puri V, Sarin SK. Critical flicker frequency: Diagnostic tool for minimal hepatic encephalopathy. *J Hepatol* 2007;47:67–73. doi:10.1016/j.jhep.2007.02.022.
- [33] Edden RAE, Puts NAJ, Harris AD, Barker PB, Evans CJ. Gannet: A batch-processing tool for the quantitative analysis of gamma-aminobutyric acid–edited MR spectroscopy spectra. *J Magn Reson Imaging* 2013;(in press). doi:10.1002/jmri.24478.
- [34] Friston KJ. *Statistical parametric mapping the analysis of functional brain images*. Amsterdam; Boston: Elsevier/Academic Press; 2007.
- [35] Mon A, Durazzo TC, Meyerhoff DJ. Glutamate, GABA, and other cortical metabolite concentrations during early abstinence from alcohol and their associations with neurocognitive changes. *Drug Alcohol Depend* 2012;125:27–36. doi:10.1016/j.drugalcdep.2012.03.012.
- [36] Gao F, Wang G, Ma W, Ren F, Li M, Dong Y, et al. Decreased auditory GABA + concentrations in presbycusis demonstrated by edited magnetic resonance spectroscopy. *NeuroImage* 2015;106:311–6. doi:10.1016/j.neuroimage.2014.11.023.
- [37] Foerster BR, Carlos RC, Dwamena BA, Callaghan BC, Petrou M, Edden RAE, et al. Multimodal MRI as a diagnostic biomarker for amyotrophic lateral sclerosis. *Ann Clin Transl Neurol* 2014;1:107–14. doi:10.1002/acn3.30.
- [38] Cho S, Jones D, Reddick WE, Ogg RJ, Steen RG. Establishing norms for age-related changes in proton T1 of human brain tissue in vivo. *Magn Reson Imaging* 1997;15:1133–43. doi:10.1016/S0730-725X(97)00202-6.
- [39] Liu J-Y, Ding J, Lin D, He Y-F, Dai Z, Chen C-Z, et al. T2* MRI of minimal hepatic encephalopathy and cognitive correlates in vivo. *J Magn Reson Imaging* 2013;37:179–86. doi:10.1002/jmri.23811.
- [40] Singhal A, Nagarajan R, Kumar R, Huda A, Gupta RK, Thomas MA. Magnetic resonance T2-relaxometry and 2D L-correlated spectroscopy in patients with minimal hepatic encephalopathy. *J Magn Reson Imaging* 2009;30:1034–41. doi:10.1002/jmri.21943.
- [41] Wang J, Qiu M, Kim H, Constable RT. T1 Measurements incorporating flip angle calibration and correction in vivo. *J Magn Reson* 2006;182:283–92. doi:10.1016/j.jmr.2006.07.005.
- [42] Tunc-Skarka N, Weber-Fahr W, Hoerst M, Meyer-Lindenberg A, Zink M, Ende G. MR spectroscopic evaluation of N-acetylaspartate’s T2 relaxation time and concentration corroborates white matter abnormalities in schizophrenia. *NeuroImage* 2009;48:525–31. doi:10.1016/j.neuroimage.2009.06.061.

- [43] Öngür D, Prescot AP, Jensen JE, Rouse ED, Cohen BM, Renshaw PF, et al. T2 relaxation time abnormalities in bipolar disorder and schizophrenia. *Magn Reson Med* 2010;63:1–8. doi:10.1002/mrm.22148.
- [44] Andreychenko A, Klomp DWJ, de Graaf RA, Luijten PR, Boer VO. In vivo GABA T2 determination with J-refocused echo time extension at 7 T. *NMR Biomed* 2013;26:1596–601. doi:10.1002/nbm.2997.
- [45] Harris AD, Puts NAJ, Barker PB, Edden RAE. Spectral-editing measurements of GABA in the human brain with and without macromolecule suppression. *Magn Reson Med* 2014;n/a – n/a. doi:10.1002/mrm.25549.
- [46] Bhattacharyya PK. Macromolecule contamination in GABA editing using MEGA-PRESS should be properly accounted for. *NeuroImage* 2014;84:1111–2. doi:10.1016/j.neuroimage.2013.08.050.
- [47] Volz S, Nöth U, Jurcoane A, Ziemann U, Hattingen E, Deichmann R. Quantitative proton density mapping: correcting the receiver sensitivity bias via pseudo proton densities. *NeuroImage* 2012;63:540–52. doi:10.1016/j.neuroimage.2012.06.076.

17

18 **Abstract**

19 Neuronal oscillatory activity in the beta band (15-30 Hz) is a prominent signal within the human
20 sensorimotor cortex. Computational modeling and pharmacological modulation studies suggest
21 an influence of GABAergic interneurons on the generation of beta band oscillations.
22 Accordingly, studies in humans have demonstrated a correlation between GABA concentrations
23 and power of beta band oscillations. It remains unclear, however, if GABA concentrations also
24 influence beta peak frequencies and whether this influence is present in the sensorimotor
25 cortex at rest and without pharmacological modulation. In the present study, we investigated
26 the relation between endogenous GABA concentration (measured by magnetic resonance
27 spectroscopy) and beta oscillations (measured by magnetoencephalography) at rest in humans.
28 GABA concentrations and beta band oscillations were measured for the left and right
29 sensorimotor and occipital cortex. A significant positive linear correlation between GABA
30 concentration and beta peak frequency was found for the left sensorimotor cortex, whereas no
31 significant correlations were found for the right sensorimotor and the occipital cortex. The
32 results show a novel connection between endogenous GABA concentration and beta peak
33 frequency at rest. This finding supports previous results that demonstrated a connection
34 between oscillatory beta activity and pharmacologically modulated GABA concentration in the
35 sensorimotor cortex. Furthermore, the results demonstrate that for a predominantly right-
36 handed sample, the correlation between beta band oscillations and endogenous GABA
37 concentrations is evident only in the left sensorimotor cortex.

39 **Introduction**

40 Oscillatory activity in the beta (15-30 Hz) frequency range is a prominent signal in the human
41 sensorimotor cortex, both at rest and during motor activity [1–4]. Beta band activity differs
42 across areas and depends on motor output (see [5] for a review). For example, beta band power
43 in sensorimotor cortex decreases during movement, whereas beta band power increases
44 following movement [6].

45 The majority of studies on beta band activity investigated the role of power (e.g., [7,8]). In
46 addition to power, there is increasing evidence that beta peak frequency (i.e., the frequency
47 within the beta band with the highest power) is an important and functionally relevant
48 parameter of oscillatory activity [9]. Beta peak frequency differs across distinct recording sites
49 within the sensorimotor cortex [1]. Furthermore, beta peak frequency differs during movement
50 and stimulation of lower and upper limbs, thereby distinguishing between different
51 somatotopic representations [10]. Finally, beta peak frequency seems to be an important factor
52 for the communication between cortical areas and muscles during movement. For example,
53 neuronal activity in the motor cortex and electromyographic activity during movement is
54 coherently coupled at ~20 Hz [11]. This 20 Hz motor cortical activity is thought to optimize
55 motor output by maximal recruitment of motor neurons at a minimum discharge in the
56 pyramidal tract [11].

57 Animal and modeling studies provide evidence for an essential role of GABAergic interneuronal
58 activity for the generation of beta oscillations in the sensorimotor cortex [12–14]. For example,
59 a study using modeled neuronal networks found increases in the power of beta band
60 oscillations to result from an increase in the synaptic conductance of GABA_A-mediated inhibition
61 [12]. Further, studies demonstrated increases in human beta power [7,8,12,15,16] as well as
62 decreases in beta peak frequency [12] (but see [16,17]) as a result of pharmacological
63 GABAergic modulation. Such modulations of beta power were evident at rest [7,12] as well as
64 after motor output [8,15,17].

65 While the abovementioned studies demonstrated a causal link between GABA administration
66 and changes in beta band power and peak frequencies, the concentration of GABA and its direct
67 modulation in the sensorimotor cortex was not measured. Thus, the quantitative relation
68 remains unclear. Magnetic resonance spectroscopy (MRS) offers a non-invasive method for in
69 vivo quantification of endogenous neurotransmitter concentrations in spatially restricted
70 cortical regions [18]. While this approach has initially been applied to estimate GABA
71 concentrations especially in occipital cortical areas (e.g., [19,20]), recent studies also focused on
72 the sensorimotor cortex (e.g., [16,21,22]). These studies demonstrated a linear relationship
73 between sensorimotor GABA concentration and post-movement oscillatory beta power. In
74 contrast, no relationship could be demonstrated between sensorimotor GABA concentration
75 and post-movement oscillatory beta peak frequency [16]. Taken together, there are consistent
76 results supporting a general relationship between GABA concentration and beta band power in
77 sensorimotor cortex areas. Contrarily, the results concerning beta band peak frequency are less
78 consistent. Therefore, the question remains whether beta peak frequency is related to GABA

79 concentrations and if such a potential relation is present at rest (i.e., without movement) and
80 for endogenous (i.e., non-modulated) GABA concentrations.

81 Here, we investigated whether the peak frequency of ongoing beta band oscillations is
82 correlated to endogenous GABA concentration in the sensorimotor cortex at rest. Beta peak
83 frequencies were determined by magnetoencephalography (MEG) and individual GABA
84 concentrations were measured by means of MRS. Peak frequencies were determined for the
85 left and right sensorimotor cortex, as well as for a control region in the occipital cortex. For
86 these three regions of interest (ROIs), we linearly related peak frequencies to GABA
87 concentrations estimated for analogue cortical areas.

88

89 **Materials & Methods**

90 **Subjects**

91 15 subjects (7 male, age: 59.9 ± 9 years (mean \pm SD)) participated after providing written
92 informed consent. The experimental protocol was reviewed and approved by the Ethical
93 Committee of the Medical Faculty, Heinrich-Heine-University Düsseldorf (study number: 3644).
94 The study was conducted in accordance with the Declaration of Helsinki. All participants had
95 normal or corrected to normal vision and reported no sensory impairments, known history of
96 neurological disorders or use of neuro-modulatory medication. Subjects were selected from the
97 healthy controls of a sample that was previously reported in [23].

98

99 **Behavioral data**

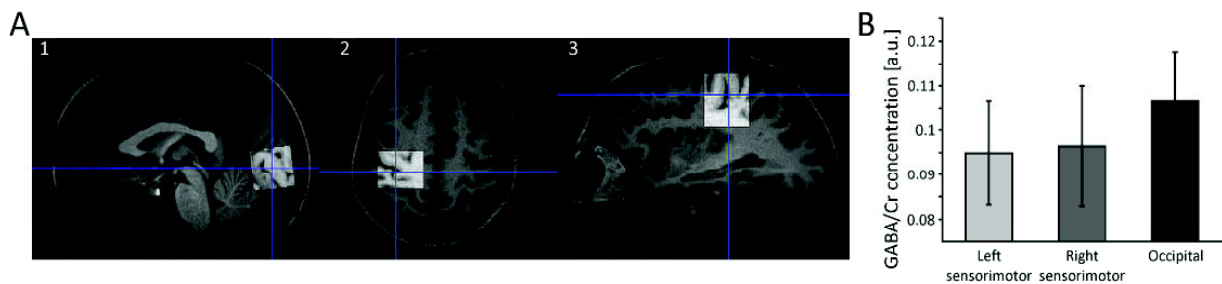
100 Individual handedness was assessed by comparing bi-manual performance (hand dominance
101 test (HDT) [24]). Categorization based on the performance measure resulted in 12 clearly right-
102 handed subjects (HDT score: 29.8 ± 8.1 (mean \pm SD)) and 3 subjects with no clear hand
103 preference (HDT score: -6.8 ± 9.7).

104 **Magnetic resonance spectroscopy (MRS) data**

105 **Spectroscopy**

106 MRS data were recorded using a 3T whole-body MRI scanner (Siemens MAGNETOM Trio A TIM
107 System, Siemens Healthcare AG, Erlangen, Germany) in connection with a 12-channel head

108 matrix coil. Subjects were instructed to lie in the scanner, relax and refrain from any further
109 activity. For the determination of neurotransmitter concentrations, MRS voxels ($3 \times 3 \times 3 \text{ cm}^3$) were
110 placed in left and right sensorimotor cortices and occipital cortex (Fig 1A). For both
111 sensorimotor cortices, voxels were centered on the respective 'hand knob' within the *Gyrus*
112 *praecentralis* [25], thus covering both motor and somatosensory cortex. The occipital MRS voxel
113 was medially centered on the occipital lobe with the inferior boundary of the voxel aligned with
114 the *Tentorium cerebelli*. For all subjects, voxel placement was performed with the focus to
115 include a maximum portion of cortical volume, as well as a minimal volume of non-cerebral
116 tissues to avoid any additional lipid contamination of the spectra. MRS voxels will be addressed
117 as MRS ROIs (in contrast to MEG ROIs) subsequently.



118
119 **Fig 1. Localization of MRS ROIs and average GABA/Cr concentrations across MRS ROIs.** A)
120 Placement of the occipital voxel in the sagittal plane (1), placement of the left sensorimotor
121 voxel, centered on the hand knob, in the axial (2) and sagittal (3) planes. B) Average GABA/Cr
122 concentrations for the left and right sensorimotor and occipital MRS ROIs. Error bars represent
123 standard deviations. No significant difference between voxels was found ($p \geq 0.16$).

124
125 After the localization of target volumes by means of T_1 -weighted planning sequences, MEGA-
126 PRESS spectra [26] were acquired (number of excitations = 192, TR = 1500 ms, TE = 68 ms, V =

127 3x3x3 cm³, bandwidth = 1200 Hz, 1024 data points). Spectral editing was performed by J-
128 refocusing pulses irradiated at 1.9 ppm and 7.5 ppm using Gaussian pulses with a bandwidth of
129 44 Hz. Processing of MEGA-PRESS data was performed with the MATLAB-based tool GANNET
130 2.0 [27], including frequency and phase correction of the single acquisitions as well as Gaussian
131 fitting of the 3 ppm GABA resonance. For subsequent analyses, the GABA-to-creatine ratio
132 (GABA/Cr) was used [28].

133 GABA/Cr estimates were not available for every MRS ROI in each subject (see results section for
134 further details). Therefore, we applied two different statistical tests: 1) GABA/Cr concentrations
135 were compared across the left, right and occipital MRS ROIs by means of a one-factor repeated-
136 measures ANOVA (with listwise deletion of values for all MRS ROIs of a single subject if a value
137 was missing in one MRS ROI). 2) We additionally computed pairwise comparisons between MRS
138 ROIs by means of paired-sample *t*-tests corrected for multiple comparisons by means of the
139 Holm-Bonferroni procedure (see [29] for a similar procedure). Although this comparison also
140 implemented listwise deletion of missing values, the respective deletions are determined for
141 each comparison separately, resulting in fewer deletions compared to the abovementioned
142 ANOVA. This served to achieve a higher statistical power since more subjects could be included
143 in the respective *t*-test comparisons.

144

145 **MEG data**

146 **Experimental Design**

147 Subjects were seated in the MEG with all visual stimuli projected on the backside of a
148 translucent screen (60 Hz refresh rate) positioned 57 cm in front of the subjects. Resting-state

149 neuromagnetic activity was recorded during two sessions with a respective duration of 5
150 minutes, with subjects being instructed to relax and refrain from any additional activity. In the
151 first session, subjects had to focus a dimmed fixation dot (diameter: 0.5 degree) presented in
152 the middle of the translucent screen (eyes open condition (EO)). After completing the first
153 session, subjects were verbally informed regarding the beginning and the instructions of the
154 second session. In the second session, subjects had to close their eyes (eyes closed condition
155 (EC)) but remain awake during the measurement. Stimulus presentation was controlled using
156 Presentation software (Neurobehavioral Systems, Albany, NY, USA).

157 **Data Recording and Preprocessing**

158 Continuous neuromagnetic brain activity was recorded at a sampling rate of 1000 Hz using a
159 306-channel whole head MEG system (Neuromag Elekta Oy, Helsinki, Finland), including 204
160 planar gradiometers (102 pairs of orthogonal gradiometers) and 102 magnetometers. Data
161 analysis in the present study was restricted to the planar gradiometers. Electro-oculograms
162 (EOGs) were recorded for offline artifact rejection by applying electrodes above and below the
163 left eye as well as on the outer sides of each eye. Further, an electro-cardiogram (ECG) was
164 recorded for offline artifact rejection by means of two electrodes placed on the left collarbone
165 and the lowest left rib.

166 Data were offline analyzed using custom-made Matlab (The Mathworks Inc., Natick/MA, USA)
167 scripts and the Matlab-based open source toolbox FieldTrip (<http://fieldtriptoolbox.org>; [30]).

168 Continuously recorded data were divided into two epochs according to the respective session
169 (EO and EC), starting 3 s after beginning and ending 3 seconds before the end of the respective
170 task. Data were band-pass filtered at 1 Hz to 200 Hz and power line noise was removed by using

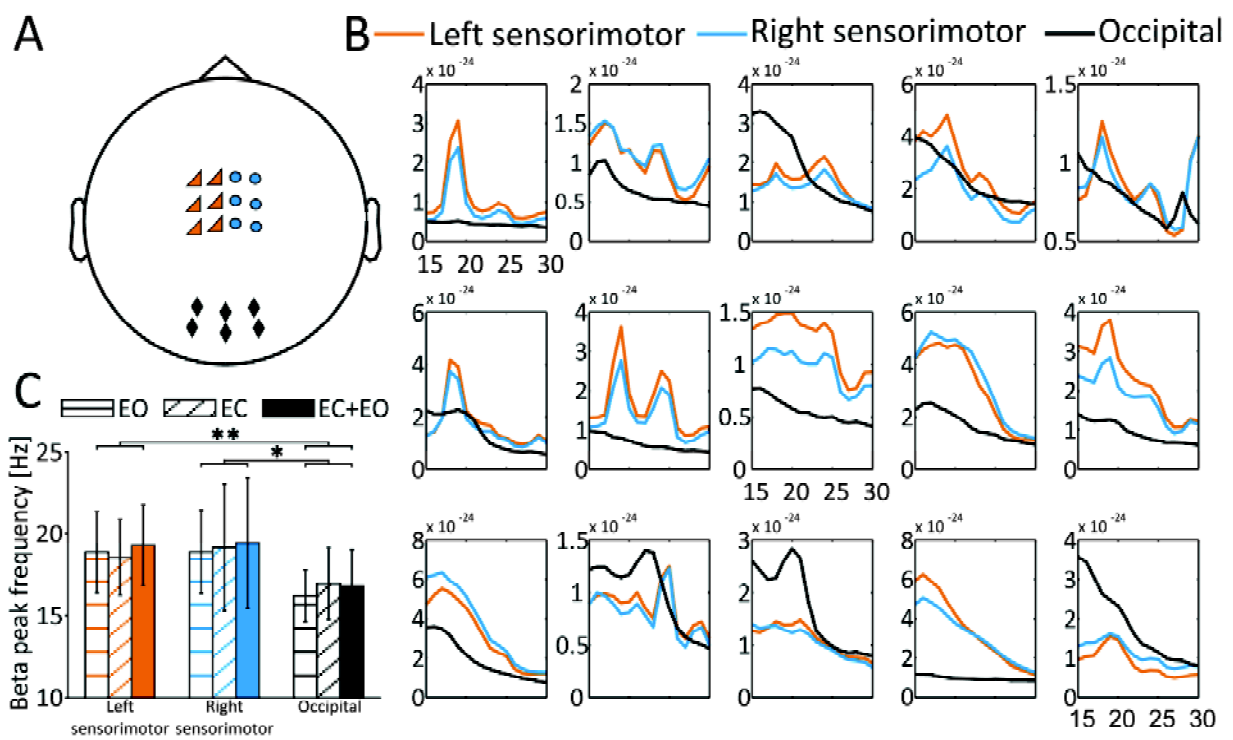
171 a band-stop filter encompassing the 50, 100, and 150 Hz components. Data were detrended and
172 the mean of every epoch was subtracted. Continuous data were segmented into trials of 1 s
173 duration with a 0.25 s overlap. Subsequently, trials were semi-automatically and visually
174 inspected for artifacts. Artifacts caused by muscle activity, eye movements or SQUID jumps
175 were removed semi-automatically using a z-score based algorithm implemented in FieldTrip.
176 Excessively noisy channels were removed. To further eliminate cardiac and ocular artifacts, an
177 independent component analysis was computed. Mutual information was calculated between
178 the resulting components and the EOG and ECG channels [31,32]. Components were sorted
179 according to their level of mutual information and subsequently visually examined regarding
180 their topography and time course. Those components showing high mutual information with
181 EOG and ECG channels as well as topographies and time courses typical for cardiac and ocular
182 artifacts were rejected. Afterwards, removed channels were reconstructed by an interpolation
183 of neighboring channels. After artifact rejection, 292 ± 34.5 (mean \pm SD) trials in the EC
184 condition and 304 ± 35.4 trials in the EC condition remained for further analysis. Subsequent
185 analyses were performed separately for the EO and EC condition as well as for a combined data
186 set created by appending the EO and EC condition (EC+EO).

187 **Frequency Analysis and Peak Frequency Determination**

188 To determine individual peak frequencies, we performed a frequency analysis encompassing all
189 frequencies of the beta-band (15 to 30 Hz; [6,33]) by applying a Fourier transformation over the
190 entire trial duration. Trials were tapered with a single Hanning taper, resulting in a spectral
191 resolution of 1 Hz. Within each condition, spectral power was averaged over all trials for each
192 frequency separately. Power was estimated independently for each of the 204 gradiometers.

193 Subsequently, gradiometer pairs were combined by summing spectral power across the two
 194 orthogonal channels, resulting in 102 pairs of gradiometers.

195 Since GABA-concentrations were assessed for three different MRS ROIs (left and right
 196 sensorimotor cortex, occipital cortex; see Fig 1A and methods section (MRS data, Spectroscopy)
 197 for details), we determined corresponding MEG ROIs by selecting 6 sensor pairs in the left and 6
 198 sensor pairs in the right hemisphere covering the respective sensorimotor cortices (Fig 2A). The
 199 selection of sensors was based on previous studies [34,35]. In addition, we selected 6 posterior
 200 sensor pairs covering the occipital cortex [36].



201
 202 **Fig 2. Sensor selection for respective MEG ROIs, individual beta peak frequencies and**
 203 **average beta peak frequencies across MEG ROIs.** A) Sensors for left sensorimotor MEG ROI
 204 (orange triangles), right sensorimotor MEG ROI (blue dots) and occipital MEG ROI (black

205 diamonds). B) Individual beta peak frequencies for all 15 subjects (EC+EO condition) for left
206 sensorimotor MEG ROI (orange lines), right sensorimotor MEG ROI (blue lines) and occipital
207 MEG ROI (black lines). C) Average beta peak frequencies separately for all conditions (EO, EC,
208 EC+EO) and all MEG ROIs. Error bars represent standard deviations. *: $p < 0.01$; **: $p < 0.05$.

209

210 Individual beta peak frequencies were determined within each MEG ROI separately for each
211 subject. For each subject, the frequency showing the maximum power within the predefined
212 beta-band (15-30 Hz) was selected as the individual peak frequency. Beta peak frequencies
213 were statistically compared between the three MEG ROIs and the three conditions by means of
214 a two-factor repeated-measures ANOVA (main factors: MEG ROI (left sensorimotor, right
215 sensorimotor, occipital) and condition (EO, EC, EC+EO)). In case of violations of sphericity,
216 Greenhouse-Geisser corrected values were reported.

217 **Correlation of MRS and MEG data**

218 In order to examine the relationship between GABA/Cr concentrations and resting-state
219 neuromagnetic brain activity, we linearly correlated individual GABA/Cr concentrations within
220 the respective MRS ROIs with the beta band peak frequencies determined for the corresponding
221 MEG ROIs. We computed correlations within each ROI (e.g., between left sensorimotor MRS ROI
222 and left sensorimotor MEG ROI), thus resulting in 3 correlations for each condition (EO, EC,
223 EC+EO). In addition, we corrected the respective correlations for the HDT handedness scores by
224 means of partial correlation (Pearson).

225

226 **Results**

227 **GABA/Cr concentrations**

228 GABA/Cr values were determined in left sensorimotor, right sensorimotor and occipital MRS
229 ROIs (Fig 1). Due to cancellation of the measurements or distorted spectra, GABA/Cr
230 concentrations could not be estimated for the left sensorimotor, right sensorimotor and
231 occipital MRS ROI in 4, 2, and 1 subjects, respectively (see Table 1 for a summary of GABA/Cr
232 estimates). For the remaining subjects, a one-factor repeated-measures ANOVA yielded no
233 significant difference between GABA/Cr concentrations in the 3 MRS ROIs ($F(2, 16) = 2.06, p =$
234 0.16 ; Fig 1B). Likewise, paired-sample t -tests yielded no significant differences in GABA/Cr
235 concentration between MRS ROIs ($p > 0.017$, after correction for multiple comparisons).

| Subject | GABA/Cr values per MRS ROI | | |
|---------|----------------------------|---------------------|-----------|
| | Left Sensori-motor | Right Sensori-motor | Occipital |
| 1 | 0.1097 | 0.1083 | 0.1054 |
| 2 | 0.0798 | 0.0713 | 0.1197 |
| 3 | 0.1035 | | 0.1087 |
| 4 | 0.0995 | 0.1011 | 0.1056 |
| 5 | 0.0844 | 0.0886 | 0.0940 |
| 6 | | 0.0914 | 0.1213 |
| 7 | | 0.0730 | 0.1134 |
| 8 | | 0.1004 | 0.1166 |
| 9 | | | 0.1110 |
| 10 | 0.0948 | 0.1045 | 0.1073 |
| 11 | 0.0920 | 0.1187 | 0.1083 |
| 12 | 0.1078 | 0.0962 | |
| 13 | 0.1085 | 0.1014 | 0.1034 |
| 14 | 0.0781 | 0.0908 | 0.0783 |

| | | | | |
|-------------|--------|--------|--------|--------|
| | 15 | 0.0862 | 0.1079 | 0.1000 |
| Mean | 0.0949 | 0.0964 | 0.1066 | |
| SD | 0.0117 | 0.0135 | 0.0110 | |

236 **Table 1: GABA/Cr values per MRS ROI**

237

238 **MEG data**

239 Beta peak frequencies could be determined in all subjects (Fig 2B; Table 2). A two-factor
 240 repeated measures ANOVA comparing beta peak frequencies for the factors MEG ROI (left
 241 sensorimotor, right sensorimotor, occipital) and condition (EO, EC, EC+EO) demonstrated a
 242 highly significant main effect for the factor MEG ROI ($F(1.43, 19.97) = 7.27, p < 0.01$; Fig 2C).
 243 Post hoc *t*-tests revealed a significant difference between peak frequencies in left sensorimotor
 244 MEG ROI vs. occipital MEG ROI ($p < 0.01$) and between peak frequencies in the right
 245 sensorimotor MEG ROI vs. the occipital MEG ROI ($p < 0.05$). For the factor condition, no
 246 significant main effect was found ($F(2, 28) = 1.17, p > 0.05$). Since no significant results could be
 247 found for the factor condition, we chose the combined condition EC+EO for visualization
 248 purposes in Fig 2B. Likewise, an ANOVA did not reveal a significant interaction between the
 249 factors ROI and condition ($F(2.06, 28.77) = 0.49, p > 0.05$).

250

251

252

253

254

255

256

257

258

259

| Subject | Beta peak frequency [Hz] | | | | | | | | |
|-------------|--------------------------|-------|-------|--------------------|-------|------|-----------|-------|------|
| | Left Sensorimotor | | | Right Sensorimotor | | | Occipital | | |
| | EO | EC | ECEO | EO | EC | ECEO | EO | EC | ECEO |
| 1 | 19 | 19 | 19 | 19 | 19 | 19 | 19 | 19 | 19 |
| 2 | 17 | 17 | 17 | 18 | 16 | 17 | 17 | 17 | 17 |
| 3 | 24 | 18 | 24 | 24 | 18 | 24 | 15 | 17 | 16 |
| 4 | 19 | 16 | 19 | 19 | 19 | 19 | 16 | 15 | 15 |
| 5 | 18 | 18 | 18 | 18 | 30 | 30 | 15 | 15 | 15 |
| 6 | 18 | 18 | 18 | 18 | 18 | 18 | 17 | 19 | 19 |
| 7 | 19 | 19 | 19 | 19 | 19 | 19 | 15 | 15 | 15 |
| 8 | 18 | 19 | 20 | 18 | 17 | 17 | 16 | 15 | 16 |
| 9 | 17 | 18 | 18 | 17 | 20 | 17 | 17 | 17 | 17 |
| 10 | 19 | 19 | 19 | 19 | 19 | 19 | 15 | 15 | 15 |
| 11 | 17 | 17 | 17 | 15 | 17 | 17 | 16 | 16 | 16 |
| 12 | 25 | 25 | 25 | 25 | 25 | 25 | 15 | 22 | 22 |
| 13 | 18 | 21 | 21 | 18 | 15 | 15 | 20 | 20 | 20 |
| 14 | 16 | 15 | 16 | 17 | 15 | 16 | 15 | 17 | 15 |
| 15 | 19 | 19 | 19 | 19 | 20 | 19 | 15 | 15 | 15 |
| Mean | 18.87 | 18.53 | 19.27 | 18.87 | 19.13 | 19.4 | 16.2 | 16.93 | 16.8 |
| SD | 2.47 | 2.29 | 2.46 | 2.53 | 3.87 | 3.98 | 1.57 | 2.17 | 2.21 |

260 **Table 2: Beta peak frequencies per MEG ROI and condition**

261

262 **Correlation of MRS and MEG data**

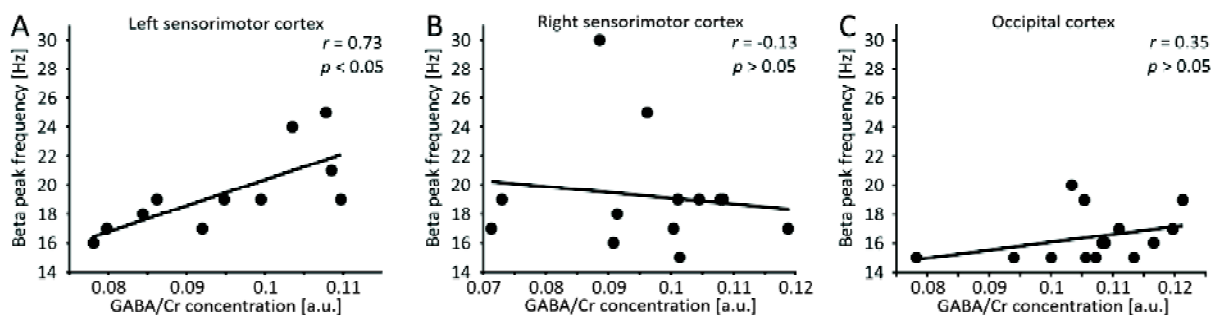
263 We computed linear correlations between GABA/Cr concentrations determined in MRS ROIs

264 and beta peak frequencies determined in MEG ROIs, separately for each of the three ROIs (left

265 sensorimotor cortex, right sensorimotor cortex, occipital cortex). Correlation analyses revealed

266 significant linear correlations in the left sensorimotor ROI (EO: $r = 0.62$, $p < 0.05$, EC: $r = 0.62$, $p <$ 267 0.05 , EC+EO: $r = 0.73$, $p < 0.05$; Fig 3A). No significant correlations were found in the right

268 sensorimotor ROI (EO: $r = -0.14$, $p > 0.05$, EC: $r = -0.07$, $p > 0.05$, EC+EO: $r = -0.13$, $p > 0.05$; Fig
 269 3B). Similarly, no significant correlations were found in the occipital ROI (EO: $r = 0.24$, $p > 0.05$,
 270 EC: $r = 0.09$, $p > 0.05$, EC+EO: $r = 0.35$, $p > 0.05$; Fig 3C). Since, within each ROI, correlations were
 271 highly similar across conditions, we selected the combined condition EC+EO for visualization
 272 purposes in Fig 3. Further, correlations within the respective ROIs statistically remained highly
 273 similar when correlations were restricted to those subjects for whom valid MRS spectra could
 274 be determined for all 3 MRS ROIs (see section MRS data above).



275
 276 **Fig 3. Correlation of beta peak frequencies and GABA/Cr concentration.** (A) Beta peak
 277 frequencies calculated for the left sensorimotor MEG ROI and the EC+EO condition correlated
 278 with GABA/Cr estimates from the left sensorimotor MRS ROI. (B) Same as (A), but now for right
 279 sensorimotor MEG and MRS ROI. (C) Same as (A), but now for occipital MEG and MRS ROI.

280
 281 We only found correlations between GABA/Cr concentrations and beta peak frequencies to be
 282 significant for the left sensorimotor ROI. Because the majority of the subjects (12/15) were
 283 classified as right-handed by means of the HDT performance measure, we additionally
 284 investigated the influence of handedness on the relationship between GABA/Cr concentration
 285 and beta peak frequency. Therefore, we partialized out the effect of handedness (assessed by

286 the HDT performance measure) on the correlations between GABA/Cr concentration and beta
287 peak frequencies. We found a significant correlation between GABA/Cr concentration and beta
288 peak frequencies for the left sensorimotor cortex for the EO and EC+EO conditions (EO: $r = 0.69$,
289 $p < 0.05$, ECEO: $r = 0.77$, $p < 0.01$), and a strong trend towards significance for the EC condition (r
290 $= 0.6$, $p = 0.07$). No significant correlations were found for the right sensorimotor and occipital
291 cortex.

292

293 **Discussion**

294 Using magnetoencephalography (MEG) and magnetic resonance spectroscopy (MRS) in healthy
295 human subjects, we investigated the relationship between beta peak frequencies at rest and
296 endogenous (i.e., non-modulated) GABA/Cr concentrations in the left and right sensorimotor
297 and occipital cortex. The results show significant positive linear correlations between peak
298 frequencies in the beta-band (15-30 Hz) and GABA/Cr concentrations for the left sensorimotor
299 cortex, i.e., higher beta peak frequency was related to a higher GABA/Cr concentration.

300 The present study is one of the first to investigate the connection between beta peak frequency
301 at rest (i.e., without movement or a movement-related task) and non-modulated GABA/Cr
302 values in the sensorimotor cortex. Previous studies that have addressed the general question if
303 sensorimotor beta activity is related to the GABAergic system, applied pharmacological
304 GABAergic modulators [7,8,12,15,17] and/or investigated movement-related sensorimotor beta
305 activity [8,15–17]. By focusing exclusively on non-modulated (i.e., no movement-related and
306 pharmaco-induced manipulation) parameters, the present study was able to show a correlation
307 between GABA/Cr concentrations and beta peak frequency at rest.

308 Beta peak frequencies differed across measurement sites. While left and right sensorimotor
309 cortices showed clear peaks in the beta-band in all subjects (Fig 2B), beta peaks were less
310 prominent in the occipital cortex, with five subjects showing no clear peak. This is in agreement
311 with the specific role of beta band activity for the sensorimotor cortex [1,4,37,38], while beta
312 band activity in occipital regions is less common. Less clear peaks in the beta band for the

313 occipital ROI might be a reason why correlations between GABA/Cr concentrations and beta
314 peak frequencies were only found for the sensorimotor cortex. This interpretation, however,
315 cannot account for the lack of a significant correlation in right sensorimotor areas, since we
316 found clear peaks in the right sensorimotor cortex for all subjects. Because GABA/Cr
317 concentrations across MRS ROIs did not differ significantly, it is also unlikely that GABA/Cr
318 concentrations are solely responsible for the unilaterality. Since 12 of 15 subjects in the present
319 study were classified as right-handed, handedness might be an explanation for the unilaterality
320 of the correlation. However, correlations remained significant even after correcting for
321 handedness. This finding suggests that handedness alone is unlikely to account for the
322 differences between left and right sensorimotor cortices. Handedness, however, is known to
323 lead to asymmetries with respect to hand representations in the sensorimotor cortex [39–41].
324 Such asymmetries might lead to regional differences in GABA/Cr concentration and/or
325 generators of beta frequencies in left and right sensorimotor areas. The rather large size of the
326 MRS ROIs poses an additional challenge, since for such voxel sizes it is not possible to separately
327 measure GABA/Cr concentrations for motor and somatosensory cortex. Although smaller voxel
328 sizes are possible [21], they result in extended measurement time for a comparable signal to
329 noise ratio. Thus, although GABA/Cr concentrations did not significantly differ between left and
330 right sensorimotor MRS ROIs, our method might have measured more GABA/Cr concentrations
331 that are unrelated to beta frequency generations in right sensorimotor cortex (i.e., more
332 “noise”). More fined-grained analyses might resolve this problem and shed further light on the
333 relation between GABA concentration and beta peak frequencies. In addition, it would be

334 interesting to assess both left and right-handed populations in future studies to further
335 elucidate the effect of handedness on GABAergic concentrations in sensorimotor cortices.

336 A general limitation of GABA measurements via MRS is that this method is unable to
337 differentiate between synaptic and extra-synaptic GABA concentrations [22]. Nonetheless,
338 GABA concentrations measured by MRS might primarily reflect extra-cellular GABA
339 concentrations, i.e., the general GABAergic tone [42]. Contrary to intra-cellular GABA
340 concentrations, extra-cellular GABA concentrations would include synaptic concentrations. Beta
341 band oscillations would be primarily related to synaptic GABA concentrations, since this
342 represents the synaptically active neurotransmitter pool [15]. Thus, our results represent
343 correlations with the overall GABA/Cr concentration of a given voxel, not exclusively for the
344 synaptically active GABA concentration. Despite all potential limitations, we were able to
345 demonstrate a significant positive correlation between GABA/Cr concentration and beta peak
346 frequency. In addition, various studies using parameters similar to the present study proved
347 that GABA MRS in sensorimotor and occipital cortices yields feasible results (reviewed in [22]).
348 The general feasibility of GABA MRS is further supported by studies that link MRS-derived
349 neurotransmitter concentrations to functional and behavioral measurements [21].

350 Neuronal oscillations are thought to depend on the balance between excitatory (i.e.,
351 glutamatergic synaptic input) and inhibitory (i.e., GABAergic synaptic input) network
352 components [12,43,44]. For beta band activity in the sensorimotor cortex, a connection
353 between GABAergic tone and beta band oscillations is supported by studies reporting increases
354 in somatosensory beta band power as an effect of GABAergic modulation by means of
355 GABAergic agonists (e.g., benzodiazepine) [7,12,15,17]. The relation between GABAergic

356 agonists and beta peak frequencies, however, is less clear. While, Jensen and colleagues [12]
357 reported a small decrease (~1.6 Hz) in resting-state beta peak frequency in bilateral
358 sensorimotor cortices after the administration of benzodiazepine, Baker and Baker [17] found
359 no modulation of beta peak frequency after the administration of benzodiazepine. The
360 GABAergic agonist benzodiazepine is considered to enhance the synaptic GABAergic drive [12].
361 Simplified, an enhanced GABAergic drive could be related to an increased GABAergic
362 concentration. This simplified assumption along with the results from Jensen and colleagues
363 [12] would contradict the positive correlation between beta peak frequency and GABA/Cr levels
364 in the left sensorimotor cortex observed in the present study. Yet, various differences between
365 the studies have to be taken into account. First, Jensen et al. [12] and Baker and Baker [17]
366 measured the influence of pharmacological GABA modulations on beta peak frequencies on the
367 within-subject level. The present study measured non-modulated GABA concentrations and
368 investigated correlations on a between-subject level. Further, while we report a correlation for
369 the left sensorimotor cortex, Jensen and colleagues [12] averaged beta peak frequency over
370 bilateral sensorimotor cortices (thereby not investigating lateral differences). Finally, we
371 measured mostly right-handed subjects, so that an influence of handedness cannot be
372 excluded. The abovementioned studies do not report handedness of their subjects, making a
373 direct comparison difficult.

374 Gaetz and colleagues [16] found no correlation between beta peak frequency during post-
375 movement beta-rebound and endogenous GABA concentrations for the left motor cortex. Post-
376 movement beta-rebound, however, is intrinsically different from resting state beta activity, as
377 measured in our study. Any differences found between our study and Gaetz et al. [16] might

378 thus be related to different tasks. Taken together, the few existing studies focusing on the
379 connection between beta peak frequency and GABA concentrations in sensorimotor cortex
380 areas strongly vary in experimental setting and assessed parameters, thereby complicating a
381 comparison to our results.

382 For future studies, it would be interesting to determine how sensorimotor beta peak frequency
383 and GABA concentration both relate on a behavioral level. There is evidence that higher
384 sensorimotor GABA concentrations correlate with slower reaction times in a motor sequence
385 learning task [45]. Here, slower reaction has been interpreted as a result of higher levels of
386 inhibition. Furthermore, higher concentrations of sensorimotor GABA have been related to
387 lower discrimination thresholds in a tactile frequency discrimination task [21]. The authors
388 associated higher GABA concentrations with a potentially higher temporal resolution of tactile
389 perception, which would enable neurons to more closely tune their responses to the stimulus
390 cycles. Such an adjustment of neuronal response to stimulus frequency is considered as the
391 underlying mechanism of the connection between sensorimotor GABA levels and frequency
392 discrimination and to result in lower frequency discrimination thresholds. The influence of
393 oscillatory beta activity on behavioral parameters is less clear. Studies relating individual beta
394 peak frequencies to measures of functional performance apart from motor-related tasks are
395 scarce. Differences in the phase of ongoing beta band oscillations in the somatosensory cortex
396 have been shown to predict the temporal perception of subsequently presented tactile stimuli
397 [46]. Here, the specific beta band frequency showing the biggest phase differences predicted
398 the temporal resolution of tactile perception. Perfetti and colleagues [47] found beta power
399 variations to successfully predict mean reaction time in a visually guided motor task, with a

400 decrease of beta power in left sensory-motor areas corresponding to faster reaction times. In
401 line with this, lower beta-power levels during the time of stimulus presentation were related to
402 a faster reaction towards this stimulus [48]. Taken together, these results suggest an
403 involvement of GABA concentrations and beta band activity within the sensorimotor cortex in
404 the temporal dimension of tactile perception. Thus, further research should investigate if GABA
405 concentration and beta band activity show similar connections to behavioral parameters
406 assessed in parallel.

407 In conclusion, the present study shows a significant linear correlation between beta peak
408 frequency at rest and non-modulated endogenous GABA concentration measured by spectrally
409 edited MRS. Significant correlations were restricted to the left sensorimotor cortex area. While
410 previous studies revealed connections between GABA concentrations and beta band power, our
411 results provide a novel connection between GABA concentrations and peak frequencies in the
412 beta band. In line with previous results from studies using pharmacological modulation of GABA
413 concentrations, these results support a specific role of GABAergic inhibition in the generation of
414 oscillatory beta-band activity within the sensorimotor system.

416 **References**

417

- 418 1. Salmelin R, Hari R. Spatiotemporal characteristics of sensorimotor neuromagnetic rhythms related
419 to thumb movement. *Neuroscience*. 1994; 60:537–50.
- 420 2. Murthy VN, Fetz EE. Oscillatory activity in sensorimotor cortex of awake monkeys: synchronization
421 of local field potentials and relation to behavior. *Journal of Neurophysiology*. 1996; 76:3949–67.
- 422 3. Pfurtscheller G, Stancák A, JR., Neuper C. Post-movement beta synchronization. A correlate of an
423 idling motor area? *Electroencephalography and Clinical Neurophysiology*. 1996; 98:281–93.
- 424 4. Kilavik BE, Zaepffel M, Brovelli A, MacKay WA, Riehle A. The ups and downs of beta oscillations in
425 sensorimotor cortex. *Special Issue: Neuronal oscillations in movement disorders*. 2013; 245:15–26.
- 426 5. Neuper C, Pfurtscheller G. Event-related dynamics of cortical rhythms: frequency-specific features
427 and functional correlates. *Thalamo-Cortical Relationships*. 2001; 43:41–58.
- 428 6. Jurkiewicz MT, Gaetz WC, Bostan AC, Cheyne D. Post-movement beta rebound is generated in
429 motor cortex: Evidence from neuromagnetic recordings. *NeuroImage*. 2006; 32:1281–89.
- 430 7. Hall SD, Barnes GR, Furlong PL, Seri S, Hillebrand A. Neuronal network pharmacodynamics of
431 GABAergic modulation in the human cortex determined using pharmaco-
432 magnetoencephalography. *Human Brain Mapping*. 2010; 31:581–94.
- 433 8. Muthukumaraswamy S, Myers J, Wilson S, Nutt D, Lingford-Hughes A, Singh K, et al. The effects of
434 elevated endogenous GABA levels on movement-related network oscillations. *NeuroImage*. 2013;
435 66:36–41.
- 436 9. Kilavik BE, Ponce-Alvarez A, Trachel R, Confais J, Takerkart S, Riehle A. Context-Related Frequency
437 Modulations of Macaque Motor Cortical LFP Beta Oscillations. *Cerebral Cortex*. 2012; 22:2148–59.
- 438 10. Neuper C, Pfurtscheller G. Evidence for distinct beta resonance frequencies in human EEG related
439 to specific sensorimotor cortical areas. *Clinical Neurophysiology*. 2001; 112:2084–97.
- 440 11. Salenius S, Portin K, Kajola M, Salmelin R, Hari R. Cortical Control of Human Motoneuron Firing
441 During Isometric Contraction. *Journal of Neurophysiology*. 1997; 77:3401–05.
- 442 12. Jensen O, Goel P, Kopell N, Pohja M, Hari R, Ermentrout B. On the human sensorimotor-cortex
443 beta rhythm: Sources and modeling. *NeuroImage*. 2005; 26:347–55.
- 444 13. Yamawaki N, Stanford IM, Hall SD, Woodhall GL. Pharmacologically induced and stimulus evoked
445 rhythmic neuronal oscillatory activity in the primary motor cortex in vitro. *Neuroscience*. 2008;
446 151:386–95.
- 447 14. Roopun AK, Middleton SJ, Cunningham MO, LeBeau FEN, Bibbig A, Whittington MA, et al. A beta2-
448 frequency (20–30 Hz) oscillation in nonsynaptic networks of somatosensory cortex. *Proceedings of*
449 *the National Academy of Sciences*. 2006; 103:15646–50.
- 450 15. Hall SD, Stanford IM, Yamawaki N, McAllister CJ, Rönqvist KC, Woodhall GL, et al. The role of
451 GABAergic modulation in motor function related neuronal network activity. *NeuroImage*. 2011;
452 56:1506–10.
- 453 16. Gaetz W, Edgar J, Wang D, Roberts T. Relating MEG measured motor cortical oscillations to resting
454 γ -Aminobutyric acid (GABA) concentration. *NeuroImage*. 2011; 55:616–21.
- 455 17. Baker MR, Baker SN. The effect of diazepam on motor cortical oscillations and corticomuscular
456 coherence studied in man. *The Journal of Physiology*. 2003; 546:931–42.
- 457 18. Durst CR, Michael N, Tustison NJ, Patrie JT, Raghavan P, Wintermark M, et al. Noninvasive
458 evaluation of the regional variations of GABA using magnetic resonance spectroscopy at 3 Tesla.
459 *Magnetic Resonance Imaging*. 2015; 33:611–17.

- 460 19. Muthukumaraswamy SD, Edden RA, Jones DK, Swettenham JB, Singh KD. Resting GABA
461 concentration predicts peak gamma frequency and fMRI amplitude in response to visual
462 stimulation in humans. *Proceedings of the National Academy of Sciences*. 2009; 106:8356–61.
- 463 20. Cousijn H, Haegens S, Wallis G, Near J, Stokes MG, Harrison PJ, et al. Resting GABA and glutamate
464 concentrations do not predict visual gamma frequency or amplitude. *Proceedings of the National
465 Academy of Sciences*. 2014; 111:9301–06.
- 466 21. Puts NAJ, Edden RAE, Evans CJ, McGlone F, McGonigle DJ. Regionally Specific Human GABA
467 Concentration Correlates with Tactile Discrimination Thresholds. *The Journal of Neuroscience*.
468 2011; 31:16556–60.
- 469 22. Stagg CJ. Magnetic Resonance Spectroscopy as a tool to study the role of GABA in motor-cortical
470 plasticity. *NeuroImage*. 2014; 86:19–27.
- 471 23. Oeltzschner G, Butz M, Baumgarten T, Hoogenboom N, Wittsack H, Schnitzler A. Low visual cortex
472 GABA levels in hepatic encephalopathy: links to blood ammonia, critical flicker frequency, and
473 brain osmolytes. *Metabolic Brain Disease*. 2015:1-10. doi: <http://dx.doi.org/10.1007/s11011-015-9729-2>
474
- 475 24. Steingrüber H. *Hand-Dominanz-Test*. Göttingen: Hogrefe; 2011.
- 476 25. Yousry TA, Schmid UD, Alkadhi H, Schmidt D, Peraud A, Buettner A, et al. Localization of the motor
477 hand area to a knob on the precentral gyrus. A new landmark. *Brain*. 1997; 120:141–57.
- 478 26. Mescher M, Merkle H, Kirsch J, Garwood M, Gruetter R. Simultaneous in vivo spectral editing and
479 water suppression. *NMR in Biomedicine*. 1998; 11:266–72.
- 480 27. Edden RA, Puts NA, Harris AD, Barker PB, Evans CJ. Gannet: A batch-processing tool for the
481 quantitative analysis of gamma-aminobutyric acid-edited MR spectroscopy spectra. *Journal of
482 Magnetic Resonance Imaging*. 2014; 40:1445–52.
- 483 28. Mullins PG, McGonigle DJ, O’Gorman RL, Puts NA, Vidyasagar R, Evans CJ, et al. Current practice in
484 the use of MEGA-PRESS spectroscopy for the detection of GABA. *NeuroImage*. 2014; 86:43–52.
- 485 29. Haegens S, Cousijn H, Wallis G, Harrison PJ, Nobre AC. Inter- and intra-individual variability in alpha
486 peak frequency. *NeuroImage*. 2014; 92:46–55.
- 487 30. Oostenveld R, Fries P, Maris E, Schoffelen J. FieldTrip: Open Source Software for Advanced Analysis
488 of MEG, EEG, and Invasive Electrophysiological Data. *Computational Intelligence and
489 Neuroscience*. 2011; 2011:9.
- 490 31. Liu Z, Zwart JA de, van Gelderen P, Kuo L, Duyn JH. Statistical feature extraction for artifact
491 removal from concurrent fMRI-EEG recordings. *NeuroImage*. 2012; 59:2073–87.
- 492 32. Abbasi O, Dammers J, Arrubla J, Warbrick T, Butz M, Neuner I, et al. Time-frequency analysis of
493 resting state and evoked EEG data recorded at higher magnetic fields up to 9.4T. *Journal of
494 Neuroscience Methods*. 2015. doi: 10.1016/j.jneumeth.2015.07.011
- 495 33. Haegens S, Nacher V, Hernandez A, Luna R, Jensen O, Romo R. Beta oscillations in the monkey
496 sensorimotor network reflect somatosensory decision making. *Proceedings of the National
497 Academy of Sciences*. 2011; 108:10708–13.
- 498 34. van Ede F, Jensen O, Maris E. Tactile expectation modulates pre-stimulus β -band oscillations in
499 human sensorimotor cortex. *NeuroImage*. 2010; 51:867–76.
- 500 35. Lange J, Halacz J, van Dijk H, Kahlbrock N, Schnitzler A. Fluctuations of Prestimulus Oscillatory
501 Power Predict Subjective Perception of Tactile Simultaneity. *Cerebral Cortex*. 2012; 22:2564–74.
- 502 36. van Dijk H, van der Werf J, Mazaheri A, Medendorp WP, Jensen O. Modulations in oscillatory
503 activity with amplitude asymmetry can produce cognitively relevant event-related responses.
504 *Proceedings of the National Academy of Sciences*. 2010; 107:900–05.
- 505 37. Pavlidou A, Schnitzler A, Lange J. Distinct spatio-temporal profiles of beta-oscillations within visual
506 and sensorimotor areas during action recognition as revealed by MEG. *Cortex*. 2014; 54:106–16.

- 507 38. Pavlidou A, Schnitzler A, Lange J. Interactions between visual and motor areas during the
508 recognition of plausible actions as revealed by magnetoencephalography. *Human Brain Mapping*.
509 2014; 35:581–92.
- 510 39. Volkmann J, Schnitzler A, Witte OW, Freund H. Handedness and Asymmetry of Hand
511 Representation in Human Motor Cortex. *Journal of Neurophysiology*. 1998; 79:2149–54.
- 512 40. Sörös P, Knecht S, Imai T, Gürtler S, Lütkenhöner B, Ringelstein EB, et al. Cortical asymmetries of
513 the human somatosensory hand representation in right- and left-handers. *Neuroscience Letters*.
514 1999; 271:89–92.
- 515 41. Triggs WJ, Subramaniam B, Rossi F. Hand preference and transcranial magnetic stimulation
516 asymmetry of cortical motor representation. *Brain Research*. 1999; 835:324–29.
- 517 42. Rae C. A guide to the metabolic pathways and function of metabolites observed in human brain 1H
518 magnetic resonance spectra. *Neurochemical Research*. 2014; 39:1-36.
- 519 43. Brunel N, Wang X. What Determines the Frequency of Fast Network Oscillations With Irregular
520 Neural Discharges? I. Synaptic Dynamics and Excitation-Inhibition Balance. *Journal of*
521 *Neurophysiology*. 2003; 90:415–30.
- 522 44. Buzsáki G. *Rhythms of the brain*. Oxford ; New York: Oxford University Press; 2006.
- 523 45. Stagg CJ, Bachtiar V, Johansen-Berg H. The Role of GABA in Human Motor Learning. *Current*
524 *Biology*. 2011; 21:480–84.
- 525 46. Baumgarten TJ, Schnitzler A, Lange J. Beta oscillations define discrete perceptual cycles in the
526 somatosensory domain. *Proceedings of the National Academy of Sciences*. 2015; 112:12187–92.
- 527 47. Perfetti B, Moisello C, Landsness EC, Kvint S, Pruski A, Onofrij M, et al. Temporal Evolution of
528 Oscillatory Activity Predicts Performance in a Choice-Reaction Time Reaching Task. *Journal of*
529 *Neurophysiology*. 2011; 105:18–27.
- 530 48. Tzagarakis C, Ince NF, Leuthold AC, Pellizzer G. Beta-Band Activity during Motor Planning Reflects
531 Response Uncertainty. *Journal of Neuroscience*. 2010; 30:11270–77.